Structure and Function in the Inferior Olivary Nucleus

Alexandre Roger Denis Mathy

I, Alexandre Roger Denis Mathy, confirm that the work presented in this thesis is my own. Where information has been derived from other sources, I confirm that this has been indicated in the thesis.

Alexandre Mathy

Dedicated to my family.

A.M.

Abstract

The inferior olivary nucleus is the source of the climbing fibres, one of the two major afferent pathways into the cerebellum. This thesis is concerned with aspects of the cellular anatomy and physiology of neurons in the inferior olive. In the first chapter, I report on the first direct patch-clamp recordings from olivary axons, and show that they fire in short bursts that can relay information about the state of olivary network and modulate plasticity in the cerebellar cortex. A remarkable feature of the olive is the widespread electrotonic coupling between neurons underlying their synchronous firing. In the second chapter I combine electrophysiological and immunohistological methods to characterize the coupling. I reveal the first morphological reconstructions of coupled pairs of olivary neurons, and show that the dendritic spines responsible for coupling neurons have very heterogeneous morphologies. Furthermore, I show that olivary dendrites may contact olivary somata and oligodendrocytes. In the third chapter, I use pharmacology and modelling to study the effect of inhibitory synapses on the coupling between olivary neurons. Confirming a popular theory, I show that GABA-A receptor activation reduces coupling between neurons, and use models to study the effect of location, timing and stochastic properties of the inhibitory input on electrical coupling. The common theme for all our findings is that the remarkable interplay between the anatomy and electrophysiological characteristics of the inferior olive underlies a unique computational unit in the central nervous system.

Table of contents

List of figures

Foreword

This thesis marks the culmination of several years of work in Michael Häusser's laboratory at University College London. It is a testament to my apprenticeship in science, and I hope it also constitutes a modest contribution to knowledge.

I got lured into neurophysiology by the hope that the mysteries of the human mind could be understood in terms of matter and mechanism. I am convinced that we have entered a golden era where significant progress is being made on this front (even if the final goal eludes us), and I feel privileged to have played a role in it – no matter how small.

Acknowledgements

One of the great joys of science is the interaction with scientists from around the world. I would like to single out Yosi Yarom, Anna Devor, Koen Vervaeke, Greg Hoge, Alberto Pereda, Michael Bennett, Chris de Zeeuw, and Marcel de Jeu for especially fruitful conversations.

I would like to acknowledge assistance with some of the data presented in this thesis. An undergraduate student under my supervision, Si Yoo, helped with the connexin 36 staining of brain slices and the reconstructions of spine morphology in Chapter 2. Maja Boznakova assisted with reconstruction of pairs of olivary neurons. The *in vivo* whole cell data in Chapter 1 was obtained by Sara Ho - a PhD student and co-author on the publication (Mathy et al., 2009) derived from that work, and is included with her permission. Latha Ramakrishnan, Kate Powell and Arifa Naeem helped with histology for the data presented in Chapter 2.

I wish to express my thanks to my family, especially to my mother, my brother Charles and my father. Their unwavering belief in me carried me through. Thanks to Nancy for her patience and understanding. I am also blessed to have many friends who have made this a very enjoyable time of my life.

Finally, I am grateful to Michael Häusser for his support. He took me on despite my limited laboratory experience and has created a great environment in which to do science. I am convinced his group will keep

going from strength to strength, and push back against the boundaries of my

knowledge.

List of abbreviations

ADP: After-depolarisation

AHP: After-hyperpolarisation

CF: Climbing Fibre

CS: Complex Spike

CX36:   Connexin 36

DAO: Dorsal Accessory Olive

DCK: Dorsal Cap of Kooy

DCN: Deep Cerebellar Nuclei

GABA: γ-Aminobutyric acid

GFP: Green fluorescent protein

IO: Inferior Olive

LTD: Long-term Depression

LTP: Long-term Potentiation

MAO: Medial Accessory Olive

NMDA: N-methyl D-aspartate

MDJ: Mesodiencephalic junction

PC: Purkinje cell

PF: Parallel Fibre

PO: Principal Olive

SSE: Synaptically evoked suppression of excitatory synapses

Chapter 1: Introduction

The cerebellum ("small brain") is a structure at the back of the brain critically involved in motor learning (Houk et al., 1996), the maintenance of posture and the production of coordinated movement (Holmes, 1917). In order to fulfil this role, the cerebellum must process information from the rest of the nervous system. A major relay for this information is the Inferior Olive, a brainstem nucleus which gives rise to one of the two input pathways into the cerebellar cortex. As such, an understanding of the structure and function of the Inferior Olive is crucial for a proper appreciation of the role of the cerebellar circuit as a whole. This thesis is concerned with important aspects of the cellular physiology and anatomy of the olive. In this introductory chapter I will review what is known about this nucleus and place it in a larger theoretical and behavioural context.

Anatomy of the Inferior Olive

Gross anatomy

Gabriele Fallopius of the Paduan school of anatomy first described the Olivary Bodies of the Medulla Oblongata in the 16th century (Bowman and King, 1973; De Zeeuw et al., 1998). They have since been found to be present –in some form- in all species of vertebrates (Voogd and Glickstein, 1998).

The Olivary Bodies contain the Superior and Inferior Olivary Complexes. The Superior Olive is involved in the auditory pathway, and will not concern us. The Inferior Olive (IO) consists of a gray convoluted folded lamella containing four main subnuclei (Figure 1): The Principal Olive (PO), the Medial and Dorsal Accessory Olives (MAO and DAO), and the Dorsal Cap of Kooy(De Zeeuw et al., 1998). Additionally, there are small structures involved in the oculomotor system called the beta-nucleus and the dorsomedial cell column. The relative size of the subnuclei varies markedly from species to species (Scheibel and Scheibel, 1955).
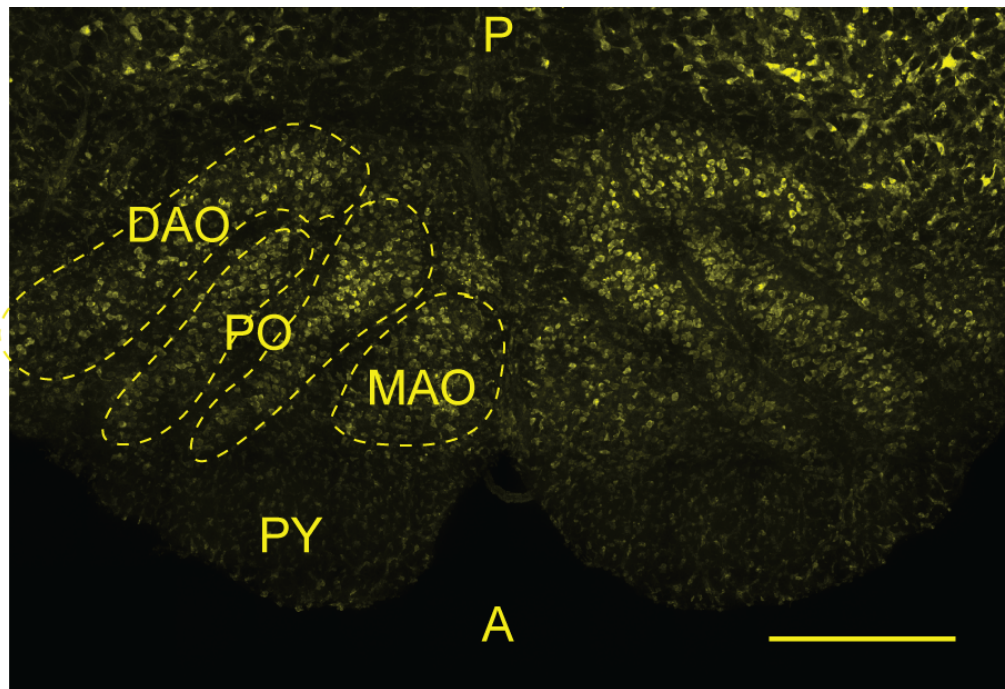
Figure 1 Histology of the IO: A Nissl stain of a transverse section of the brainstem of a P18 rat showing the subdivisions of the inferior olive. P: Posterior A: Anterior PY: pyramidal tract DAO: Dorsal Accessory Olive PO: principal olive MAO: Medial accessory olive. Note that the Dorsal Cap of Kooy is not present in this section (Scale bar: 500 μm).

Cellular anatomy

The IO contains almost exclusively principal neurons, although there is a small population of diminutive interneurons, the significance of which is as of yet unclear (Walberg and Ottersen, 1989).

The principal neurons can be morphologically divided into two types. Neurons of the first type (called Type 1) have straight dendritic arbours, whereas the dendrites of the Type 2 neurons curl back towards the soma – a quite uncommon feature in neuroanatomy (Ramon y Cajal, 1911; Scheibel and Scheibel, 1955). The envelope of the dendritic trees is spheroid in shape, although neurons at the edge of the nucleus are polar (with the dendrites pointing inwardly to the core of the IOC). The Type 1 neurons are more common in the posterior regions of the olive and seem to be a phylogenetically more ancestral type (Scheibel and Scheibel, 1955).

Relationship with the cerebellar network

The crystalline structure of the cerebellum has fascinated generations of neuroscientists (Figure 2), ever since it was elucidated by Cajal and his colleagues (Ramon y Cajal, 1911). The cortex has three layers, called (from superficial to deep) the molecular, Purkinje and granular layer. The principal neurons of the cerebellar cortex are called Purkinje cells and are oriented in the sagittal plane with their cell bodies arranged in the Purkinje layer with their complex dendrites radiating outward in the molecular layer of the cortex.

They are the only output of the cortex and send their axons to the deep cerebellar nuclei and vestibular nuclei where they make an inhibitory connection.

There are two input pathways into the cerebellum. The mossy fibres arise from the pontine nuclei and contact granule cells in the lower layer of the cerebellar cortex. The granule cells then send their axons upwards to the molecular layer of the cortex where they branch once into the parallel fibres, which run perpendicular to cerebellar folia. Each Purkinje cell receives hundreds of thousands of excitatory synapses from parallel fibres.

The second input to the cerebellar cortex is the climbing fibre pathway. The climbing fibres arise from the (on average ten) collaterals of axons of inferior olivary neurons (Shinoda et al., 2000; Sugihara et al., 1999; Sugihara et al., 2001; Szentagothai and Rajkovits, 1959). The fibres make a remarkable synapse with the Purkinje cell dendrites: They wrap around the proximal portion of the Purkinje dendritic tree rather like a vine, and make contacts at many sites on the proximal dendritic tree. Each Purkinje cell receives a single climbing fibre. The climbing fibre synapse is also excitatory and is one of the most powerful synapses in the central nervous system (Eccles et al., 1966).
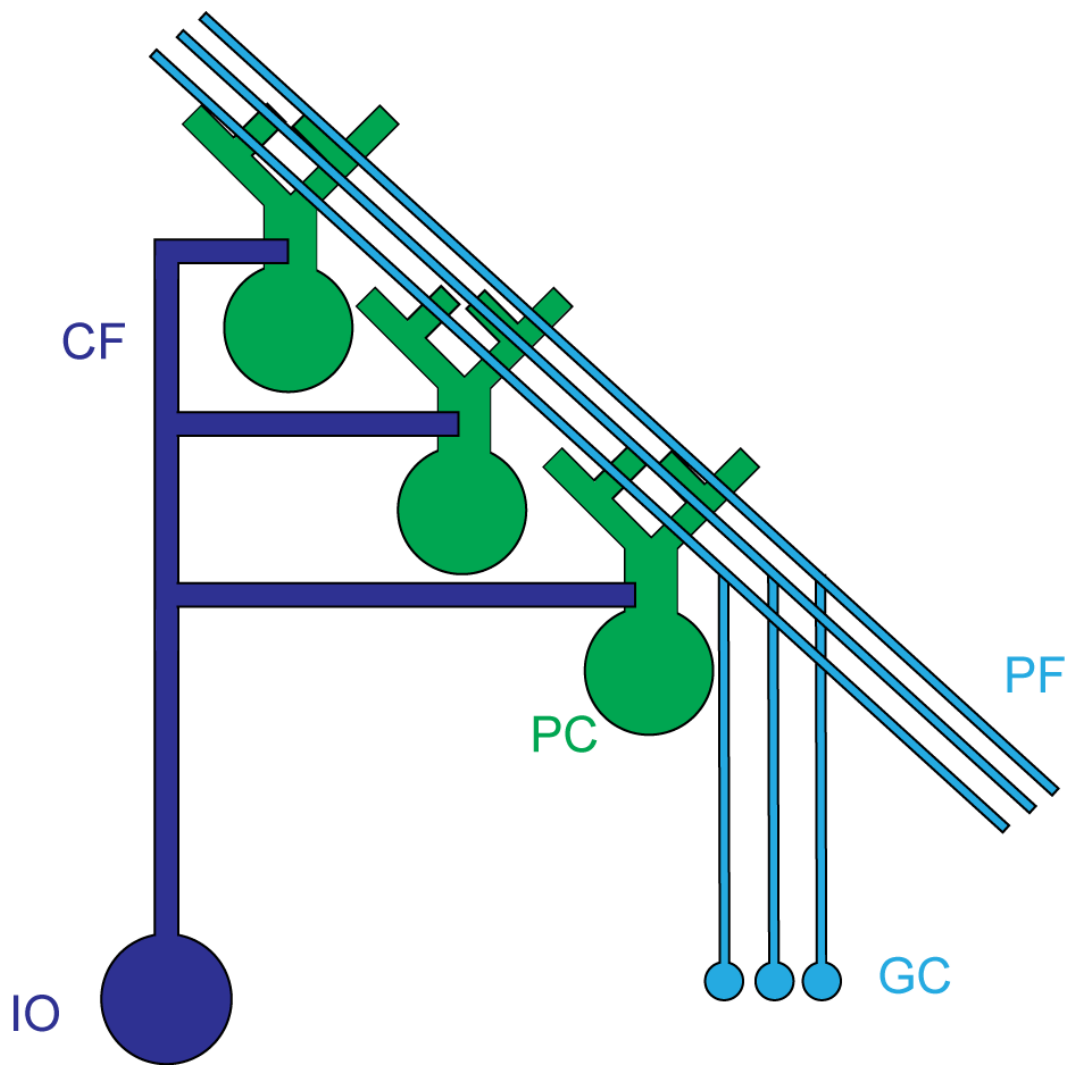
Figure 2 Input pathways to the cerebellum. Each olivary neuron (IO) sends several (averaging about ten) collaterals to the cerebellar cortex. These collaterals are the climbing fibres (CF) which each innervates one Purkinje cells. The Purkinje cells (PC) also receive around two hundred thousand parallel fibre (PF) synapses from the granule cells (GC).

The cerebellar cortex contains several types of interneurons, which play a crucial role in the computation performed by the circuit. The molecular layer interneurons consist of basket and stellate cells, and both inhibit Purkinje cells. The Golgi cells are in the granular layer and inhibit both the granule cells and Purkinje cells.

As I have described above, each Purkinje cell receives one, and only one climbing fibre connection, while it receives many tens of thousands of

parallel fibre synapses.   However, at birth, Purkinje cells are actually innervated by more than one climbing fibre. Gradually, during development, these climbing fibres degenerate until one is left. The learning rule that this pruning follows is the subject of serious inquiry (Bosman and Konnerth, 2009; Hashimoto et al., 2000).

Architecture of the olivocerebellar network: zones, microzones, modules and loops

On top of the strict organization of connections at the cellular level, the cerebellum has a remarkable architecture at the network level.

First of all, the cerebellar cortex is organized in parasagittal longitudinal strips called zones – which can span several (and often all) folia (Voogd and Glickstein, 1998). The Purkinje cells in a given zone project to one (and only one) nucleus – one of the deep cerebellar nuclei or the vestibular nuclei. The climbing fibre is organized by a similar principle: a group of inferior olive neurons (organized in a columnar fashion) project only to a given cerebellar zone (or two non-contiguous zones that project to the same output nucleus) (Armstrong et al., 1974; Groenewegen et al., 1979). Within a zone, it has been found that the climbing fibres innervating Purkinje cells within a narrow sagittal strip (200-500 µm) have very similar response properties (at least in somatosensory areas). Such a strip is called a microzone (Andersson and Oscarsson, 1978; Armstrong et al., 1974; Ekerot et al., 1991). Climbing fibres
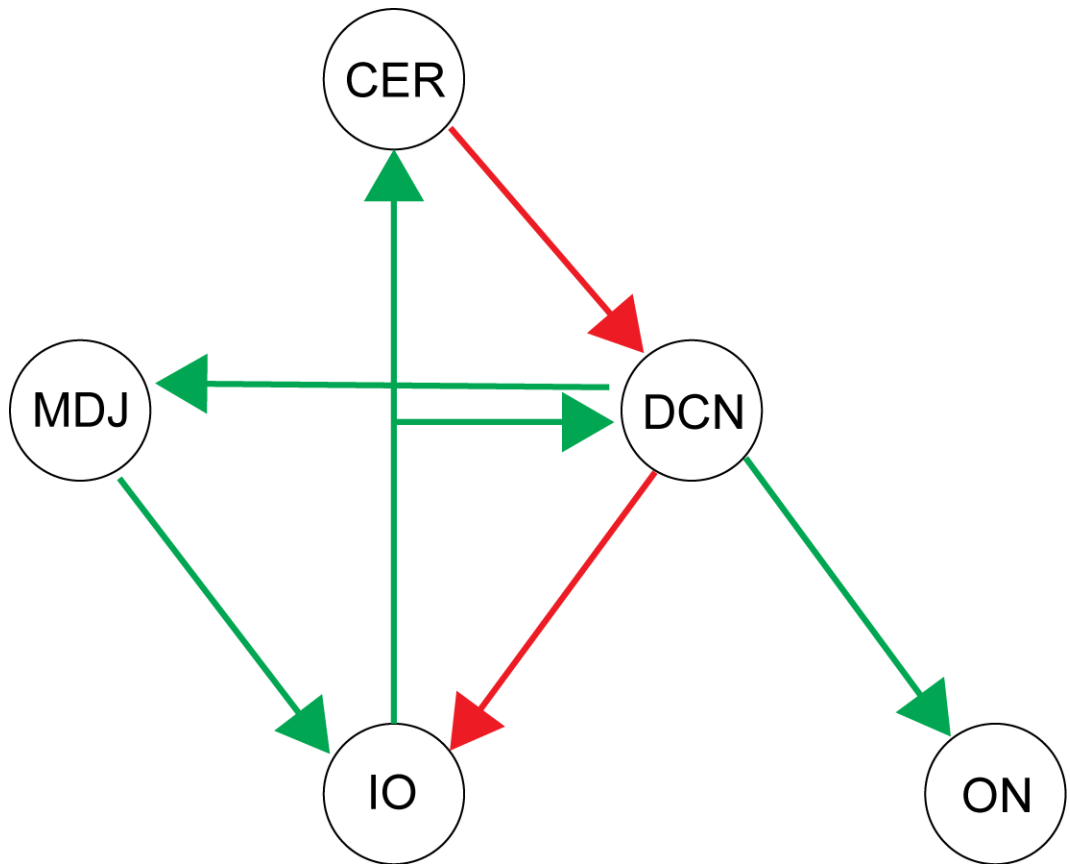
Figure 3 Network architecture of the olivocerebellar system. Red and green arrows represent inhibitory and excitatory connections respectively. MDJ: Mesodiencephalic junction. IO: Inferior Olive. CER: Cerebellar cortex DCN: Deep Cerebellar Nuclei. ON: Output nucleus (i.e. red nucleus, vestibular nucleus)

also send collaterals directly to the DCN, where they provide an excitatory connection. This projection respects the zonal principle and targets the nucleus which receives axons from Purkinje cells innervated by the same climbing fibres (Ruigrok, 1997). Finally, the DCN contain GABAergic neurons, which project back to the group of cells of the olive from which they got their input (Ruigrok and Voogd, 1990, 2000).

The reciprocity and zonal organization of the different components of the olivocerebellar network has led to the notion that it is composed of separate,

parallel *modules* (Apps and Garwicz, 2005) and that these are the fundamental units of cerebellar computation. Furthermore, the IO-cortex-DCN-IO circuit is named the *olivocerebellar loop* (De Zeeuw et al*.,* 1998*)*, (Figure 3) since each of its elements can indirectly feedback onto itself. Whether this loop structure is respected at the cellular level rather than merely at the grosser microzonal scale is an open question.

Afferent connections

Aside from the inhibitory connection from the deep cerebellar nuclei, the olive gets a variety of different inputs. Spinal afferents provide direct excitatory input via the spino-olivary tract (Armstrong, 1974). This pathway provides somatosensory and proprioceptive information to the cerebellum. Mapping studies have shown that there is a somewhat topographical organization of these afferents (Gellman et al., 1983), which, through the zonal architecture I discussed above, is preserved in the cerebellar cortex.

A collection of nuclei (including the nucleus of Darkschewitsch) at the mesodiencephalic junction sends excitatory terminals to the olive (Onodera, 1984). These nuclei also receive excitatory input from glutamatergic cells of the deep cerebellar nuclei (De Zeeuw and Ruigrok, 1994), so that the DCN-MDJ-IO circuit is also arranged in a loop structure.

Electrophysiological studies suggest that many parts of the nervous system can evoke responses in the inferior olive: stimulation of motor cortex (Crill, 1970; Lang et al., 2006b), prefrontal cortex (Dias-Ferreira et al., 2010), caudate nucleus (Sedgwick and Williams, 1967), and the cranial nerves

(Baker et al., 1972) can all activate climbing fibres. The IO also gets a significant serotonergic input from the nucleus reticularis gigantocellularis which is located dorsally to the IO (Bishop and Ho, 1984; Wiklund et al., 1981), and dopaminergic input from the nigrostriatial system (Deutch et al., 1989).

Physiology of the Inferior Olive

Olivary firing

Upon depolarisation or synaptic stimulation, olivary neurons fire in a characteristic sequence (Crill, 1970; Llinas and Yarom, 1981a, b):

A fast spike, followed by a long (10-30ms) after-depolarisation (ADP), and terminated by an after-hyperpolarisation (AHP) (Figure 4).

The fast spike is abolished by bath application of tetrodotoxin (TTX), and is therefore the result of sodium channel currents. The after-depolarisation depends on high-threshold (P/Q type) calcium channels. A recent study with mice in which the gene for CaV2.1 channels was knocked out showed that the ADP was markedly reduced (although not absent) (Choi et al., 2010).

The AHP is probably caused by calcium-dependent potassium (SK and BK) channels (Lang et al., 1997), although the precise identity of the channels hasn't yet been demonstrated.
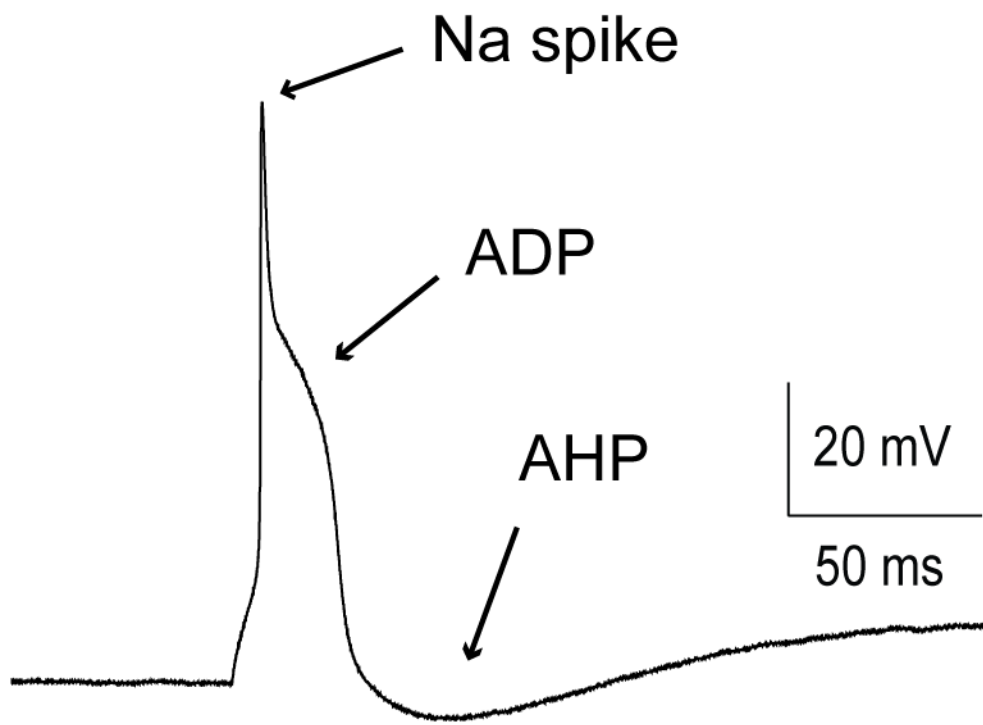
Figure 4 Spike from an olivary neuron from a rat recorded with a patch-clamp electrode. When olivary neurons are depolarized (in this case by 800pA current injection) beyond threshold, they first fire a sodium spike, followed by an after-depolarisation (ADP), and an after-hyperpolarisation (AHP).

When the neuron is hyperpolarized, the I_h current is activated (Bal and McCormick, 1997; Yarom and Llinas, 1987), and T-type calcium channels are deinactivated. Upon release from hyperpolarisation, these channels cause a rebound current, upon which a sodium spike can be triggered. The rebound spike is absent in CaV3.1 null mutants (Choi et al., 2010). Aside from the channels mentioned, there is pharmacological evidence that IO neurons express N-type calcium channels (Urbano et al., 2006) and inward rectifying (Kir) potassium channels (Placantonakis et al., 2000).

Olivary neurons do not usually fire spontaneous action potentials in slice preparations. *In vivo* they fire at low frequencies (0.5-2Hz) (Hobson and McCarley, 1972; Lang et al., 1999; Mano, 1970).

The original detailed characterization of olivary excitability (Llinas and Yarom, 1981b) attempted to localize the cellular compartments involved in generating the currents I have described. This was done by recording membrane potential with a sharp intracellular electrode and extracellular potentials with a second electrode. Based on these recordings, the authors interpreted where the current sources and sinks were located in the neuropil. They concluded that the currents underlying ADP were mainly dendritic, while the rebound spikes resulted from currents through somatic channels.

A recent report has revealed that neurons of the dorsal cap of Kooy (as opposed the other nuclei of the olive) do not fire in the way described above: their spikes do not display the ADP (Urbano et al., 2006). The cells spontaneously fire action potentials, and can fire at higher rates (up to 8 Hz). Since the dorsal cap of Kooy is involved in the regulation of ocular movement, the difference in firing patterns might be explained by the different computation implemented by this system, a subject I will return to later in this introduction.

Electrotonic coupling of olivary neurons

Initially, electrophysiological evidence of horizontal excitation between olivary neurons led researchers to believe that olivary neurons make connections through recurrent axonal collaterals (Armstrong, 1974; Eccles et al., 1967) in the nucleus (indeed some researchers still maintain that these collaterals exist (Sotelo, 2003)). Later, electrophysiological evidence and electron microscopy of the olivary neuropil revealed that there were gap junctions between olivary neurons (Llinas et al., 1974; Sotelo et al., 1974).

Gap junctions can form between spines of olivary neurons. The spines of the neurons meet together in a glomerulus (Figure 5), which is ensheathed by a glial covering. Each spine furthermore receives inhibitory and excitatory input from the deep cerebellar nuclei and the mesodiencephalic junction respectively (de Zeeuw et al., 1990b).

There is a dendritic organelle called the lamellar body which seems to be associated with the production of gap junctions, but for which a definite function has yet to be found (De Zeeuw et al., 1995a; De Zeeuw et al., 1997)
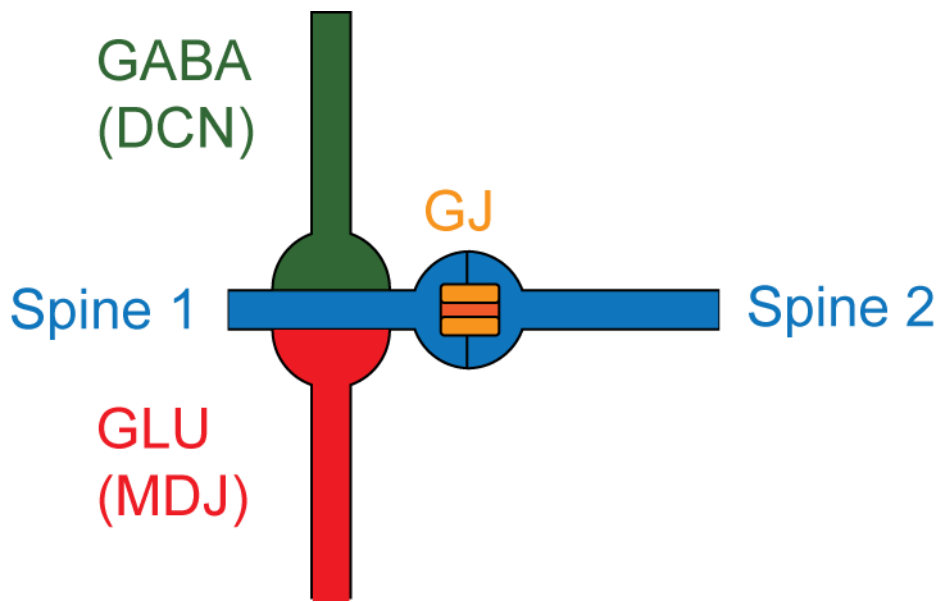
Figure 5 The olivary glomerulus: 4-7 olivary dendritic spines from neighbouring neurons contact each other in a glomerular structure. Some of the spines form gap junctions (GJ). Each spine is also innervated by a glutamatergic input from the mesodiencephalic junction and a GABAergic input from the deep cerebellar nuclei.

Ionic current flow through gap junctions (Bennett et al., 1963) is the physical substrate for electrotonic coupling. A gap junction consists of two connexons (or hemi-channels): protein complexes that meet in the extracellular space between the cells. A connexon is either a homomer or heteromer of six connexin proteins, arranged so as to form a central pore. This pore will permit the passage of small ions and other molecules such as cAMP, IP3, ATP and glutamate (Harris and Locke, 2009). When the gap junction is formed by connexons of different types, it is named heterotypic.

There are twenty one connexin proteins, each conferring different properties to the gap junction they form. All connexins share the same basic structure: cytoplasmic C- and N-terminus tails, two extracellular and one intracellular loop. Connexins are expressed in many organs around the body. For instance Connexin 43 permits the propagation of the cardiac action

potential in myocytes, while connexin 36 couples insulin secreting cells in the pancreas (Charpantier et al., 2007). Connexin 36 and connexin 45 are the main proteins involved in neuronal gap junctions (Nagy et al., 2004). Connexin 36 appears to be main constituent of olivary gap junctions (De Zeeuw et al., 2003; Long et al., 2002). Connexin36 has a small unitary conductance (15pS) compared to other connexins (Srinivas et al., 1999).

Traditionally gap junctions have been regarded as forming a static, passive pore between cells. It is true that, in many circumstances, gap junctions behave in an Ohmic fashion. However, treating them as mere resistances disregards the fact that gap junctions can be modulated in several interesting ways.

First of all, gap junctions are to a certain extent voltage gated. However, the voltage gating is quite slow, and it is not yet clear what role it plays under physiological conditions. For connexin 36, the voltage dependence in the physiological range is negligible (Srinivas et al., 1999)

Secondly, conductance of gap junctions can be strongly affected by intra and extracellular pH. For most connexins, acidification reduces and alkalinisation increases the permeability of the junctions. This modulation can be quite dramatic (Bukauskas and Verselis, 2004). However for connexin 36 (the protein which is most relevant for this thesis), the relationship is inverted (Gonzalez-Nieto et al., 2008), so that acidification actually increases the conductance of the junction slightly. The presumed mechanism for the pH-dependence of coupling is protonation or de-protonation of amino acid residues in the connexin protein causing conformational change of the connexins at the junction.

Increasing intra and extracellular calcium concentrations can decrease coupling. Indeed, some early studies suggest that very high concentrations of calcium cause the channels to close. However it is unclear what the physiological role of calcium is in modulating gap junctions (Connors and Long, 2004).

There are several ways to determine coupling between cells. The most direct way to demonstrate coupling is to make electrophysiological recordings of the membrane potential of two neurons and inject current in one cell while measuring the response in the other (Landisman et al., 2002; Mann-Metzer and Yarom, 1999).

The olive has an unusual feature that allows assessment of intercellular coupling: antidromic stimulation of climbing fibres results in a 'climbing fibre reflex' measured in the cerebellar white matter, which is the consequence of the spread of the antidromic impulse via the electrically coupled network and back up the climbing fibre(Blenkinsop and Lang, 2006).

The most used technique to establish electrotonic coupling between neurons is to evaluate dye coupling, where a single cell is filled with a dye that diffuses through gap junctions. The extent of coupling is then quantified by counting the number of cells that have been indirectly stained (Mills and Massey, 1995). The permeability of the different connexin proteins to dyes varies quite markedly (Charpantier et al., 2007; Kanaporis et al., 2011), and therefore an appropriate dye has to be found for the system under study. Neurobiotin and Lucifer Yellow (Hanani, 2011) are popular choices.

 Finally, anatomical methods allow the detection of gap junction plaques. With transmission electron microscopy of thin sections (Sotelo et al., 1974)

the gap junctions have a characteristic appearance. Immunohistochemical techniques such as Freeze-fracture immunogold labelling (FRIL) can increase the detection rate (Rash et al., 2005). The advent of antibodies with fluorescent tags has allowed confocal microscopic methods to be used to detect gap junction plaques (Nagy et al., 2003; Rash et al., 2001).

When one estimates the number of connexin channels from anatomical data and compares to the conductance measured between neurons, it is apparent that only a small portion of the connexin channels are open (Vervaeke et al., 2010). This raises the distinct possibility that they form a reserve pool of channels, which provide a resource for plasticity.

Subthreshold oscillations

Early experiments in cat showed that the administration of harmaline (de Montigny and Lamarre, 1973, 1974; Llinas and Volkind, 1973), an alkaloid drug that induces olivary neurons to fire rhythmically at around 10Hz, caused a motor tremor of the same frequency to appear in the animals. This was interpreted as evidence that oscillatory activity in the IO could be important in the generation of motor programs. It was also known that complex spikes in the cerebellum, the counterpart of olivary firing, were often periodic in the 1-10Hz range.

The basis for this periodicity became clear when, in 1986, two groups demonstrated, using intracellular recordings from guinea pig brainstem slices, that olivary neurons display subthreshold oscillations (STOs) of their membrane potential (Benardo and Foster, 1986; Llinas and Yarom, 1986).

The oscillations are 1-10Hz in frequency and 1-20mV in amplitude, and often sinusoidal in character (Figure 6). These findings have now been replicated many times across several species (rat, mouse, ferret)(Bal and McCormick, 1997; Devor and Yarom, 2002a; Leznik et al., 2002; Long et al., 2002; Placantonakis et al., 2000) and, recently *in vivo* in anesthetized preparations(Chorev et al., 2007; Khosrovani et al., 2007).
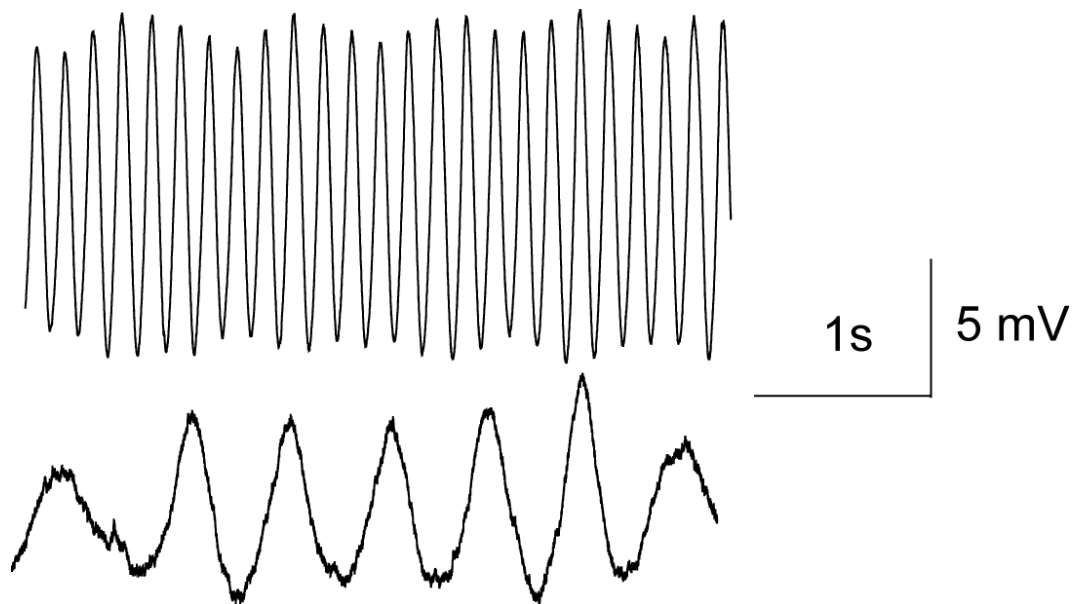
Figure 6 Subthreshold oscillations: Two intracellular recordings from inferior olive neurons showing large amplitude sinusoidal subthreshold oscillations.

The occurrence of olivary oscillations varies considerably between reports. Some authors report the oscillations as quite infrequent (Llinas and Yarom, 1986), while in other hands most of the cells oscillate (e.g. 85% in (Khosrovani et al., 2007)). This is presumably due to species differences, the details of the slicing and anaesthesia protocols employed, as well as the criteria for defining the oscillation.

The character of the oscillations is also somewhat controversial. Some researchers claim that the oscillations are very stable and present during the whole of a recording (Khosrovani et al., 2007), but others state that the oscillations are interrupted by frequent periods of quiescence or that the amplitude and frequency of the oscillation is modulated considerably during a recording (Chorev et al., 2007; Devor and Yarom, 2002a).

What drives these remarkable oscillations? The original studies (Benardo and Foster, 1986; Llinas and Yarom, 1986) showed that they were resistant to TTX application and intracellular current injection, but that blocking calcium currents (by application of nickel and cadmium ions or removing the extracellular calcium) abolished the oscillations. More recently, a study in two knockout mouse lines which lacked the subunits for either the high (CaV2.1) or low threshold (CaV3.1) calcium channels showed that these mice had a much lower occurrence of STOs when compared to wild-type(Choi et al., 2010). Bal and McCormick provided evidence that the Ih current (Bal and McCormick, 1997) was important in determining the resting potential of the cells and therefore the occurrence of oscillations by modifying the inactivation of the low-threshold calcium channel. Others have shown steady state depolarisation of olivary neurons reduces the amplitude of the oscillations (Leznik and Llinas, 2005; Long et al., 2002). One study (Khosrovani et al., 2007) categorizes the oscillations into two types: LTOs (low-threshold oscillations in the 1-3 Hz range) and SSTOs (sinusoidal subthreshold oscillations in the 6-9 Hz range); being driven by low-threshold and high-threshold calcium channels respectively.

From these findings it is clear that intrinsic conductances in each cell are involved in the generation of the STOs. However, there is additional evidence suggesting that the oscillations are also a network phenomenon mediated by electrotonic coupling between IO cells. Firstly gap junction blockers interfere with the oscillation (Leznik and Llinas, 2005). Secondly, in connexin 36 knockout mice, the oscillations are still present, but unsynchronized between cells (Long et al., 2002). While developmental compensation in these mice makes the interpretation of these results problematic (De Zeeuw et al., 2003), a study using a lentiviral knockdown of connexin 36 in the IO provided evidence that to support an oscillation, olivary neurons need to be coupled to a small ensemble of other IO cells(Placantonakis et al., 2006). It seems therefore that, while olivary neurons are intrinsically oscillatory, they only produce strong oscillations as part of a synchronous ensemble.(Lampl and Yarom, 1997; Manor et al., 2000)

The original work of Benardo and Foster (Benardo and Foster, 1986; Llinas and Yarom, 1986) further showed that the subthreshold oscillation was tightly synchronized across neighbouring neurons that were coupled by gap junctions. This finding has been replicated many times (Devor and Yarom, 2002a; Leznik and Llinas, 2005; Long et al., 2002). Two studies used voltage sensitive dye imaging to characterize the oscillations at the network level. In one case (Leznik et al., 2002), the IO showed synchronous clusters of cells, while in the second (Devor and Yarom, 2002c), the subthreshold oscillations propagated across the nucleus in a wave-like pattern. In agreement with this,

an *in vivo* study using chronic electrode recordings in the cerebellum (Jacobson et al., 2009) suggests that rather than being exactly in phase, olive neurons can have stable phase differences between neurons while oscillating at the same frequency. A networked compartmental model of olivary neurons (Schweighofer et al., 1999) shows the phase difference between the oscillation of coupled inferior olivary can be varied with the magnitude of the coupling.

It is still unresolved how large an oscillating cluster of cells is. A dye coupling study suggests olive cells are coupled to a varying small number of cells (up to 35) contained within their dendritic field(Hoge et al., 2010). However it is known that these dendrites can sometimes extend across the midline to make contacts with the contralateral olive(De Zeeuw et al., 1996).

The oscillations are modulated by a number of factors. Synaptic stimulation of brain stem slices disrupts the STOs (Benardo and Foster, 1986; Lampl and Yarom, 1993), while bath application of NBQX reduces their amplitude modulation somewhat (Devor and Yarom, 2002a). Blocking GABA-A receptors with picrotoxin creates more synchronous clusters of olive cells as visualized by voltage sensitive dyes (Leznik et al., 2002), while local GABA application abolishes the oscillations (Devor and Yarom, 2000). Blockers of the NMDA receptor have been shown to block STOs, while bath application of NMDA causes oscillations sensitive to nifedipine (Placantonakis and Welsh, 2001) but not to TTX. Meanwhile, application of harmaline causes the

neurons firstly to oscillate and then fire at the crest of oscillation (Llinas and Yarom, 1986).

What is the impact of oscillations on olivary firing? Some authors claim that oscillations precisely and periodically time spikes (the "clock" hypothesis), but this is controversial. *In vivo*, while olivary neurons preferentially fire at the crest of an oscillation (Chorev et al., 2007) they can fire at a wide range of other phases (Khosrovani et al., 2007). Others have argued that synaptic response to a stimulus is delayed until the peak of an oscillation (Kistler and De Zeeuw, 2005; Lampl and Yarom, 1993), but the mechanism for this is poorly understood and contradicted by data that shows the olive responds to stimulation at low latencies (Gellman et al., 1985).

If it is disputed how oscillations affect spike output, an inverse relationship has been quite clearly demonstrated by several groups: After the neuron spikes, the subthreshold oscillations resets to a given phase (Khosrovani et al., 2007; Llinas, 2009). This phase reset is a network phenomemon affecting several cells at once, and has been hypothesized to represent the retrieval of a new motor program in the olivocerebellar system.

Serotonin and the olive

As mentioned above, the olive receives a significant serotonergic input from a nucleus situated dorsally to it. Serotonin has several interesting physiological effects on olivary neurons.

In slice experiments, application of serotonin increases the input resistance of the neurons and potentiates the I_h current as well as depressing the t-type calcium and K_{ir} currents, thereby suppressing subthreshold oscillations (Placantonakis et al., 2000). *In vivo*, this should translate to a reduction in the rhythmic of climbing fibre activity, but the evidence for this contradictory (Barragan et al., 1983; Biscoe et al., 1973; Headley and Lodge, 1976; Headley et al., 1976; Sugihara et al., 1995).

There is some suggestion that the oscillatory effects of harmaline on the olive are in fact mediated by the serotonergic pathway since chemical ablation of this input suppresses the harmaline induced tremor (Sjolund et al., 1977).

A recent study has shown that serotonergic input can strongly and transiently suppress excitatory (glutamatergic) input via an endocannabinoid-dependent pathway (Best and Regehr, 2008).

Impact of olivary firing in the cerebellum

The climbing fibre-Purkinje cell synapse is very powerful and essentially never fails. When activated, it produces a large compound response in Purkinje cells called the complex spike (Eccles et al., 1966).

The Purkinje cell also fires spikes spontaneously at high frequencies. These spikes are comparable in shape to classical Hodgkin-Huxley type action potentials and are therefore referred to as Simple Spikes. Activation of parallel fibre synapses can modify simple spike output.

The interaction between complex spikes and simple spikes has been a source of intense study. For instance, after a complex spike, the Purkinje cell stops

firing simple spikes for a period of a few tens of milliseconds. This is called the CF-pause (Bloedel and Roberts, 1971; Latham and Paul, 1970).

In vivo, it has been shown that the Purkinje cell is bistable in its firing pattern: it can switch from a quiescent downstate, to an up state where it fires simple spikes at high rates. These states can last for several hundreds of milliseconds. A study suggests that the occurrence of complex spikes can trigger transitions between these up and down states (Loewenstein et al., 2005). However, it is controversial to what extent the up and down states occur in Purkinje cells recorded from awake, unanaesthetised, animals (Schonewille et al., 2006).

Purkinje cells send their inhibitory output to cells of the deep cerebellar nuclei where complex spike causes a hyperpolarisation in these cells. Upon release, the DCN cells fire a rebound burst of spikes(Hoebeek et al., 2010). However, As I have mentioned above, olivary axons also make direct synapses unto deep cerebellar nuclei cells, and can therefore potentially also have a direct effect on DCN firing (Lang and Blenkinsop, 2011) .

There is some evidence that Climbing Fibres also interact with molecular layer interneurons in the cerebellum through spill-over transmission of glutamate binding onto AMPA and NMDA receptors (Szapiro and Barbour, 2007).

Climbing fibre dependent plasticity

Climbing fibre activity is known to mediate several forms of plasticity in the cerebellum.

Long-term depression (LTD) of parallel fibre synapses is a form of associative plasticity where repeated pairings of a climbing fibre input with parallel fibre stimulation results in the depression of PF synaptic strength(Ito, 2001). Originally predicted by Albus and Marr to provide the substrate for cerebellar learning, there has been much work on the signalling cascades underlying LTD (Crépel et al., 1996) and the relative timing of parallel fibre and climbing fibre input has been shown to affect the magnitude of the depression caused (Safo and Regehr, 2008; Wang et al., 2000).

Another form of plasticity is Climbing-Fibre LTD (Hansel and Linden, 2000), which is a depression of the climbing fibre response itself in response to repetitive stimulation.

It was also shown in slice preparations that climbing fibre activation causes long term potentiation of inhibitory synapses onto Purkinje cells (Kano et al., 1992). This phenomenon is called Rebound Potentiation, and the implication is that climbing fibre input in a certain region of cerebellum can determine its inhibitory tone, thereby affecting the excitability of the circuit.

Complex spike rhythmicity

While the oscillatory properties of olivary neurons are well established, how this is actually translated into patterns of spiking at the network level is still an issue of debate (Kitazawa and Wolpert, 2005). The main bone of contention is whether climbing fibre activity is rhythmic, and how this

relates to the behaviour of the animal. Periodically firing climbing fibres have been demonstrated in awake animals during behaviour and rest (Lang et al., 1999; Llinas and Sasaki, 1989; Welsh et al., 1995), but this periodicity varies considerably between cells, and is strongest when the behaviour itself is rhythmic. In rats, olivary neurons fire rhythmically during the step cycle (Smith, 1998), although this doesn't seem to be the case in cats (Armstrong et al., 1988). Another study in cat (Bloedel and Ebner, 1984) found that in response to touch, olivary neurons do not fire rhythmically in a single trial, but there are two to four peaks in the autocorrelograms of the PSTH over many trials, indicating there are rhythmic increases in excitability of IO neurons after a sensory input, which could be explained by the phase reset phenomenon discussed in the previous section. Importantly, studies in awake monkeys and cats (Armstrong and Rawson, 1979; Keating and Thach, 1995, 1997) deny the presence of periodic CF firing at all. A modelling study (Schweighofer et al., 2004) suggests that the firing of olivary neurons may in fact be chaotic, rather than periodic. This means the climbing fibre can encode considerable amounts of information in its interspike intervals.

It is by now clear that IO neurons are not functioning as simple pacemaker cells. An *in vivo* study blocking AMPA receptors in the olive showed that the firing rate drops by 50% (Lang, 2001), showing that the output of the olive is both synaptically and intrinsically generated. This means that other areas of the nervous system may drive the olivocerebellar system to the beat of their own drum. It has been suggested therefore that the IO acts as a resonating

circuit, preferentially transmitting input of certain frequencies from the motor cortex to the cerebellum (Lang et al., 2006b; Marshall and Lang, 2004).

Complex spike synchrony

In the cerebellar cortex, Purkinje cells within a 500 μm sagittal strip discharge complex spikes in synchrony (Bell and Kawasaki, 1972; Lang et al., 1999; Sasaki et al., 1989; Schultz et al., 2009). The synchrony has been shown to be due to a combination of electrotonic coupling between IO cells (Blenkinsop and Lang, 2006), the subthreshold oscillations themselves (Lang et al., 1997), the branching of a single olivary axon into multiple climbing fibres (Lang et al., 2006a), and shared synaptic input between neighbouring olivary neurons (Kistler et al., 2002; Wise et al., 2010).

The fact that rodents and humans with impaired gap junction function show motor learning deficits is an indication that synchronous olivary activity is important for normal cerebellar function (Van Der Giessen et al., 2008; van Essen et al., 2010). One study also found that the coordination of muscles during tremor was disrupted in rats with impaired electrotonic coupling (Placantonakis et al., 2004).

The patterns of synchrony are not fixed, but modulated during behaviour (Welsh et al., 1995). Blocking either excitatory or inhibitory synaptic input to the olive increases the synchronicity with which the cells fire action potentials (Lang, 2002). This has been posited to be due to the synaptic

shunting of intercellular current. Furthermore, since the inhibition coming from the DCN is one arm of an olivocerebellar loop, a patch of IO neurons could be regulating its own pattern of synchrony dynamically (Marshall and Lang, 2009). This had led several groups to formulate theories of the olivocerebellar system as being able to dynamically generate different spatiotemporal patterns of climbing fibre activation for the coordination of motor synergies (Jacobson et al., 2008; Llinas, 2009). The rationale for taking this olive-centric view of the system is that the climbing fibre system has a much more dramatic effect on the output of the cerebellum (via the CF pause (Davie et al., 2008), and the modulation of PCs bistability (Loewenstein et al., 2005) and rebound firing in the DCN (Hoebeek et al., 2010)) than does the PF pathway, which can only weakly modulate the intrinsic firing of Purkinje cells.

Climbing fibre coding

What is the meaning of the signal carried by the climbing fibre? Despite many years of debate, there is still no consensus on the matter (Simpson et al., 1996). Here I review some of the roles ascribed to climbing fibre coding in different systems.

Events, errors and gating

One of the most puzzling aspects of the climbing fibre pathway is the nature of the information that could possibly be transmitted at such low firing frequencies. As I have discussed, the olive certainly receives plenty of sensory input, but could not faithfully encode it completely by classical rate

coding. This observation led Olov Oscarsson to surmise that the role of the olive was to compare inputs from two pathways and only fire when the difference was large enough (Oscarsson, 1980). The inputs could for instance represent a descending cortical signal encoding a desired or predicted sensory signal, and an ascending spino-olivary signal encoding an actual signal from the periphery. A natural development of this idea is that the olive is computing an error signal between intended or desired actions and outcomes (Andersson and Armstrong, 1987; Lou and Bloedel, 1992a, b).

A related hypothesis is one that sees the IO as flagging up discrete somatosensory events. Extracellular recordings from cats have shown IO cells to respond readily to somatosensory and proprioceptive stimulation at low latencies (Gellman et al., 1983). However, the climbing fibres seem remarkably insensitive to the duration, intensity or direction of the stimulation, and respond mostly at the onset of the stimulation. This is compatible with the notion of climbing fibres as *event detectors* (Rushmer et al., 1976).

It was later found that in awake animals, the olive doesn't report all sensory events indiscriminately, but suppresses self-generated input. For instance, when the animal is walking, it receives strong sensory input from its paws when stepping onto a surface. This input will not generate climbing fibre signals, but providing an unexpected input to the same paw (either by touch or by lowering a rung on which the animal was going to step) leads to robust olivary responses (Andersson and Armstrong, 1987; Apps et al., 1997; Devor, 2002; Gellman et al., 1985; Lidierth and Apps, 1990). This has led to the theory that the olive is a gate (Devor, 2002), only allowing unexpected events

through. Importantly, the suppression of inputs is not generated within the olive itself, but seems to be mediated by inhibition from external nuclei (Weiss et al., 1990). It should be noted that the idea that olivary cells respond to unexpected events is not completely at odds with the notion discussed above that climbing fibres transmit error signals.

It is likely that climbing fibre signalling does not fit neatly into one single paradigm. For example, an important study in monkeys (Kitazawa et al., 1998) using a reach-to-target task found that complex spikes encode information in two phases: early after task initiation, the climbing fibre signals information about the destination where the monkey reaches, whereas later in the task it is more likely to fire if the monkey has made an error in reaching for its target.

Role of the inferior olive in ocular motion

The inferior olive is implicated in the control of the oculomotor system (Barmack, 2006). Its role has been studied extensively in two behaviours which have provided an important paradigm for understanding the role of climbing fibres. : the vestibulo-ocular reflex (VOR) and the optokinetic reflex (OKR).

 The VOR denotes involuntary eye movements produced by the brain to compensate for head rotation. In physiological conditions, the VOR will stabilize visual input by responding to a head rotation in a given direction with eyes movements in the opposite direction. The optokinetic reflex (OKR),

on the other hand, allows the eyes to smoothly track a moving target in the visual scene when the head remains fixed.

It is known that the flocculo-nodular cerebellum, which receives input from the dorsal cap of Kooy of the inferior olive, is crucial for these behaviours (Simpson et al., 1996). The dorsal cap of Kooy of the olive is very sensitive to optokinetic stimulation and seems to encode a low velocity retinal slip signal (Barmack and Simpson, 1980), which is essential to modifying the gain of the eye movements. Note that this slip signal can be well interpreted in terms an error signal, as described above. Many studies have exploited this by independently manipulating the visual and vestibular stimulation the animal receives, because this will require adaptation of the ocular movements, for which plasticity in the cerebellum is essential (see for instance (Schonewille et al., 2011)). Intriguingly, during sinusoidal head rotations, the parallel fibres and climbing fibres of the flocculus tend to fire in anti-phase (Barmack and Yakhnitsa, 2011a; De Zeeuw et al., 1995b). This had led to the idea that the role of the climbing fibre is to cause simple spikes to occur in anticorrelation to events that cause the climbing fibre to fire (Dean et al., 2002). There is recent evidence that the cells of the dorsal cap of Kooy have different electrophysiological properties to the rest of the IO, raising the distinct possibility that the computation carried out by this circuit is distinct from the rest of the cerebellum (Urbano et al., 2006).

Role of the inferior olive in conditioned response learning

Another behaviour in which the contribution of the inferior olive has been well characterized is Pavlovian associative learning; and in particular, eyeblink conditioning. In this paradigm, a conditioned stimulus (CS) which causes the animal to close its eyelid (such as an airpuff to the periocular region), is paired with an unconditioned stimulus (US) such as a tone. After several such pairings, a presentation of the US alone will cause the eyeblink response in the animal. When, after learning, the US is presented several times without co-occurrence of the CS, the response to the US will extinguish. There is good evidence to suggest that the US is carried by the climbing fibres, and the CS travels via the mossy fibre pathway (Hesslow and Ivarsson, 1996; Mauk et al., 1986; Sears and Steinmetz, 1991). Furthermore, it has been shown that inhibition from the DCN to the IO plays a crucial role in suppressing climbing fibre spiking during trials where a conditioned response is evoked by a US, and that blocking this inhibition prevents extinction of the response (Medina et al., 2002) .

Abstract models of cerebellar function and the olive

Marr-Albus theory

In 1969, taking inspiration from the rapid advances being made in cerebellar physiology (Eccles et al., 1967), David Marr published an influential theoretical model of the function of the cerebellar cortex (Marr, 1969). In summary, the theory postulates that each Purkinje cell learns to respond to certain patterns of activation of its parallel fibre inputs when those patterns

co-occur with climbing fibre input by modification of PF synapse strength. In other words, the CF is the teacher signal in a form of associative plasticity.

Marr predicted that the parallel fibre input would be potentiated, whereas James Albus advanced a similar theoretical analysis of the cerebellum which (correctly) predicted a depression of synaptic strength (Albus, 1971). The role of the granule cell layer is to provide an overcomplete (or "sparse") representation of the sensory input, which provides the Purkinje with a rich palette of associations to learn.

In Marr's original paper, he saw the IO neurons as either relaying a simple motor command from motor cortex (in his words an "elemental movement" from which more complex motions are built up), or signalling a sensory event from the periphery. While there is considerable support for the latter (see above), the former view is contradicted by the fact that microstimulation of olivary neurons does not cause movement (Gellman et al., 1983).

It was considered a vindication of Marr's model when long-term depression (LTD) of parallel fibre input by climbing fibre activation was discovered (Ekerot and Kano, 1985; Ito, 2001; Ito et al., 1982). However, whether LTD is really the substrate for motor learning is still hotly debated. Several studies have shown no impairment in learning when LTD is blocked either pharmacologically or genetically (Schonewille et al., 2011; Welsh et al., 2005b). There is increasing evidence that there are many loci for neuronal plasticity in the cerebellum, and that the precise plasticity mechanism engaged in the cerebellar circuit depends on the nature of the specific memory being acquired. (Boyden et al., 2006; Boyden et al., 2004)

Modern learning theories

There are many modern variants of Marr and Albus' original idea (Houk et al., 1996). Several of these for models are based on concepts from control theory. For instance, (Kawato and Gomi, 1992) see the cerebellum as implementing an inverse kinematics controller, such that the cerebellum learns to output the correct motor command for a desired outcome. A contrasting model sees the cerebellum as learning a forward model of the sensory consequences of motor action (Miall et al., 1993).

Another popular family of models is based on adaptive filter theory. In these theories, the main role of the cerebellum is gain modulation (Ebner and Bloedel, 1981). The learning rule of the cerebellum is thought to be covariance based, so that parallel fibres gradually learn to be active when the climbing fibre is not. The climbing fibres still provide the learning signal for changing the gain, however the importance of LTD is de-emphasized, and the (controversial) climbing fibre mediated plasticity of interneuron responses is thought to be more important (Dean and Porrill, 2008, 2010, 2011; Dean et al., 2002).

The olivocerebellar system as a spatiotemporal pattern generator

Because climbing fibres have such a widespread impact on firing patterns in the cerebellum, an olive-centric view of the olivocerebellar system has gained prominence (Jacobson et al., 2009; Llinas, 2009; Welsh et al., 1995). In this perspective, the function of the cerebellum is to generate specific spatiotemporal patterns of activity for coordinating motor output (De Zeeuw

et al., 2011). The role of parallel fibre input is minimal, since it can at most weakly affect Purkinje cell firing (which intrinsically fire simple spikes at high rates regardless of parallel fibre input), and the spatiotemporal patterns in the cerebellum are therefore mainly created by climbing fibres (Barmack and Yakhnitsa, 2011b).

There is not yet a standard version of this theory, but the common thread is that subthreshold oscillations are the main determinant of olivary firing. In the early versions of this theory, the inferior olive was thought to deliver a simple clock signal at the peak of subthreshold oscillations (Llinas et al., 1997; Llinas and Welsh, 1993), however the existence of such a regular climbing fibre signal is strongly disputed (Keating and Thach, 1995, 1997; Kitazawa and Wolpert, 2005). Modern theories are more sophisticated: the oscillations themselves are controlled and synchronised by the synaptic input to the olive, part of which comes from one limb of the olivocerebellar loop, and therefore climbing fibre spiking is only rhythmic during sustained periods of oscillations (Chorev et al., 2007). Phase differences in the oscillations between neighbouring neurons could allow for patterns of activation more interesting than simple synchrony between olivary neurons (Devor and Yarom, 2002c; Jacobson et al., 2009).

How a specific oscillatory pattern is "loaded" into the olivocerebellar system is the least worked-out aspect of the theory, with suggestions that this role could be carried out the PF input (Jacobson et al., 2009), or by the phase reset of the subthreshold oscillation (Llinas, 2009) by strong synaptic input into the inferior olive.

Pathology of the Inferior Olive

Damage to the dentatorubral-olivary pathway (otherwise known as the Guillain-Mollaret triangle) causes a secondary degeneration of the olivary nucleus. While this kind of trans-synaptic degeneration is common in the nervous system, the olive is unique in that it enlarges rather than atrophies. This process is called Olivary Hypertrophic Degeneration (Ruigrok et al., 1990b) and is used clinically as radiological evidence (Kitajima et al., 1994) for damage to the aforementioned pathway.

The spinocerebellar ataxias are a large family of genetic neurodegenerative diseases that cause varied symptoms of motor dysfunction. Many of the subtypes cause degeneration of the inferior olive (Koeppen, 2005). Other neurodegenerative diseases where there is evidence for olivary involvement include olivopontocerebellar atrophy (Berciano et al., 2006), Leigh's disease (Cavanagh, 1994).

Autopsies from patients with autism suggest that the inferior olive is implicated in this disorder, which has led to the theory that desynchronisation of neural responses in the olivocerebellar system and elsewhere could cause some of the pathology (Bauman and Kemper, 2005; Welsh et al., 2005a)

Since the discovery of harmaline induced tremor, which is dependent on the inferior olive, there have been attempts to implicate the nucleus in other tremors (Loewenstein, 2002). Essential tremor is a progressive neurological disorder which is characterized by a tremor in 4-12 Hz frequency range. PET studies have implicated episodes of tremor with increased olivary

metabolism (Elble, 1996). The olive also appears to be involved in oculopalatal tremor (which can arise as a symptom of olivary hypertrophic degeneration) (Chang et al., 1993; Kim et al., 2007; Yokota et al., 1989). Recently, a study into alcohol abuse conducted with monkeys found that olivary neurons in subjects that had been subjected to months of daily alcohol administration significantly increased the rebound currents (Ih and the low threshold calcium current) involved in oscillations(Welsh et al., 2011). Since the rebound currents have been found to be essential for harmaline-induced tremor (Park et al., 2010), the ethanol induced plasticity of olivary responses could underlie the withdrawal tremor that appears after chronic alcohol abuse.

Conclusion

We have reviewed the anatomy and physiology of the inferior olive and placed them in a functional context. We have discussed the leading theories of the code carried by the climbing fibres and their role in motor coordination and learning within the olivocerebellar network. While much progress has been made over the last century, there is still no consensus on the computation carried out by this remarkable structure.

Chapter 2: Axonal bursts in olivary neurons

Introduction

It has long been understood that the ultimate output of a neuron – that is, the packets of neurotransmitter it releases onto its postsynaptic partners – is determined by the action potentials arriving at the neuron's axonal boutons. It is rare, however, for experimentalists to actually record action potentials at the level of the axon. Instead, spikes are usually measured at the soma, and this is assumed to track neuronal output. In general, this causes no special difficulties, because somatic waveforms are not ambiguous with regard to the occurrence of action potentials, and axons are extremely reliable channels of communication.

There are, however, some classes of neurons where the voltage deflections at the soma are quite complex, and may not be easily interpreted in terms of spikes propagating down the axon (Khaliq and Raman, 2005; Monsivais et al., 2005). The neurons of the inferior olive exhibit such a complex somatic waveform: Upon depolarisation, the neuron fires a fast spike followed by a short (10 ms) afterdepolarisation (ADP), followed by a long (100ms) afterhyperpolarisation (AHP). In this chapter, I will describe recordings from olivary axons to directly characterize how this sequence is translated into axonal output, and further explore the impact of olivary spiking on plasticity in the cerebellum.

Results

Simultaneous paired recordings from somata and axons of inferior olive neurons reveal a burst response

Whole-cell patch recordings of somata of inferior olive neurons were obtained under infrared oblique illumination. The identity of the neurons was confirmed by their characteristic electrophysiology. The intracellular solution contained AlexaFluor 488, and several minutes were allowed for the dye to diffuse. The fluorescent dye emission image was overlaid on top the infrared image, and this allowed the visualization of the morphology of the neuron. A loose-seal recording was made on the cut end ("bleb") of the neuron's axon with a second electrode containing external solution, at distances up to 275 μm.

Both upon depolarisation by current injection and synaptic stimulation, olivary neurons fired in a characteristic pattern: at the soma, a fast sodium spike was followed by an after-depolarisation (ADP) and an after-hyperpolarisation (AHP). On top of the ADP, one to six wavelets of small amplitude (<10 mV) were superimposed (Figure 7B-C). In the axonal recording, the wavelets were mirrored by action potentials that were similar or identical to the action potential mirroring the primary sodium spike. In other words, the neurons fired short bursts (on average 2.2 ± 0.16 spikes, range 1–6 spikes, at an instantaneous frequency of 273 ± 9 Hz, range 127–476 Hz; n = 23 cells).

Upon release from hyperpolarisation, the neurons fired a low-threshold spike that could be accompanied by a fast spike in the soma. Only when this somatic fast spike was present was there also an axonal spike (Figure 7D).
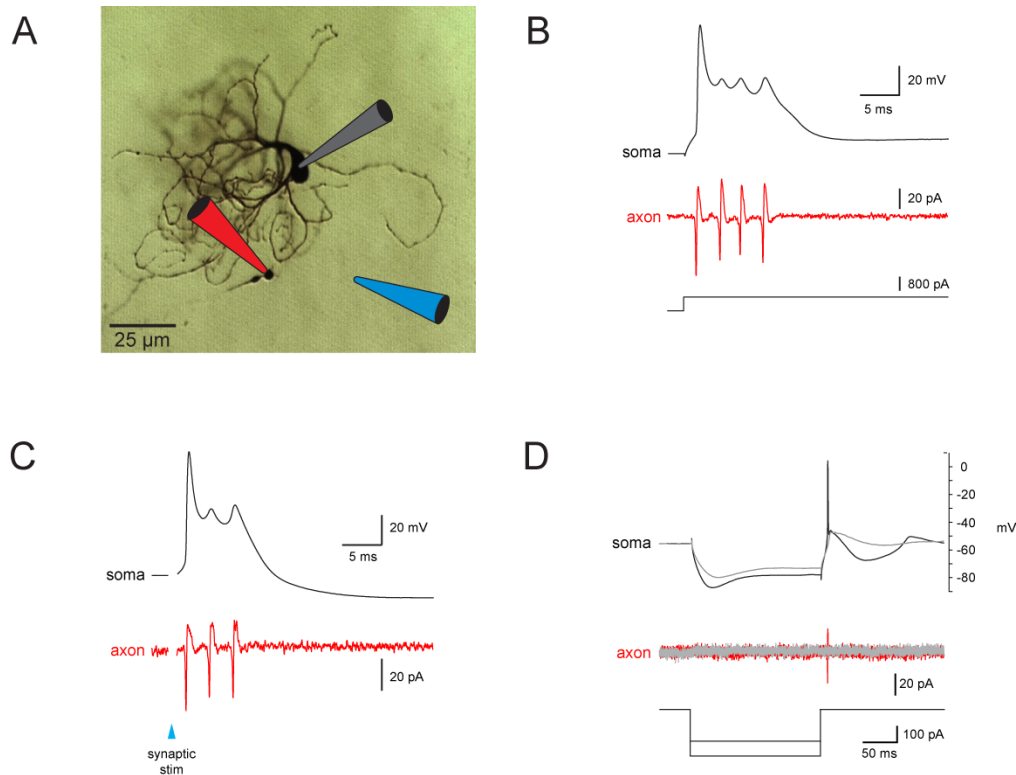
Figure 7 Axonal recordings from olivary neurons reveal burst responses. A: recording configuration B: Somatic and axonal responses to current injection (black and red trace). Three somatic wavelets are translated in to axonal spikes. C: response to synaptic stimulation D: release of hyperpolarisation causes a low threshold calcium spike with (black/red traces) or without (grey traces) an axonal spike.

Bursts are generated in olivary axons

Neurons from which axonal recordings were obtained were filled with 0.5% biocytin, which allowed reconstruction of the axonal morphology. There was no correlation between axon length and the input resistance of the cell

(mean 97 ± 7.5 MΩ; r = −0.088, p > 0.05), suggesting the excitability of the cells was left relatively intact. In axons shorter than 50 μm, however, cells generally didn't fire additional spikes beyond the primary spike, which was clearly present in axon and soma (n=6 out of 8 cells). The number of axonal spikes fired in a burst increased with the length of the axon remaining after slicing, with reliable bursting occurring only in axons longer than 100 μm (Figure 9A-B). It was also found that for short axons, the secondary spikes tended to be smaller than the primary spike, but that in long axons, the secondary spikes were the size of the primary spike (Figure 9C). The fact that the integrity of the bursts depended on the presence of a certain length of axon suggested an axonal locus of burst generation.

An estimate of the delay between axonal and somatic signals was obtained by measuring the temporal difference between the occurrence of the peaks of the axonal spike and the first time derivative of the somatic voltage (Figure 8). For the primary and secondary spikes, negative delays were obtained for axons shorter than 100 μm, confirming that they are generated in the proximal axon (Figure 9D).
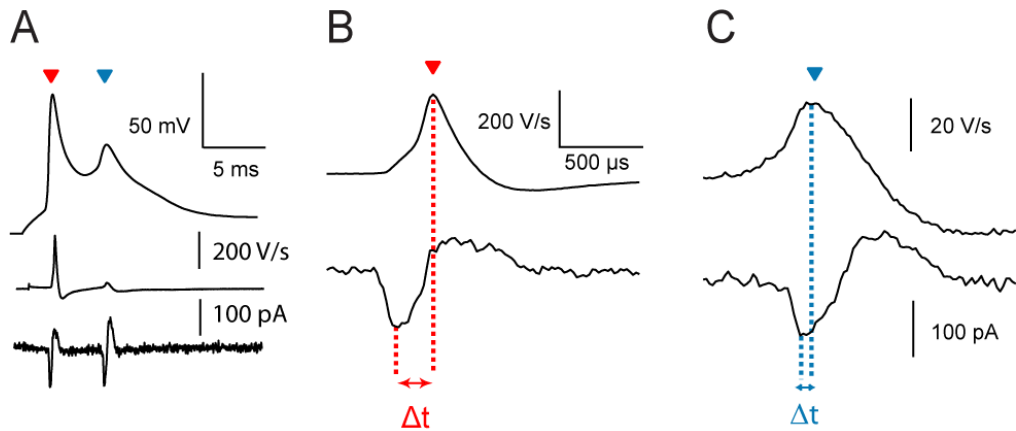
Figure 8 Measuring propagation delays. A) Top trace: somatic recording showing a primary spike and one wavelet. Middle trace: dV/dt of this trace. Bottom trace: corresponding axonal spikes. Delays were calculated between the peak of the dV/dt and the axonal spike (magnified for primary spike and wavelet in B and C).
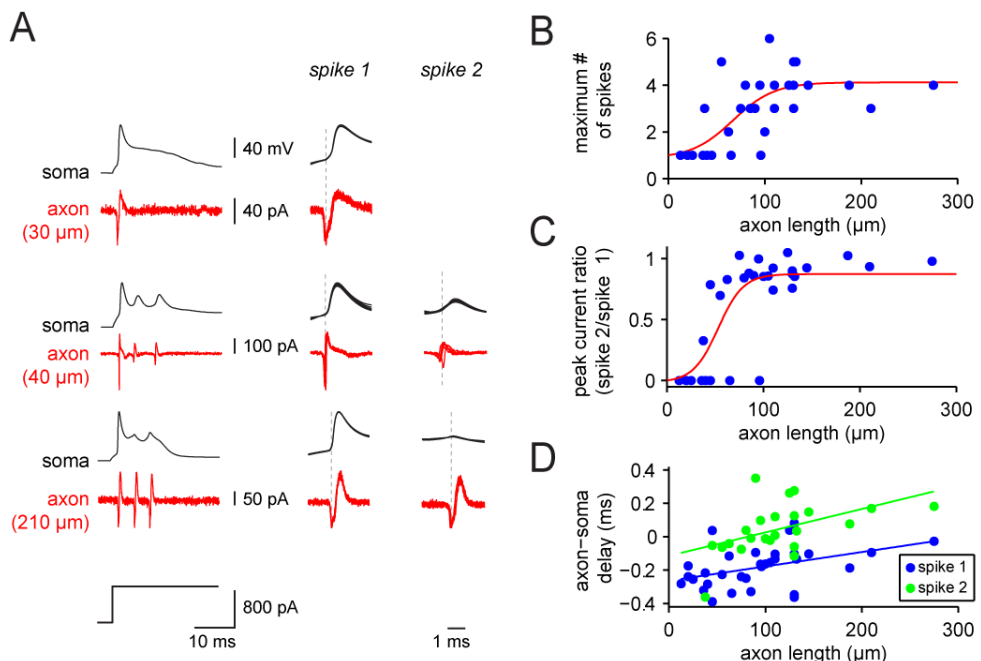
Figure 9 Axonal initiation of bursts. A) Recordings of olivary responses taken from three cells with different lengths of spared axons. The middle and right column show five superimposed traces of the first and second spikes at slower sweep speed. B) Maximum number of spikes in burst response as a function of length of axon spared. C) Ratio of the amplitude of the second spike to the first spike as recorded in the axon. D) Axon-soma delay of first and second spike as a function of axon length (n=23 cells).

Whole-cell recordings from olivary axons

Olivary axons are myelinated, with the sheath starting approximately 50 μm away from the soma (de Zeeuw et al., 1990c). I was unable to obtain whole cell recordings in myelinated blebs, but in shorter axons (<60 μm), the blebs were unmyelinated and it was possible to gain whole-cell access. In agreement with the loose seal recordings detailed above, these short axons did not display secondary spikes (since they lack the site for secondary spike initiation), but did provide some insight into the integrative properties of olivary neurons (Figure 10).

Firstly, the primary spike was still present. It was bigger and occurred earlier in the axon (n=5), indicating an axonal locus for its initiation. The ADP was subject to a strong attenuation, while the AHP was relatively spared (Figure 10B). The IO neurons exhibited subthreshold oscillations (STOs) that were only mildly attenuated by the axon (Figure 10C). This is likely to be due to their low frequency (1-10 Hz), so that they escape the low-pass filtering of the axonal cable. This evidence is consistent with a somatodendritic locus for the generation of the ADP, AHP and STOs, with spikes being generated in the axon.
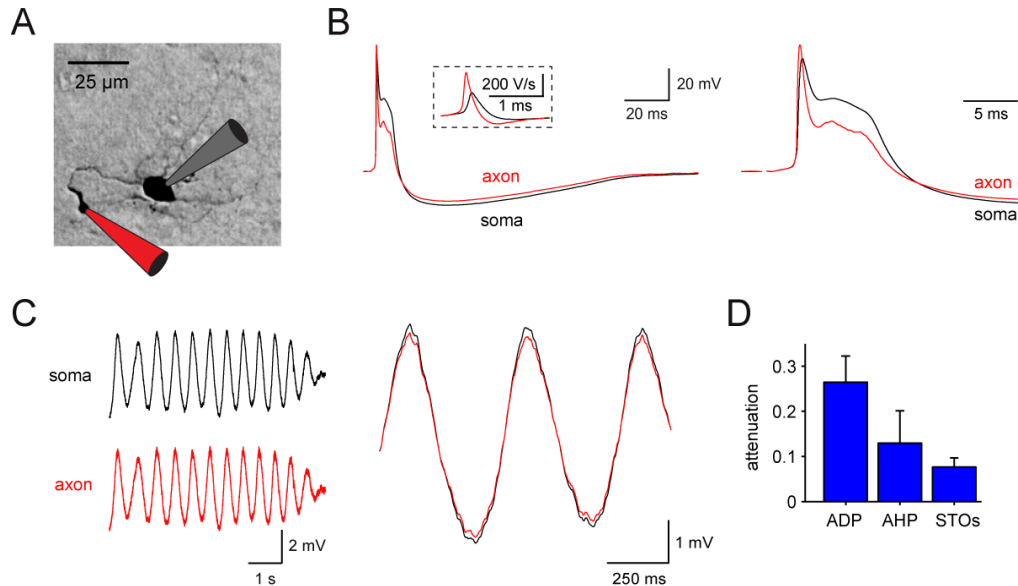
Figure 10 Whole-cell recordings from axons of olivary neurons. A) Biocytin fill of an olivary neuron. A whole cell recording was obtained from the terminal bleb. B) Overlaid trace of somatic and axon trace at slow and fast sweep speed (left and right respectively) during olivary spike evoked by synaptic stimulation. Inset: dv/dt of the traces shows spike occurs in the axon first. C) Subthreshold oscillation recorded in the soma and axon. Overlay on the right showing mild attenuation. D) Attenuation of the afterdepolarisation, afterhyperpolarisation and subthreshold oscillations (n=5 cells)

Imperfect transmission of bursts

In general, axonal spikes and somatic wavelets perfectly mirrored one another. However, in 7 out of 10 recordings from cells with longer axons (>125 μm), somatic wavelets were occasionally seen without an axonal counterpart. Since the wavelets were present at the soma, I interpreted this as failed axonal propagation of a spike generated in a part of the axon more proximal than the site of recording (Figure 11).

When an axonal spike was present, it was without exception reflected by a somatic wavelet. This indicates that back-propagation from the axonal initiation site to the soma is probably perfect, presumably because it occurs

mainly passively. For each spike in a burst, I assessed the reliability of propagation. I found that the primary spike always propagated, while the second, third, fourth, and fifth spikes in the burst exhibited propagation probabilities of 0.85 ± 0.03, 0.82 ± 0.04, and 0.66 ± 0.09, and 0.89 ± 0.10, respectively (Figure 11B), indicating that propagation is relatively reliable—despite occasional failures—across the burst.

The timing of the spikes was very stable between trials, with low coefficient of variations (CV) for the inter-spike intervals (ISIs) (0.12 ± 0.02, 0.20 ± 0.03, 0.18 ± 0.06 for the first, second and third ISI respectively (n=23)). The temporal spiking pattern is therefore highly stereotyped for a burst, with just the number of spikes varying between trials.
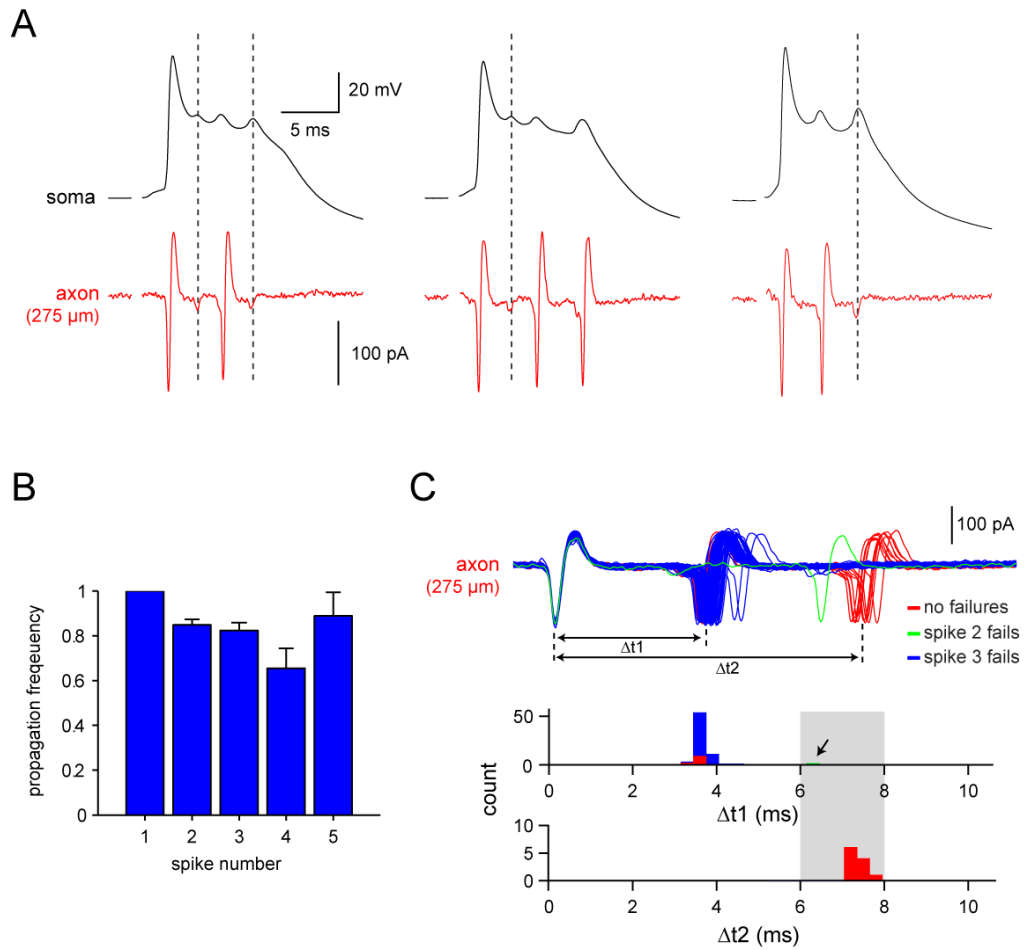
Figure 11 Olivary bursts are subject to occasional failures of propagation. A) Sample traces showing propagation failures of all but the primary spike with synaptically evoked bursts. B) Frequency with which each spike in the burst propagated as a function of the order it occurred in the burst. (n=10 cells) C) Overlay of 50 traces from an axon where bursts were evoked synaptically. Bottom: histogram of the two ISIs in the bursts. The arrow points to cases when the second spike failed, and thus resulted in a large ISI.

Bursts are modulated by subthreshold oscillations

The subthreshold membrane potential oscillations exhibited by olivary neurons range from 1 to 10 Hz in frequency and from 1 to 20 mV in amplitude (Llinas and Yarom, 1986). To determine if oscillations can modulate synaptically triggered axonal bursts, I mimicked subthreshold oscillations by injecting a sinusoidal current into the soma, with a frequency

of 5 Hz and producing a mean peak-to-peak amplitude of 9.6 ± 0.6 mV. Spikes were initiated by EPSPs activated by synaptic stimulation timed at different phases of the oscillation (n = 14 cells). The number of spikes in the axonal burst was modulated in phase with the oscillation (Figure 12). For the example shown in Figure 12A, the mean number of spikes triggered by synaptic stimulation in the absence of oscillations was 2.07 ± 0.03, with a low coefficient of variation (CV) of 0.17. During oscillations, synaptic input triggered from zero to three spikes (mean 2.40 ± 0.17, coefficient of variation 0.49), with the number of spikes depending on the timing of the EPSP relative to oscillatory phase. This indicates that the phase of the oscillation can modulate the output of olivary neurons (Figure 12B). I used the CircStat circular statistics toolbox for Matlab (Berens, 2009) to determine whether this modulation was significant, I used the Rayleigh test for non-uniformity, using the number of spikes at each of the 10 phases as the weight factor. I found that there was a highly significant deviation from uniformity (P=6.9x10^{-13}, 60 trials per phase across 14 cells).

In olivary neurons that exhibited spontaneous oscillations (Figure 13), I investigated whether the spike output was affected by the phase of the oscillation. The mean oscillation frequency was 5.6 ± 0.65 Hz (n = 7 cells) and the peak-to-peak amplitude was 6.6 ± 0.94 mV. Because synaptic stimulation abolishes oscillations in olivary slice preparations (Lampl and Yarom, 1993), I injected short current pulses (2 ms; 300–1800 pA) at different phases of the oscillation (Figure 13B) to trigger spikes and characterized the axonal spike output by counting the number of wavelets on the ADP. Confirming my results with injected oscillations, I found that the spike output varied with

the phase of the oscillation (Figure 13C). As above, I used the Rayleigh test for non-uniformity, this time using 6 bins for the phases, and again using the number of spikes in the response as the weight factor. As with the injected oscillations, the modulation was found to be significantly deviating from uniformity (P=2.2x10^{-3}, 2440 trials across the 7 cells).
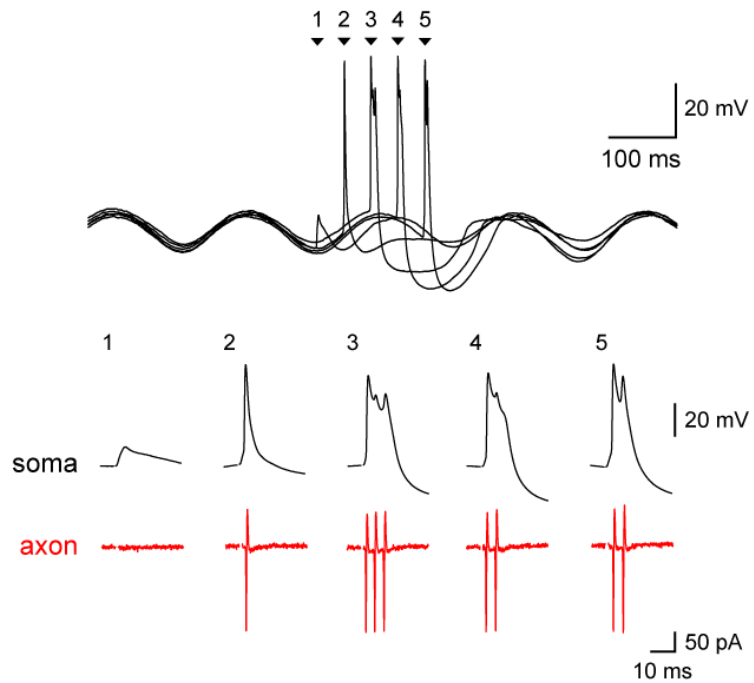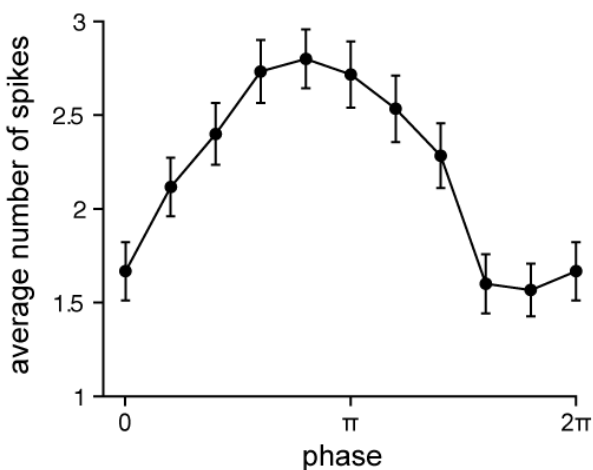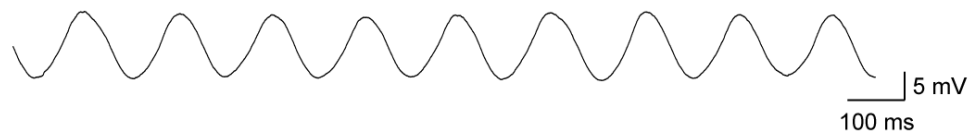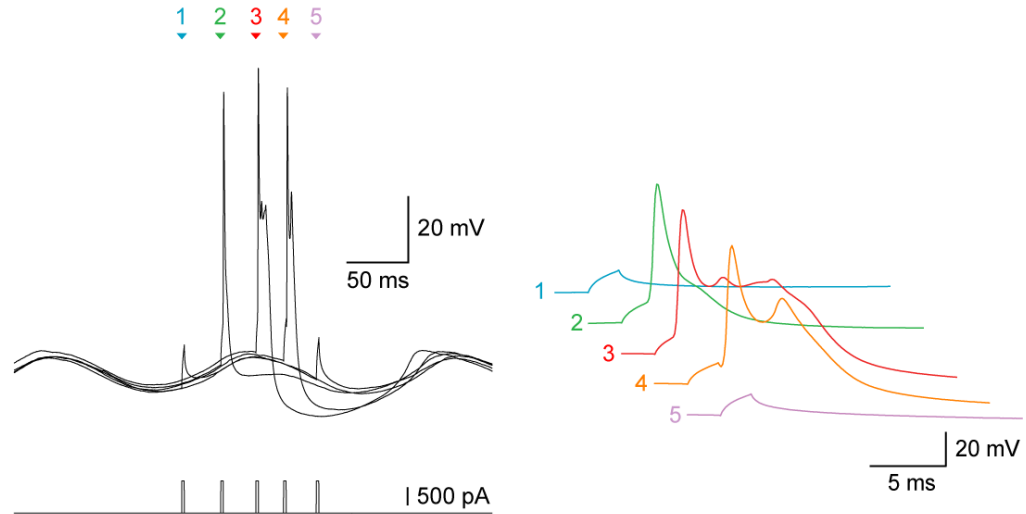
A

B

Figure 12 Modulation of bursts by injected STOs. A) An oscillation was injected into the cell and a response evoked at different phases of the oscillation. The number of spikes in the burst was found to be higher at the crest of the oscillation. The top trace shows an overlay of 5 phases. Lower traces: somatic and axonal responses at the different phases. B) Population data (n=14 cells).

A

B

C
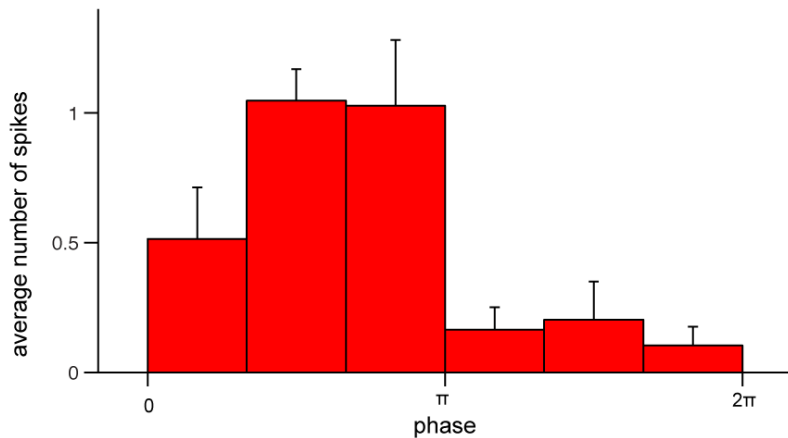
Figure 13 Modulation of bursts by spontaneous STOs. A) Spontaneous voltage oscillation in an olivary neuron. B) Current pulses (2ms) were injected at different phases of the oscillation. Left: overlay of 5 phases. Right: somatic responses at the different phases. C) The number of spikes in the response varies with the phase (n=7 cells).

Burst length is determined by calcium dependent currents

I obtained somatic recordings from cells where the intracellular solution contained 10 mM of the calcium ion chelator BAPTA. In these cells, the

duration of the ADP was considerably prolonged (mean 37.8±10.9 ms, range 28-60 for synaptic stimulation, N=3 cells), and the number of wavelets increased (mean 6.6±0.89 spikes, range 4-8) (Figure 14). Such long-lasting bursts were never seen with normal internal solution (mean duration: 9.97±0.84 ms, N=23 cells). This is consistent with the termination of the ADP being principally determined by calcium-dependent potassium channels. Therefore, we hypothesize that intracellular calcium accumulation will tend to shorten the burst response from olivary neurons.

A

B
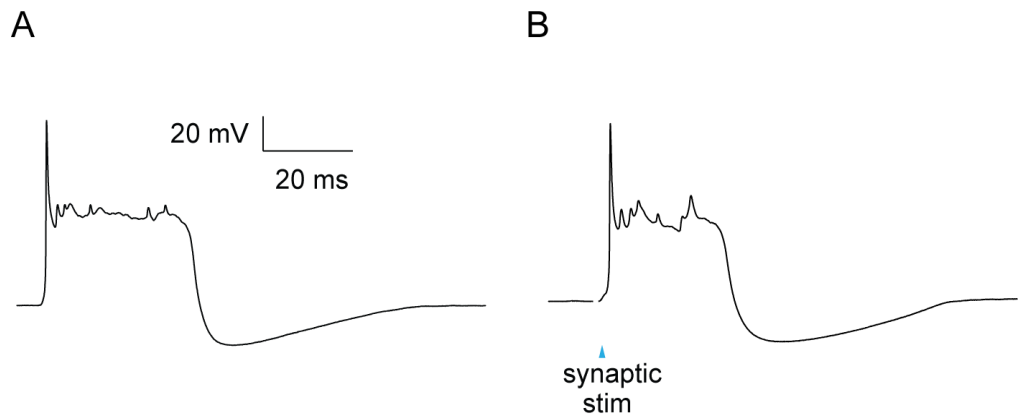
Figure 14 Calcium dependence of bursting. Spontaneous (A) and synaptically evoked (B) spikes in somatic recordings with 10 mM BAPTA in the internal solution. Note that the ADP is dramatically lengthened and the number of spikelets increases compared with spikes obtained with normal internal solution.

Paired pulse depression of burst response

In three cells, I examined the interaction between two subsequent spikes evoked by two current pulses separated by varying delays. I found that at short delays, the second ADP was shorter and therefore the second burst was smaller than the first (Figure 15). The mechanism for this paired pulse depression is obviously intrinsic, and not synaptic, since in my experiments I evoked it with current injection. Rather, it is likely to be due to a combination

of calcium accumulation shortening the ADP (as detailed in the previous section) and the second spike falling within the AHP of the first spike and therefore having to combat the hyperpolarizing potassium current.
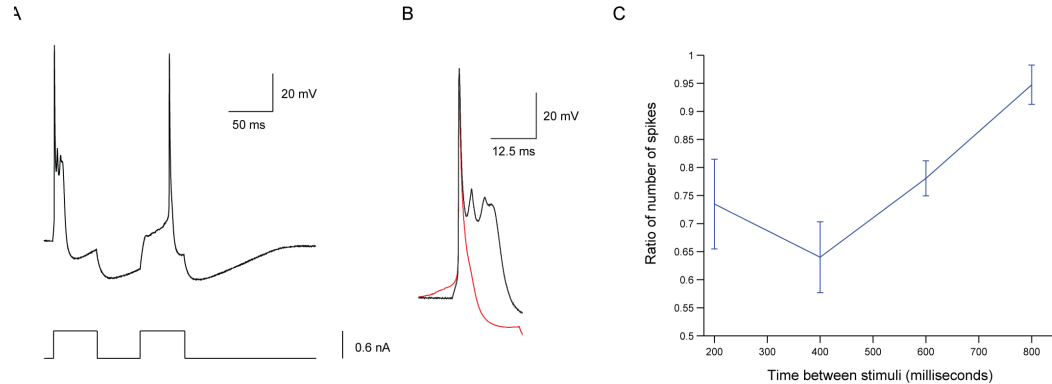
Figure 15 Paired pulse depression of burst response. A) Two current pulses are delivered to a cell. Note that the ADP in response to the first pulse is considerably larger than the second. B) Overlay of the two responses (first spike in black, second spike in red) C) Ratio of the number of spikelets in the first burst to the second burst as a function of the time between the current pulses (n=3 cells).

Bursts back-propagate into the olivary dendritic tree

The original pioneering investigations into the electrophysiological properties of olivary neurons posited that the ADP was dendritically generated by calcium channels (Llinas and Yarom, 1981b). This was based on recordings of field potentials during olivary spiking.
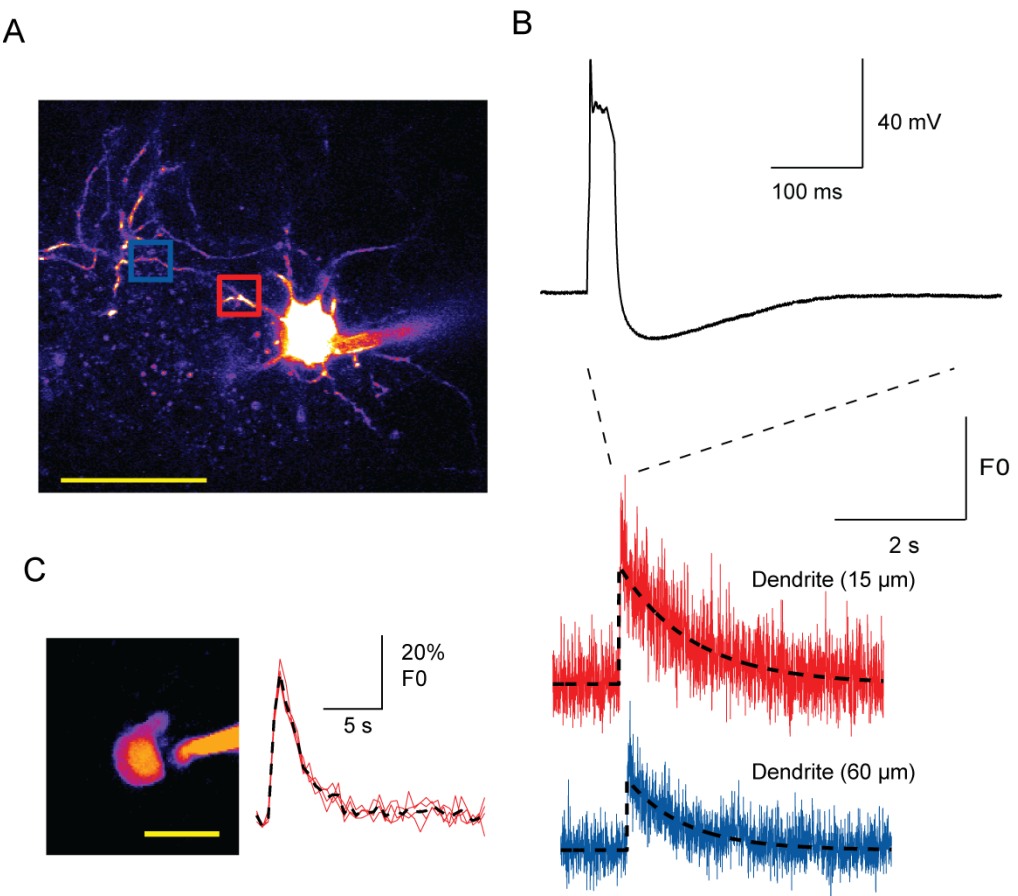
Figure 16 Two-photon imaging of calcium transients in olivary neurons. A) Maximum intensity projection of a neuron filled with 200 μM Oregon-Green BAPTA1. Scale bar 50μm. B) Calcium transients at two dendritic locations (middle and bottom – overlay of 5 traces, and exponential fit - black dashed trace) in the dendrite during single olivary bursts triggered by current injection (800 pA). C) Somatic transients: Single z-plane from another neuron (left, scale bar: 20μm.) The soma was selected as a region of interest in a frame scan, and showed large calcium transients during single olivary spikes (overlay of 3 traces, average is shown in dashed black trace).

I decided to use more direct techniques to determine the dendritic spread of olivary signals. With two-photon microscopy of cells loaded with 200μM Oregon Green BAPTA1, I imaged calcium transients during olivary spikes evoked by current injection. A single olivary spike produced large calcium transients visible during single trials in the dendrites (peak $\Delta F/F0=1.08\pm0.43$, decay time constant 825 ± 290 ms, n=3 cells, line scans performed at 10-200 μm from the soma) (Figure 16B). Interestingly, large

and fast calcium transients were also seen at the soma (Figure 16C). (peak $\Delta F/F0=0.29\pm0.08$, n=3 cells, ROI containing soma from frame scan). It is quite likely therefore that a mix of somatic and dendritic calcium channels are involved in the generation of the ADP.

A compartmental model for burst generation

To synthesize my findings, I extended an existing compartment model of olivary neurons (Schweighofer et al., 2004; Schweighofer et al., 1999). The original model has somatic and dendritic compartments with active channels and produces a somatically initiated spike with the ADP-AHP sequence when depolarized. The dendrites contain high-threshold calcium and calcium activated potassium channels, while the soma contains sodium, potassium, I_h, and low-threshold calcium channels. I kept the dendritic and somatic compartments of the model intact, and I added an axonal compartment (Figure 17A). When no channels are added to this compartment, the ADP is mildly attenuated (Figure 17B). Finally, I added axonal sodium and potassium channels to the axon (see methods chapter for their specification). This causes axonal bursts remarkably similar to the ones recorded experimentally (Figure 17B). The axonal spikes are displayed as somatic wavelets on top of the ADP, just as in my electrophysiological recordings.
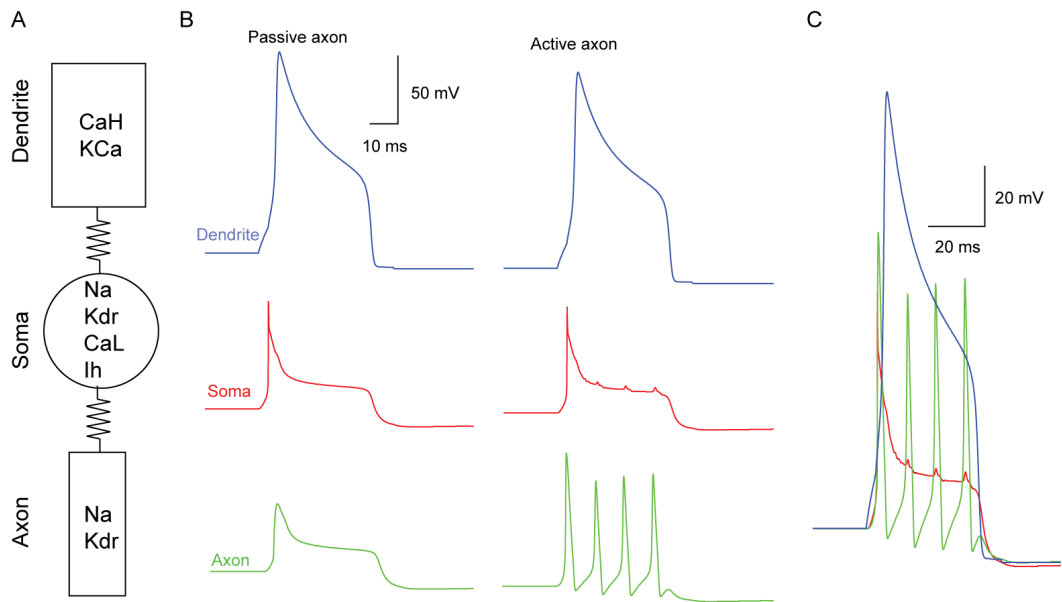
Figure 17 A compartment model reproduces olivary bursting. A) Three compartments are linked by resistances. The axonal compartment has sodium and potassium channels. A 50ms square current pulse (8 μA/cm²) is injected into the dendrite and causes a complex response in all three compartments B) When axonal sodium and potassium channels are turned off, an attenuated ADP is visible in the axon (left column). When the channels are on, the axon bursts, with small wavelets visible in the soma (right column) C) active axon with all three traces overlaid.

I found that the magnitude of the resistance linking the soma and axon was crucial in determining the burst pattern (Figure 18). At high axosomatic resistance (or low conductance), the axon is effectively autonomous and fires spontaneously (Figure 18A). At intermediate resistances, the axon fires only during the ADP (Figure 18B and C). Intriguingly it is possible to encounter resistances in this range where wavelets are absent in the soma despite axonal bursting (Figure 18B).

When the resistance is low, the flow of depolarizing current during the ADP is such as to inactivate sodium channels in the axon (Figure 18D) and prevent repetitive firing.

A limitation of the model is that the ADP widths and burst patterns are fixed in size, and it cannot therefore reproduce the modulations of burst size I saw in my experiments.
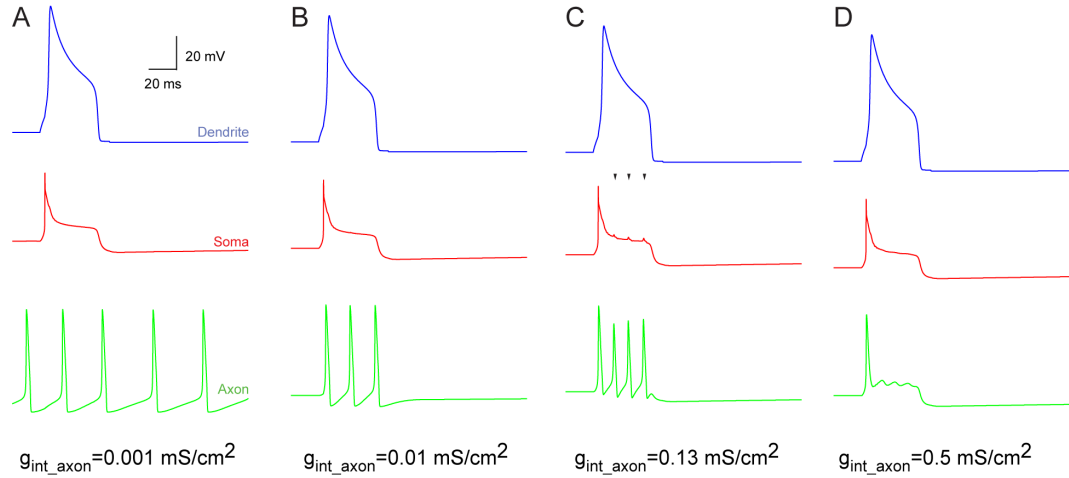
Figure 18 Effect of varying the axo-somatic conductance on burst generation. A) When the conductance between the soma and the axon is low, the axon is effectively decoupled and fires autonomously. B) Increasing the conductance causes the axon to fire a three-burst restricted to the period of dendritic depolarisation. C) A further increase leads to one more axonal spike and the appearance or somatic wavelets. D) At very high conductances, the depolarisation of the axon during the ADP plateau causes inactivation of axon sodium channels and the abolition of the burst.

Bursty synaptic input can be transmitted by the CF-Purkinje cell synapse

The CF-PC cell synapse is depressing (Dittman and Regehr, 1998), which raises the question whether it can still effectively transmit information at the high frequencies I have recorded for the climbing fibre spikes. Unfortunately, the studies of paired pulse depression of the climbing fibre synapse have used time intervals much larger than the typical intra-burst ISI (Silver et al., 1998). I obtained voltage-clamp recordings from 3 Purkinje cells to study transmission in this range. To permit clamping of the CF evoked synaptic currents added 5mM QX-314 to my internal solution. I used a regular burst of 5 stimulations with ISIs between 2 and 5 ms. While the synapse depressed,

the depression stabilized for >2 stimuli, and the aggregate synaptic charge transfer was significantly larger for a burst than for a single stimulus (Figure 19B). This shows that the CF synapse is able to convey high-frequency olivary bursts.

Corroborating this evidence, Sara Ho, from my lab, obtained *in vivo* voltage clamp recordings from Purkinje cells in anaesthetised rats with a QX-314 based internal solution and found bursts of EPSCs (See (Figure 19A), and refer to (Mathy et al., 2009) for the full account)
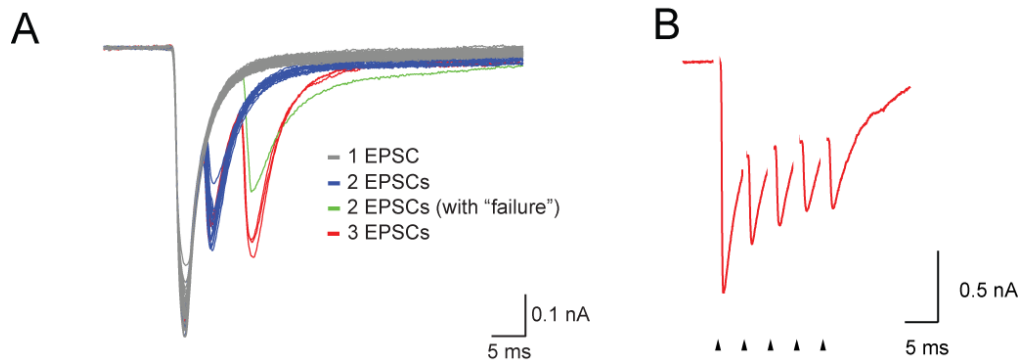
Figure 19 Climbing fibre burst transmission to Purkinje cells. A) *In vivo* **recording from Purkinje cell (courtesy of S. Ho) shows multi-peaked EPSCs (note the occasional failures of propagation) B) This can be reproduced with repetitive stimulation of CF input in slice recordings from Purkinje cells with 5 mM QX-314 in the internal solution (arrows denote synaptic stimulation).**

Bursts affect short-term plasticity in the cerebellum

Pairing a short burst of PF stimuli with CF input can transiently and selectively depress the PF synapses, a form of associative short-term plasticity known as synaptically evoked suppression of excitatory synapses (SSE; Brenowitz and Regehr, 2005). I tested whether CF bursts could enhance SSE. For induction of SSE, I used a burst of four to six PF stimuli at 100 Hz followed by either a single CF stimulus or a burst of three or five CF

stimuli at 400 Hz. When the CF stimulus was omitted, there was no change in synaptic efficacy at the PF synapses (2.5% ± 3% depression relative to baseline; n = 18 trials from 3 cells). When PF inputs were paired with a single CF stimulus, PF synapses were depressed by 12% ± 2.6% (n = 17 trials). When the PF stimulus was paired with a burst of three or five CF stimuli, the PF synapses were depressed by 23% ± 7% and 50% ± 2.4% (n = 17 trials), respectively. There was a significant correlation (r = 0.61, p < 0.001) between the number of CF stimuli in the induction protocol and the degree of PF depression (Figure 20).
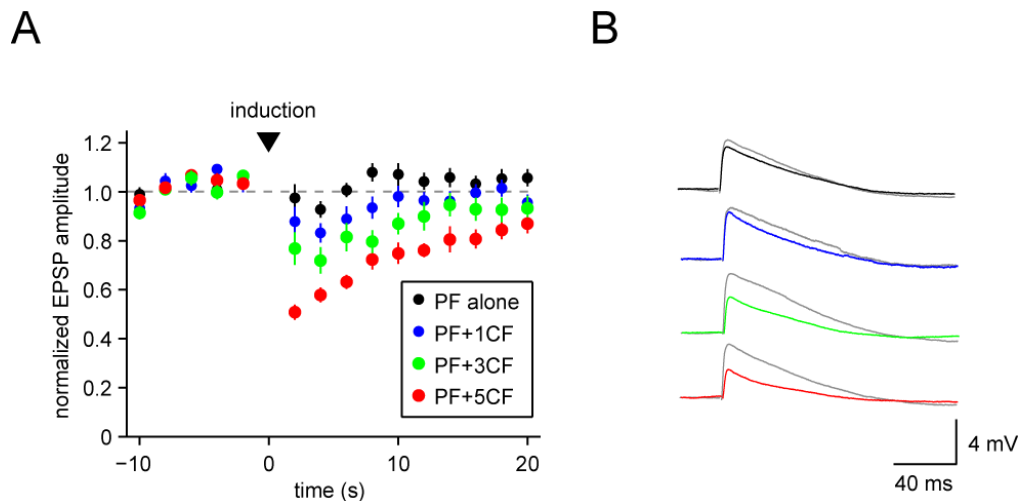
Figure 20 Synaptically evoked suppression of excitation is modulated by climbing fibre bursts. A) Time course of parallel fibre synaptic strength in three Purkinje cells when the cells are stimulated by parallel fibres alone (black), or parallel fibres with 1 (blue), 3 (green) and 5 (red) climbing fibre stimuli at 400Hz. (n=3 cells) B) PF-EPSPs for the different conditions in one of the Purkinje cells (measured 2 seconds after induction, average of 5 trials, baseline EPSPs, 2 seconds before induction, are coloured in gray).

Bursts affect long-term plasticity in the cerebellum

Parallel fibre (PF) synapses are known to undergo long-term depression (LTD) when stimulated in conjunction with CF input (Ito, 2001; Wang et al., 2000). I therefore investigated whether the CF bursts had an effect on the

induction of PF LTD. I used an induction protocol which paired five PF stimuli (at 100 Hz; (Chadderton et al., 2004) with either a single CF stimulus or a CF burst (five stimuli at 400 Hz; Figure 8A). I used only a small number of pairings (25) delivered every 2 s, which should normally provide only a relatively weak stimulus for plasticity (Jorntell and Hansel, 2006).
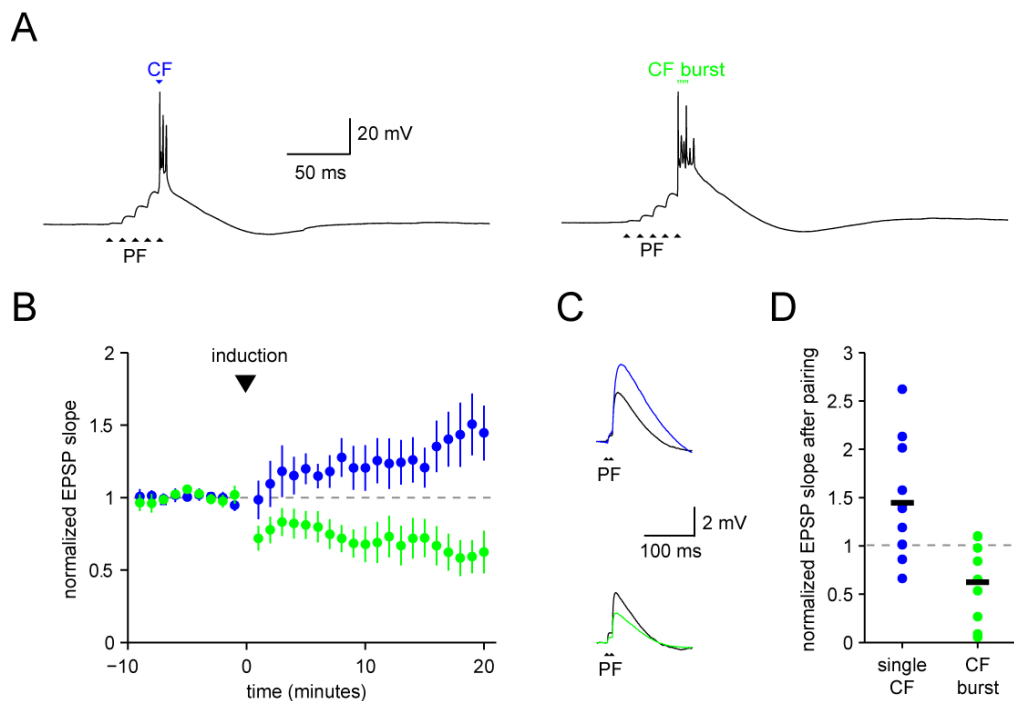
Figure 21 Long-term depression of parallel fibre synapses is modulated by climbing fibre bursting A) Induction consisted of a parallel fibre burst paired with either a single climbing fibre stimulus or a burst of five stimuli at 400Hz. B) Time course of EPSPs for the single CF stimulus (blue trace, n=9 cells) and the burst CF induction (green trace, n=10 cells) C) Representative traces, averaged over a minute, for two cells induced with either protocol before (black trace) and after (coloured traces) induction. D) Population data of the normalized EPSP slopes fifteen minutes after induction.

Indeed, the induction protocol with a single CF stimulus produced potentiation in the control group (139% ± 20% compared to baseline; n = 10; p = 0.033). In contrast, when a single CF stimulus was replaced by a CF burst (5 stimuli at 400Hz) in the induction protocol, robust LTD was observed

(63% ± 15% compared to baseline; n = 9; p < 0.01; Figures Figure 21B–D). These results demonstrate that CF bursts can enhance the probability of LTD induction using conjunctive PF-CF stimulation.

Discussion

Burst response in olivary axons

I have presented the first axonal recordings from olivary axons, which give rise to the climbing fibres of the cerebellum. I have shown that olivary neurons fire in variable short bursts, consisting of one to six spikes. The first action potential is present as a full amplitude spike in the soma, while the remaining spikes are present as small wavelets on top the ADP.

There has been previous evidence that olivary axons are capable of burst responses. In intracellular recordings from olivary neurons in the cat, the spike-ADP-AHP was first described, as were the wavelets on top of the ADP (Crill, 1970; Crill and Kennedy, 1967). Impulse collision experiments later suggested that the wavelets could propagate up the olivary axon (Armstrong et al., 1968). *In vivo* intracellular recordings with sharp electrodes from Purkinje cells have previously shown EPSP-like events with multiple peaks (Armstrong and Rawson, 1979; Eccles et al., 1966; Maruta et al., 2007). The way this data was obtained makes the interpretation difficult: Upon impalement with the electrode, the neuron depolarizes (referred to as an "injury discharge"), which causes the voltage dependent conductances to be sufficiently inactivated to view subthreshold activity.

Mechanism of burst generation

I have shown that the spikes in the burst appear in the axon first, and that neurons with short axons do not have full-blown secondary spikes. On the other hand, the ADP is strongly attenuated in the axon, pointing to a somato-dendritic origin. Furthermore, I have shown that single bursts cause large dendritic calcium transients. This suggests that the mechanism for burst generation involves the back-propagation of the axonal spike to the dendrites, where high-threshold calcium channels are activated. This depolarises the axon enough to support repetitive bursting. At the soma, the depolarisation is high enough to inactivate sodium channels. Finally, calcium dependent potassium channels are activated that curtail the burst. I have synthesised these findings in a simple three-compartment model that can reproduce the burst response in olivary neurons.

The model I propose is analogous to bursting in pyramidal cells (Williams and Stuart, 1999), where dendritic back-propagation causes a calcium channel dependent depolarisation underlying repetitive spiking in the axon. In that case, however, the depolarisation is rather modest, and so sodium channel inactivation is minimal, allowing the secondary spikes in the burst to remain of considerable amplitude. In the inferior olive, the ADP depolarises the soma to around 0mV, a level at which sodium channels will be inactivated, and therefore the secondary spikes are only visible as small deflections at the soma. Recently, it was shown in Layer 5 neocortical pyramidal that bursting requires an intact node of Ranvier (Kole, 2011),

indicating that axonal bursting might be a widespread feature of neural processing.

Transmission of bursts

The *in vivo* recordings show that secondary spikes propagate in the climbing fibre (the axon of the olivary neurons) all the way to the cerebellar cortex, where they trigger a compound EPSC in the postsynaptic Purkinje cells. I have shown that there are occasional failures of transmissions of secondary spikes - where a wavelet is not mirrored by an axonal spike - but that these failures are rare. This is in contrast to Purkinje cells, where most of the secondary spikelets of the complex spike response fail to propagate down to the DCN (Clark et al., 2005; Khaliq and Raman, 2005; Monsivais et al., 2005). Previously, it was thought that each spikelet in the complex spike must arise from a synaptic event (Armstrong and Rawson, 1979) however it is now clear that even a single stimulation can cause the complex spike (Davie et al., 2008). We have shown elsewhere (Mathy et al., 2009) that bursty input to Purkinje cells can add extra spikelets to the complex spikes and affect the post-CS pause.

Oscillatory modulation of bursty firing

When oscillations were first discovered in the olive it was assumed that their purpose was to precisely time output spikes (Llinas and Yarom, 1986). However I found that spikes could be evoked at various phases of the oscillations. A recent *in vivo* study (Khosrovani et al., 2007) confirmed this with sensory stimulation. I have shown that the relation between oscillations and spike output can be more subtle: By triggering olivary bursts on top of

injected and spontaneous oscillations, I have shown that the number of spikes in the bursts can code for the phase of the oscillation. I propose that the mechanism for this is quite straightforward: as the neuron is more depolarised (i.e. at the crest of the oscillation), there is more activation of calcium channels during an evoked spike, thereby causing a longer ADP and more spikelets.

There have been recent suggestions (De Zeeuw et al., 2011) that *in vivo*, rather than coding for the phase of the oscillations, the bursts in fact code for the amplitude of the oscillations in a paradoxical way: high amplitude oscillations cause shorter bursts. This result is puzzling to me, since, even if the oscillations *in vivo* are so heterogeneous that the phase coding isn't robust under those conditions, the size of the bursts should still co-vary with increasing pre-stimulus membrane potential. This would lead high amplitude oscillations to cause longer bursts.

If the paradoxical amplitude coding stands the test of time, I offer here two possible explanation for the discrepancy: As my recordings using a BAPTA-based internal have shown, calcium buffering is critical in determining the length of the bursts, and it is quite plausible that the resting calcium levels are higher in a cell that has large oscillations *in vivo* and therefore calcium-dependent potassium channels are more readily recruited, resulting in a shorter burst for large oscillations. Another possibility is that the spike rate in high amplitude oscillations is high enough for the paired pulse depression of bursting to become relevant.

Whether it is the phase or the amplitude that the bursts are coding, I believe there is now clear evidence that the number of spikes in the burst does convey information about the state of the olivary network. This is in contrast to early results (Crill, 1970; Crill and Kennedy, 1967), that indicated that the average number of wavelets didn't vary with stimulus intensity, but these studies did not relate the wavelets to the membrane potential of the cell, nor were subthreshold oscillations known about at the time.

Impact on cerebellar plasticity

Using recordings in cerebellar slices, I have shown that climbing fibre bursts can enhance short-term and long-term associative plasticity of parallel fibres in the downstream cerebellar Purkinje cells. In the case of short-term plasticity, I have shown that the depression obtained increases monotonically with the number of spikes in the burst. This means that climbing fibre bursts can be read out by Purkinje cells, and therefore impact the computation performed in the cortex. There are many other forms of plasticity in which climbing fibres are involved, for instance long-term depression of climbing fibre EPSCs (Hansel and Linden, 2000; Szapiro and Barbour, 2007). Going forward it will be important for physiologists to study induction protocols which take into account the bursting nature of climbing fibre spiking.

A model for the function of the inferior olive

It has been shown previously that subthreshold oscillations in olivary neurons reset their phase after the firing of a spike (Khosrovani et al., 2007;

Llinas, 2009). Since I have shown the bursts in the spikes to be related to the phase of the oscillation at which they were elicited, it is a logical conclusion that in a sequence of olivary spikes, the number spikes in a burst will encode the time that has elapsed between bursts. In other words, the number of spikes in a burst could encode the ISI between it and its predecessor. This means that olivary spiking could be more like a "stopwatch" than a "clock". Support for this is provided by a study recording intracellularly from Purkinje cells (Maruta et al., 2007) that found that the number of components in compound CF-EPSPs increases with the delay from the last compound response.

Implications for function of the cerebellum

There are two main theories of cerebellar function. In the Marr-Albus (Albus, 1971; Marr, 1969) models (or- in their modern incarnation- adaptive filter models (Dean and Porrill, 2008, 2010)), the climbing fibre signals a motor error that serves as a trigger for associative plasticity. The competing model sees the olivocerebellar system as a generator of spatiotemporal patterns (Jacobson et al., 2008), sculpted by the subthreshold oscillations.

I have shown that olivary bursts can signal information about the subthreshold oscillations and that this can impact plasticity in the cerebellar cortex. This is an indication that timing and memory functions of the cerebellum might complement each other (Mauk et al., 2000), and that the theories are not as incompatible as their proponents claim.

Chapter 3: Electrotonic coupling between olivary neurons: insights from paired recordings and fluorescence microscopy.

Introduction

Olivary neurons are connected by gap junctions (Sotelo and Llinas, 1972), which endows them with electrical coupling that is thought to underlie complex spike synchrony in the cerebellar cortex (Blenkinsop and Lang, 2006). This synchrony has been posited to represent an important code for motor coordination and learning (Van Der Giessen et al., 2008; Welsh et al., 1995).

Electron microscopic studies have shown that gap junctions form between spines of olivary neurons (de Zeeuw et al., 1989; Gwyn et al., 1977). Several spines are arranged together in a glomerular structure, which receives both excitatory and inhibitory input. While the ultrastructure provides a statistical snapshot of olivary connectivity, we know remarkably little about how a given olivary neuron interacts with its neighbours and the surrounding neuropil. I sought to better understand the coupling between neurons by combining electrophysiological recordings from olivary neurons with microscopic methods to look at the morphological correlates of coupling.

Results

Paired recordings from olivary neurons reveal that coupling is common but weak

I obtained simultaneous patch-clamp recordings from 72 pairs of olivary neurons from acute brain slices obtained from P18-22 Sprague-Dawley rats. I targeted somata within 60 μm of each other, and found that about 80% of them were coupled (defined as at least a 0.2mV deflection in one of the cells in response to a -800pA, 500ms current injection in the other cell, averaging 10-15 traces), in line with previous reports (Devor and Yarom, 2002b; Hoge et al., 2011).

The coupling between the cells, as measured by the coupling coefficient and coupling conductance, was found to vary markedly (Figure 21) but was very weak in general (median coupling coefficient: 0.0107, median coupling conductance 346 pS). These weak coupling parameters were reflected in the fact that while the after-depolarisation and the rebound spike were transmitted between coupled cells, I never observed fast spikelets, which are commonly seen in other neuronal networks coupled by gap junctions (Figure 23)(Beierlein et al., 2003; Dugue et al., 2009; Gibson et al., 1999; Long et al., 2005; Schmitz et al., 2001; Vervaeke et al., 2010). Note that in the olive, the dendritic path leading to the gap junction probably contributes significantly to the coupling resistance (see next chapter). In about a third of the pairs I saw sinusoidal subthreshold oscillations, 1 - 10Hz in frequency, 1 - 20mV in amplitude) that were synchronized between the cells. I also found that

coupling between cells was occasionally asymmetric (coupling ratio 1.28±0.13, N=72 pairs).
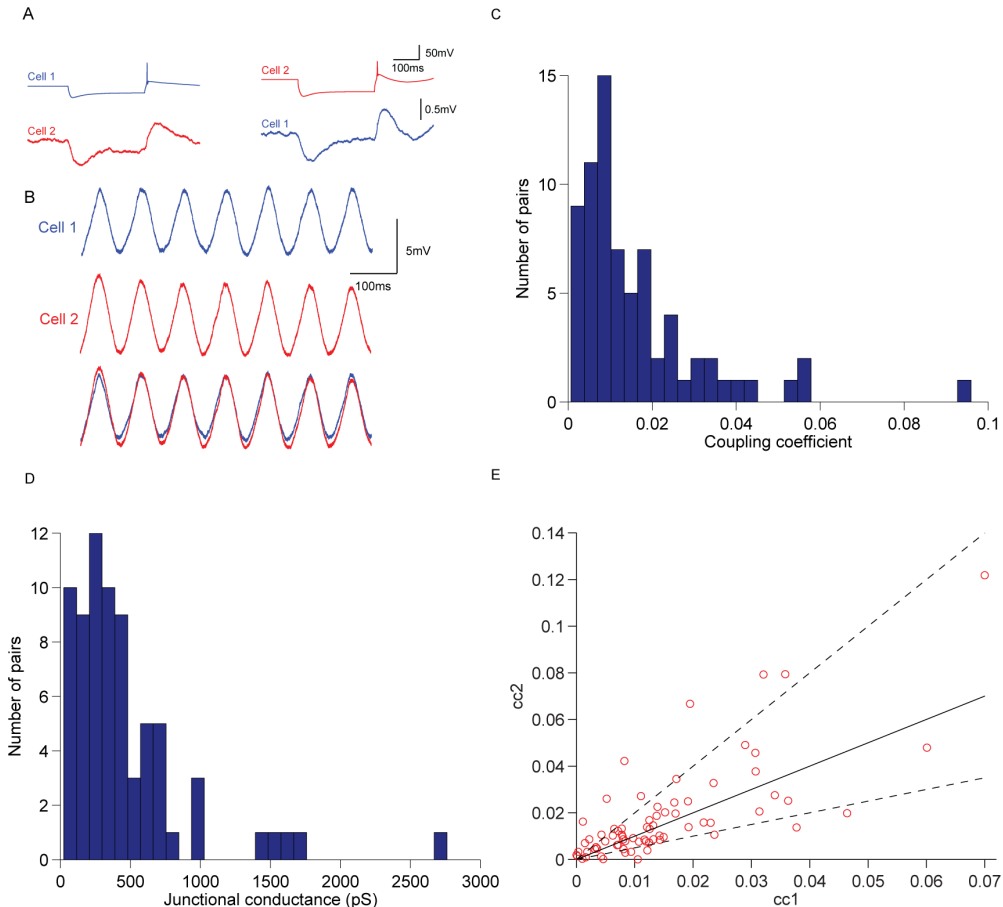
Figure 22 Paired recordings from inferior olive neurons. A) Response to hyperpolarizing current (800 pA) injected alternately in the two cells B) Synchronized subthreshold oscillation in another pair of coupled neurons. Bottom trace shows the two traces overlaid, revealing their synchronization. C) Distribution of coupling coefficients (n = 72 pairs). D) Distribution of junctional conductances. E) Coupling coefficient measured in one direction (cell 1 to cell 2) versus the other direction (cell 2 to cell 1). Note that there can be considerable asymmetry. The straight line is the unity line, and the dashed lines have slope 2 and 0.5

Since the junctional conductance (see Methods chapter) of my pairs ranges between 25 pS and 3000 pS, (with a typical conductance around 300 pS), and the conductance contributed by a single connexin36 gap junction plaque is

typically around 100 pS (Srinivas et al., 1999; Vervaeke et al., 2010), I hypothesize that a pair of olivary neurons is likely to be linked by more than a single gap junction.

A rough estimate of how many can be obtained by dividing the total coupling conductance by the single plaque conductance, bracketing the number of plaques between 0 and 30, with a typical number of 3. Note that this estimation does not take into account indirect coupling, which may contribute a significant proportion of the coupling (Amitai et al., 2002).
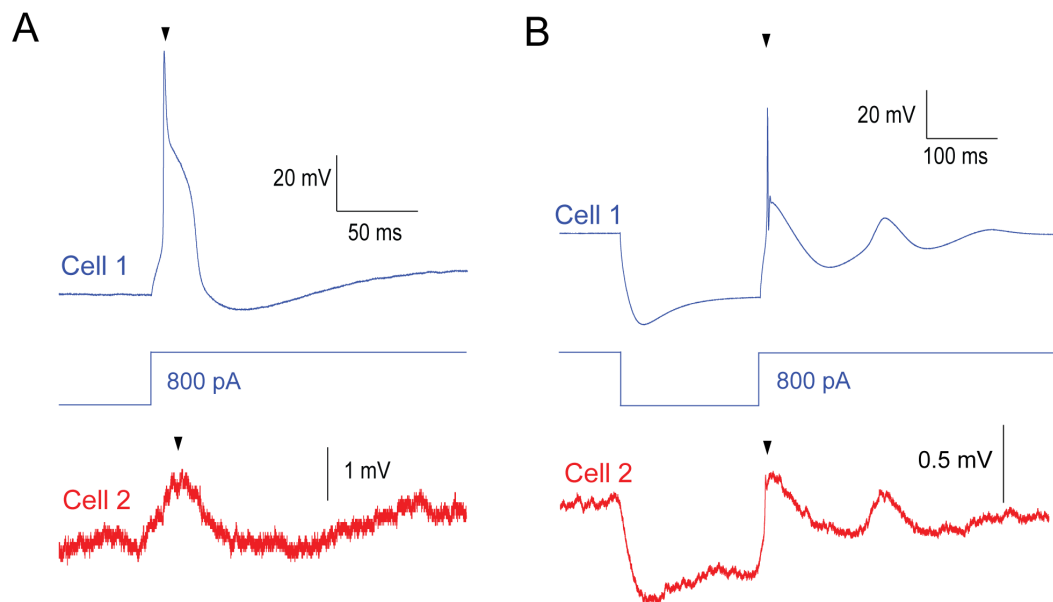
Figure 23 Coupling of olivary currents. A) An olivary burst response is evoked by somatic depolarisation. Note that the fast sodium spike is absent in the coupled cell. B) A rebound spike is evoked by hyperpolarisation. The subthreshold currents are coupled but the spike is not.

Confocal microscopy of coupled neurons

To gain insight into the morphological correlates of coupling, I filled my cells with 0.5% biocytin, fixed the slices in 5% paraformaldehyde after recording,

processed them for steptavidin-Alexa488 staining, and imaged them on a spinning disc confocal microscope.

I found that most cells had the type 2 curly morphology (Figure 24) (see introductory chapter), probably because my recordings were mostly from the principal olive and medial accessory olive (Hoge et al., 2011; Scheibel and Scheibel, 1955). In line with other reports (Devor and Yarom, 2002b; Hoge et al., 2011), I found that type 2 cells only couple to other type 2 cells (13 out of 13 pairs), and I had one pair of type 1 cells.

Occasionally, dye coupling of biocytin could be observed to cells that weren't patched (Figure 26). The dye coupling I obtained was less frequent and spread to fewer cells (on average to 3.5 ± 1.3 cells, with a maximum of ten coupled cells) than a recent report using neurobiotin (Hoge et al., 2011), but this probably due to differences in gap junction permeability for these two dyes. While, infrequently, neurites from the indirectly labelled cells were faintly stained, I was never able to trace them back to a putative gap junction location, as has occasionally been possible in other coupled neurons – for instance hippocampal neurons (Schmitz et al., 2001).
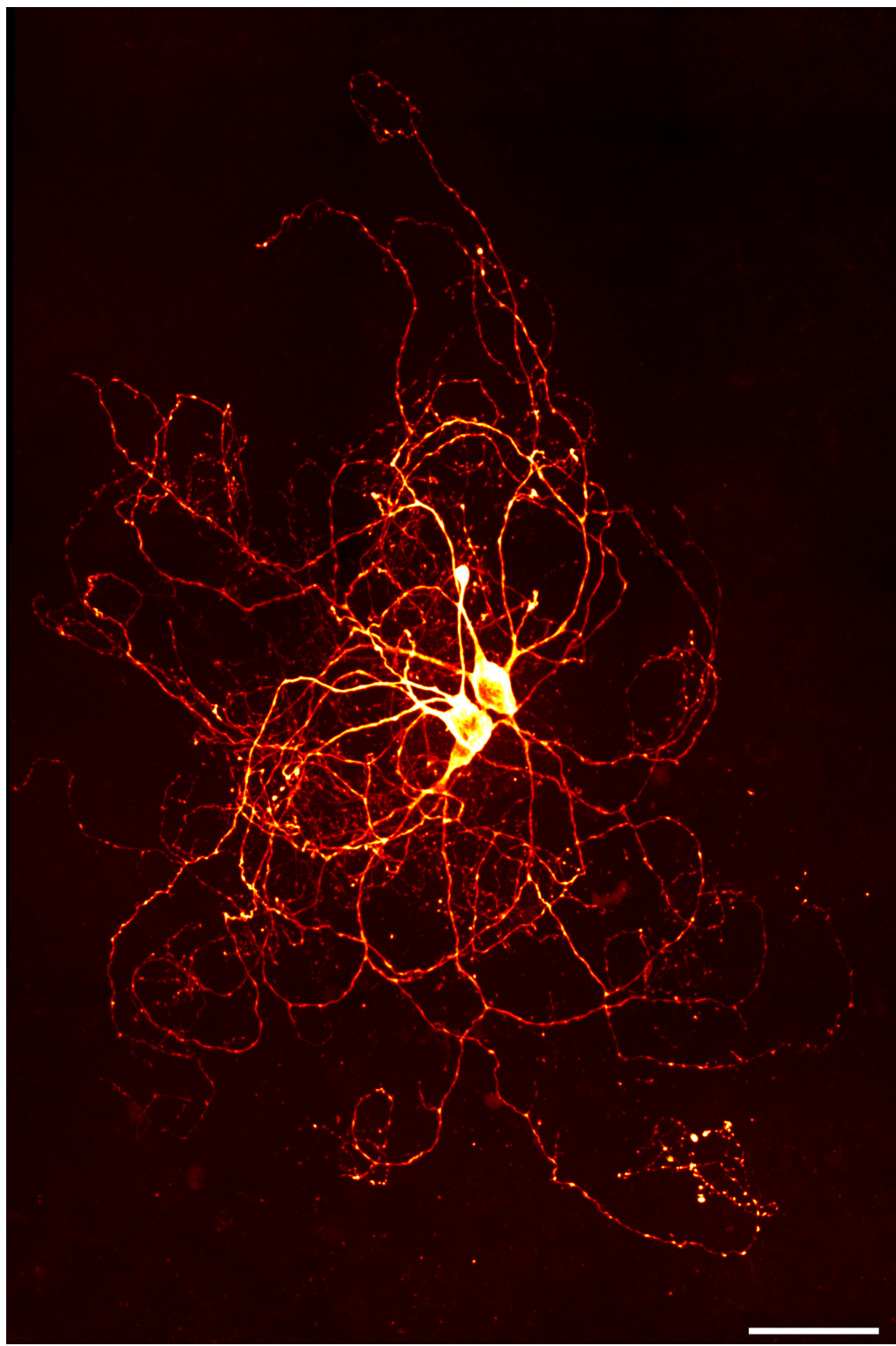
Figure 24 A pair of electrotonically coupled neurons filled with 0.5% biocytin, processed with streptavidin-Alexa488 and imaged on a spinning disc confocal microscope. (Maximum intensity projection, scale bar: 50 μm)
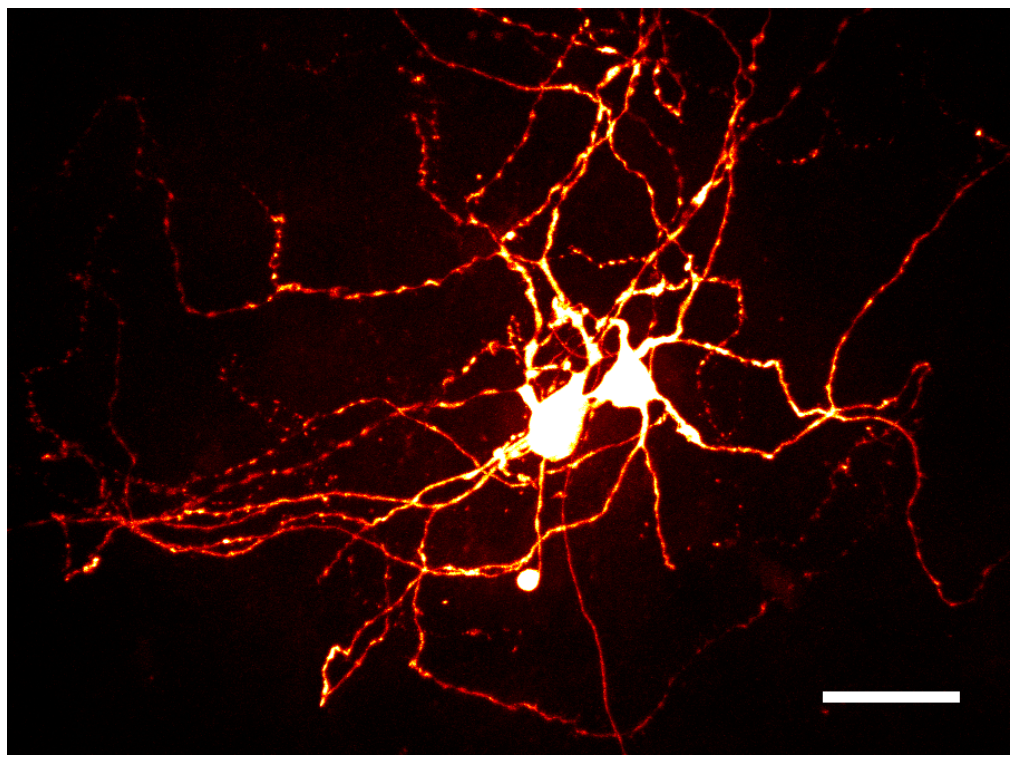
Figure 25 A pair of electrically coupled type I neurons (Maximum intensity projection, Scale bar 50 μm).
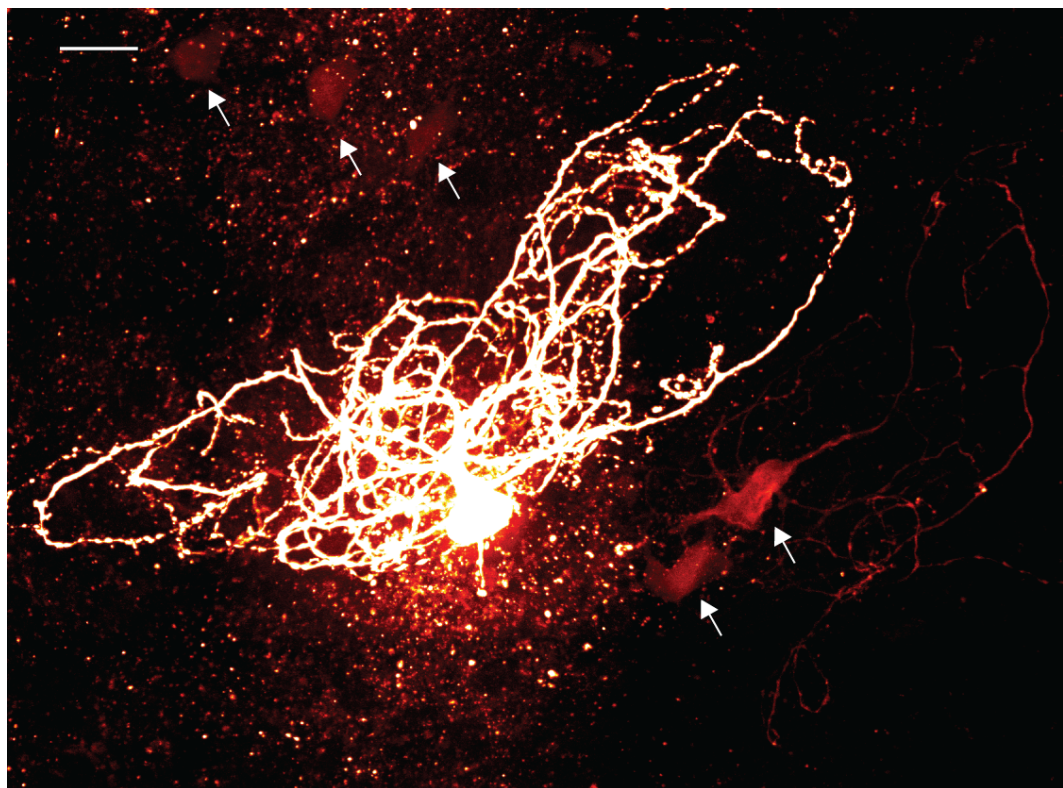
Figure 26 Dye coupling in olivary neurons. The brightly stained neuron was patched with 0.5% Biocytin. There are five faintly stained neurons (white arrows), which were stained indirectly (maximum intensity projection. Scale bar: 50 μm).

88

Reconstruction of pairs

While there have been reconstructions of the morphology of single olivary neurons (Ruigrok et al., 1990a), there are no published accounts of reconstructions of coupled olivary neurons. I therefore thought it would be instructive to attempt this.

I obtained paired recordings from two pairs of type 2 neurons filled with 0.5% Biocytin, fixed the slices and processed them with a streptavidin-Alex488 protocol. I obtained high-resolution stacks of the pairs on a spinning disc confocal system (resolution 0.2x0.2x0.8 μm with a 40X oil immersion objective, NA 1.1). The stacks were then loaded into the Trees Toolbox (Cuntz et al., 2011) and the neurites from each neuron were traced by Maja Boznakova, an assistant in the laboratory, under my supervision.

The dendritic morphology of olivary neurons is extremely complex (Ramon y Cajal, 1911), making reconstructions difficult and fraught with ambiguities. The dendrites of the cells make many sharp turns at angles unknown to most other neurons. The distal dendrites have a tendency to curl into tight whorls, occasionally making appositions with the same dendritic tree.

A   B
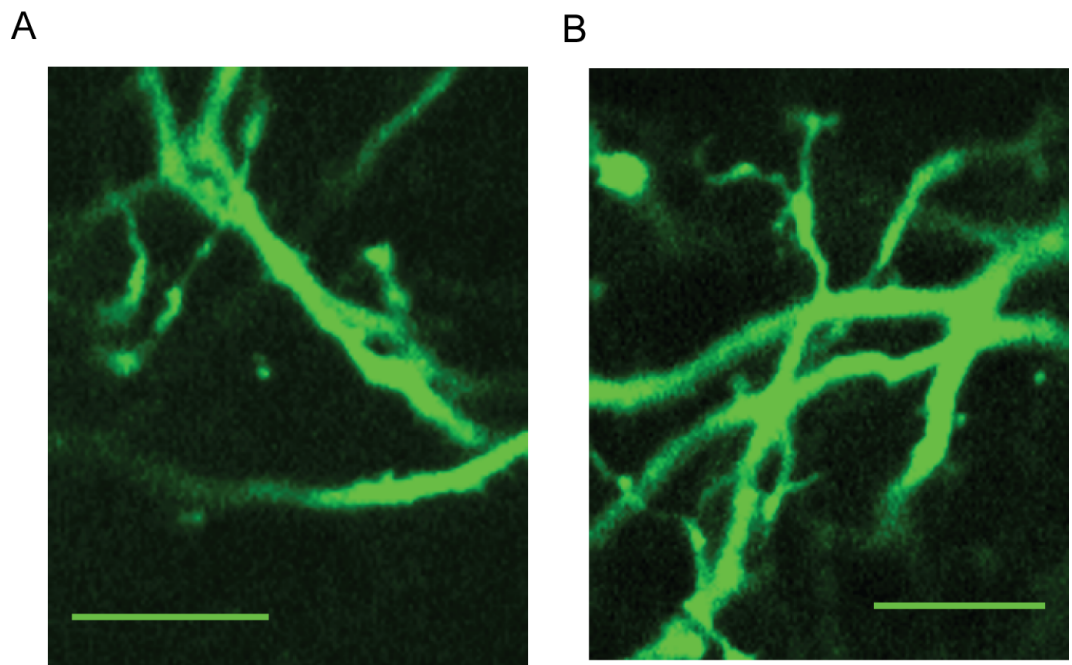
Figure 27 Close up of dendrites from two coupled neurons filled with biocytin and imaged using confocal microscopy. The dendrites of the two neurons cross over and make many "tangles" with themselves and each other (scale bar: 10 μm).

In the pairs, I found that the dendrites from the two neurons had the tendency to make various tangles and, there were many crossover points between dendrites (Figure 27). I also found that the dendrites from both neurons could run in parallel to each other for a few microns, with possible appositions between them. Coupling between olivary neurons occurs at least in part (and maybe mostly) between dendritic spines (Sotelo et al., 1974). While I sporadically saw spines in the neuropil at this resolution, to my disappointment, I never saw clear evidence of contacts between two dendritic spines of a pair of connected neurons. The reconstructions of the two pairs are shown in Figure 28 and Figure 29. These pairs had coupling coefficients of 0.003 and 0.005 respectively. During the reconstruction, each subsection of dendrite was approximated by a small cylinder to account for its length and diameter. To look for putative contacts between the dendritic

trees, I implemented an algorithm that finds the closest distance between two line segments. I then used this algorithm to look for cylinders from both neurons where the distance between the centre lines of the cylinders was smaller than the sum of their radii (see Methods chapter). These constitute putative contact points, and are plotted as green circles in the reconstructions. Many circles were found to overlap, because several dendritic sections within a small area met the criteria for closeness, indicating a region of putative contact between the dendritic trees. The first pair had 11 such regions of possible contact, while the second pair had 9. While these spots can provide, to a first approximation, a region to look for gap junctions, I do not believe that there is a strong unambiguous morphological signature of gap junctions in the pairs I reconstructed, and therefore other techniques, such as electron microscopy, would be required to make a microcircuit level reconstruction.
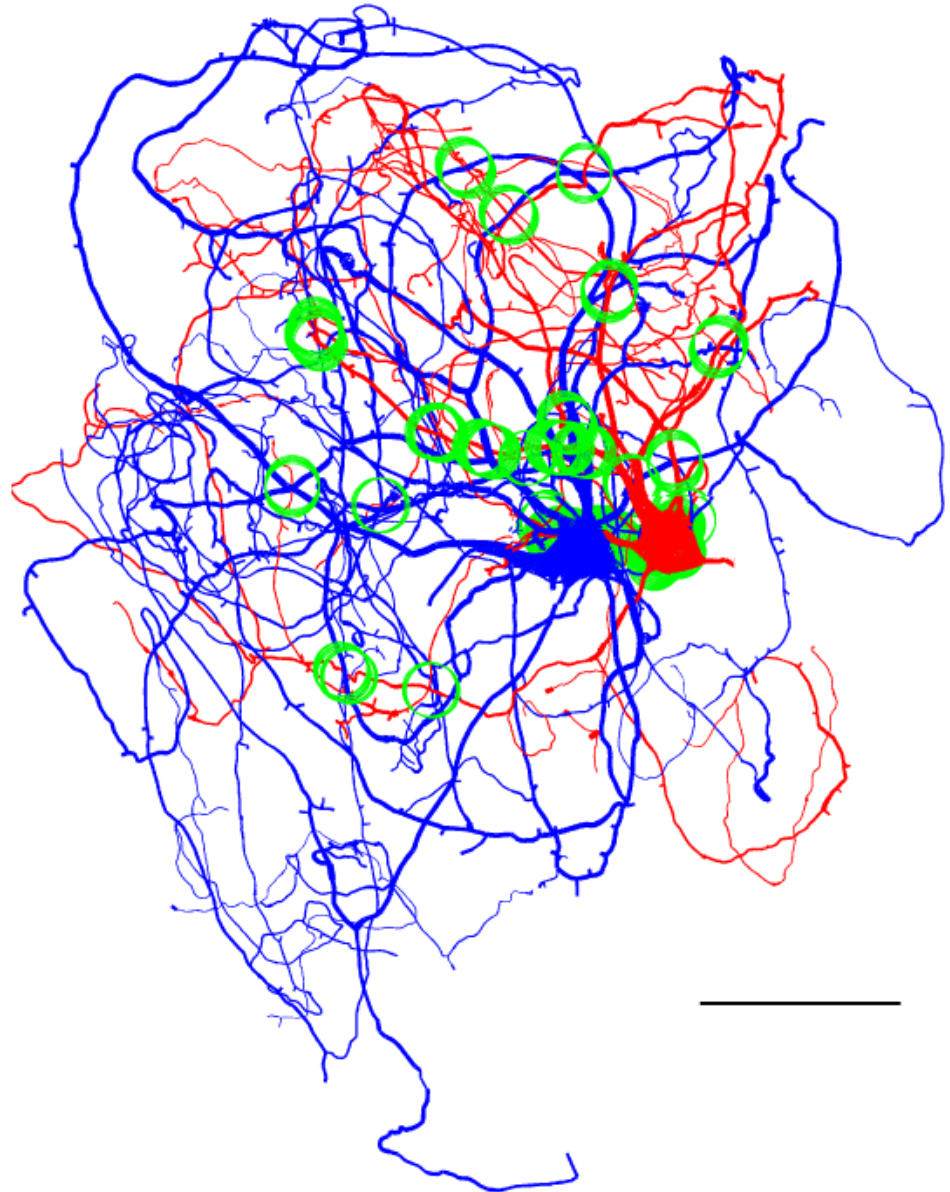
Figure 28 Reconstruction of a coupled pair of olivary neurons. The green circles denote areas where the dendritic sections from both neurons are close enough to make contact (Scale bar: 40 μm, axons not shown). Coupling coefficient: 0.003.
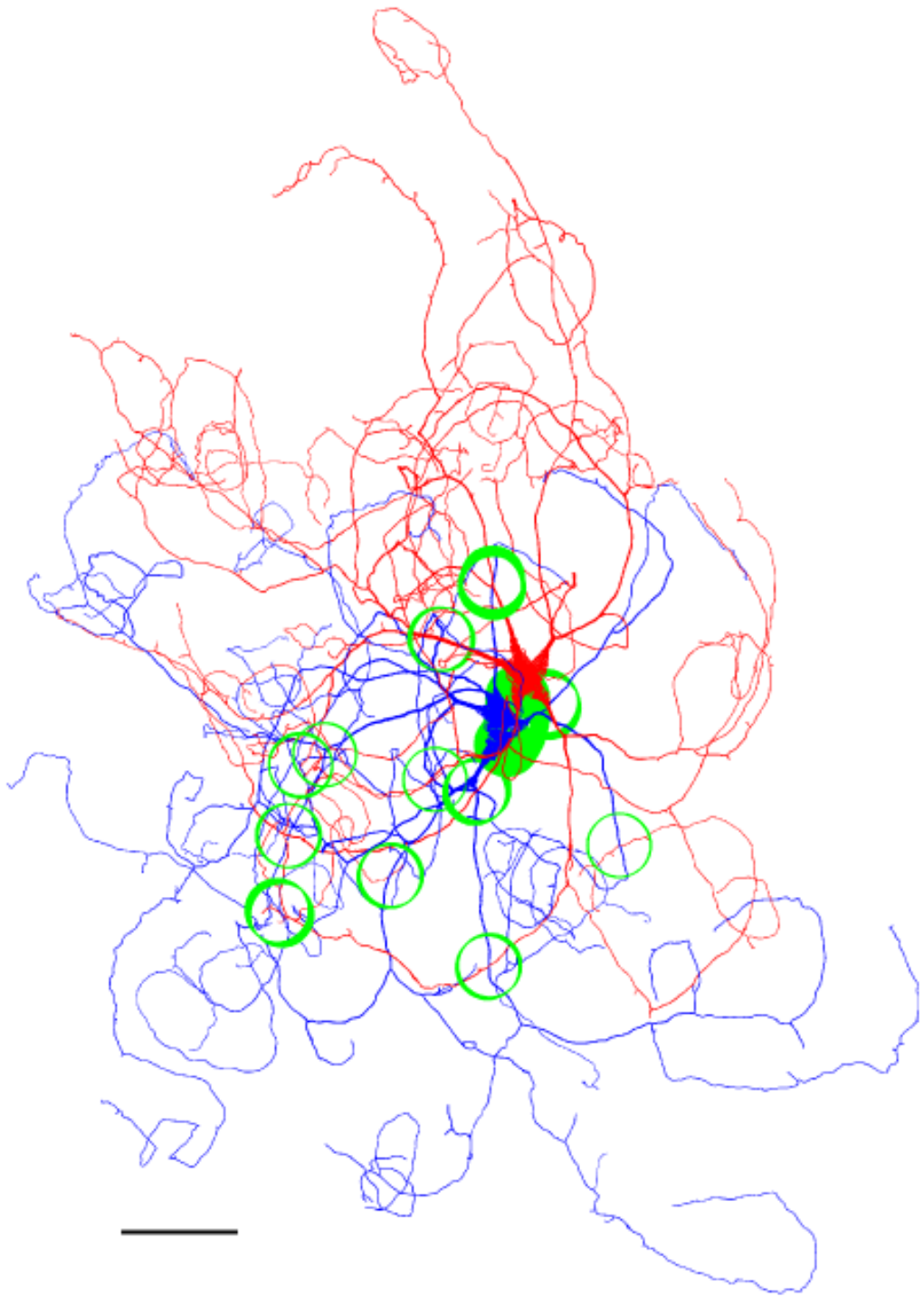
Figure 29 A reconstruction of a second olivary pair (Coupling coefficient: 0.005). (Scale bar: 40 μm, axons not shown).

Spines and connexin36 labelling in the inferior olive

At higher resolutions (80x80x200nm, 100X oil-immersion objective, 1.3 NA), I was unambiguously able to resolve spines in the dendritic tree. In accord with previous accounts (de Zeeuw et al., 1990b; Gwyn et al., 1977), I found that the spines could be categorized into several types (Figure 30).
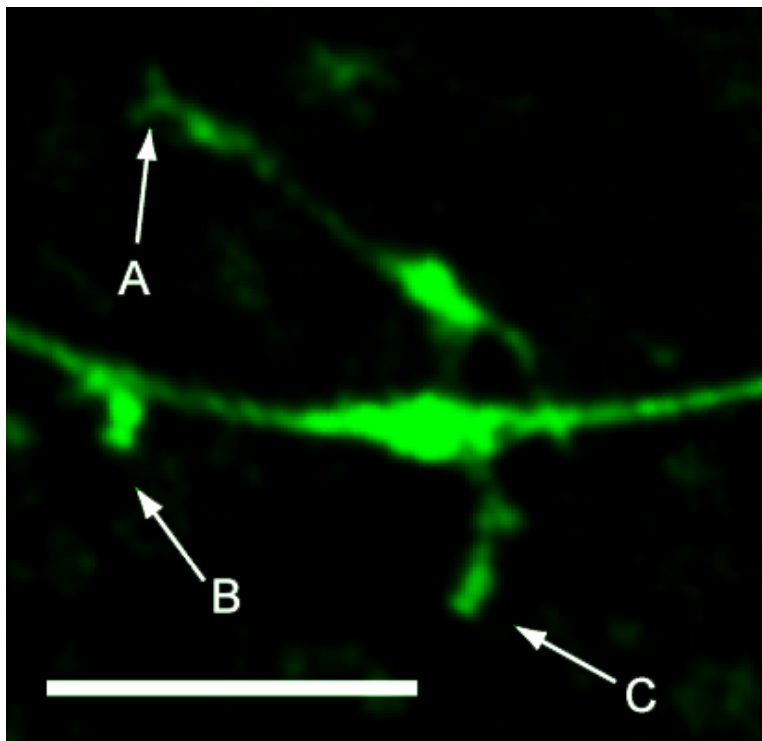
Figure 30 Spines of olivary neurons. A dendrite from a single olivary neuron filled with biocytin showing 3 different types of spines. A) Long racemose spine with two heads; B) short stubby spine; C) Spine with mushroom-like morphology. Note that spine A and C arise from a dendritic varicosity (scale bar 5 μm)

The first type was stubby and short (up to 1 μm), with no clearly distinguishable neck. The second category was of the mushroom type, about 1 μm long, with a bulbous spine head. The third type had a complex racemose morphology with up to three spine heads. These spines could be very long - sometimes exceeding 5 μm - and tortuous. Finally, I occasionally saw very

thin filamentous spines. The spines tended to originate from dendritic varicosities, and were more densely distributed in the distal dendritic tree, although they could be found at all levels in the dendritic tree. Since gap junctions are known to form between spines of olivary neurons, I decided to use immunohistochemical methods to relate the morphology of spines to their involvement in coupling. Connexin 36 is the main protein constituting olivary gap junctions (Long et al., 2002) (De Zeeuw et al., 2003), so I decided to detect gap junction plaques using a polyclonal rabbit primary antibody against the c-terminus tail of Connexin 36 (Invitrogen). This antibody has previously been shown to stain gap junction plaques in the olive (Placantonakis et al., 2006). My student, Si Yoo, and I first established the method in acute brain slices prepared in the same manner to the slices I use for electrophysiology. Similarly to previous reports (Marina et al., 2008; Placantonakis et al., 2006), I found that, under identical imaging conditions, slices incubated with primary and secondary antibodies gave a punctate labelling in the inferior olive (with a mean puncta density of 0.57±0.003 puncta per μm^3), while slices incubated only with secondary antibody didn't stain in this pattern (Figure 31).
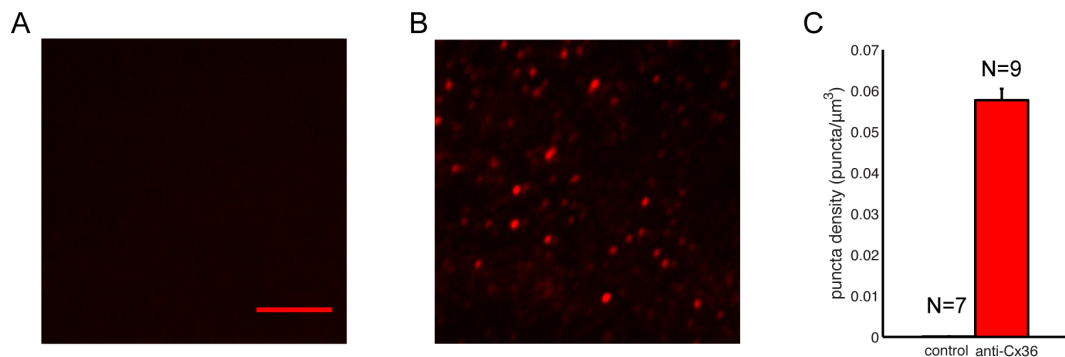
Figure 31 Connexin 36 staining of inferior olive neurons. A) Control with only secondary antibody in 1:500 dilution. B) Slice incubated with both primary and secondary antibody displays a punctate pattern of staining (Scale bar 5 μm). C) Automatic puncta labelling for 7 control image stacks from 2 slices stained with only primary and 9 stacks from 2 slices with both secondary and primary antibody. Note that there are no puncta in the control stack.

I next applied this staining protocol to slices from which recordings had been obtained from coupled neurons. I processed the slices both for biocytin and connexin 36 immunostaining. I found that I could achieve satisfactory staining of both neurites – including spines - and immunopuncta (Figure 32) with this protocol. I applied this protocol to two slices, each with a recorded pair. Again, despite good impregnation of the samples, the complexity and extent of the cells made it unfeasible to establish the presence of spiny contacts between the cells.

 I imaged four stacks containing contiguous fields of view depicting dendrites from the best-stained slice. I deconvolved the images thus obtained with a software package called Huygens (SVI software), and Si Yoo manually reconstructed all 375 spines that could be detected in these stacks (Figure 33). I quantified the length of the spines (Figure 33B), and found that there was a wide variation, but that most spines were short (mean length 1.14±0.04 μm).

I implemented an automated technique (Fish et al., 2008) for detecting immunopuncta. Briefly, this technique segments out clumps of contiguous pixels using an iteratively adjusted threshold, and selects clumps within a given size range. Empirically, I found that setting this range between 0.2 and 0.8 μm^3 worked well for my data.
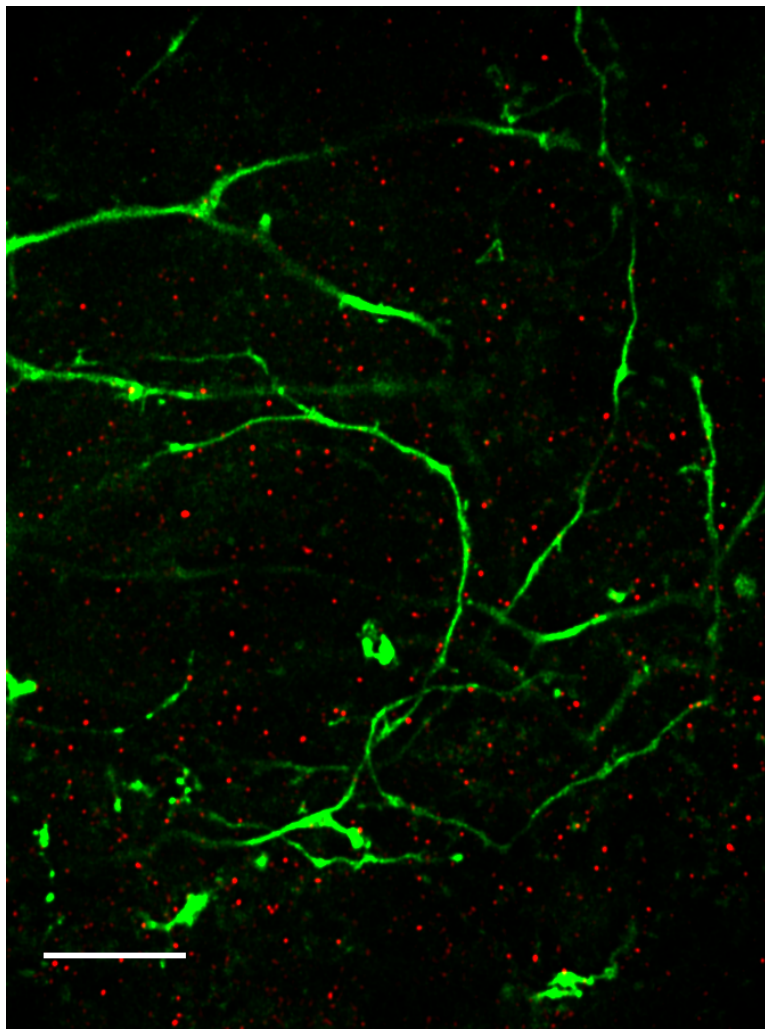
Figure 32 Connexin 36 staining (red) of slice containing a filled pair of olivary neurons (Scale bar: 10 μm).

I looked for colocalisation between spines and puncta by applying my automated puncta detection algorithm to a small image volume around each of the spines I had manually traced. I defined a punctum as colocalized with a

spine if it shared more than 3 pixels with the spine. I found that all types of

spines could be associated with puncta on the head or shaft (Figure 33A), and

found that around 40% of spines overall had at least one associated

immunopunctum (Figure 33). The longer spines (>1 μm) were significantly

more likely to be associated with a punctum than shorter spines (62±18%

versus 24±12%, p<0.01, Chi-squared test for proportions). Incidentally, I

found that immunopuncta could commonly also be associated with dendritic

shafts, a finding confirmed by a previous report (Placantonakis et al., 2006) .
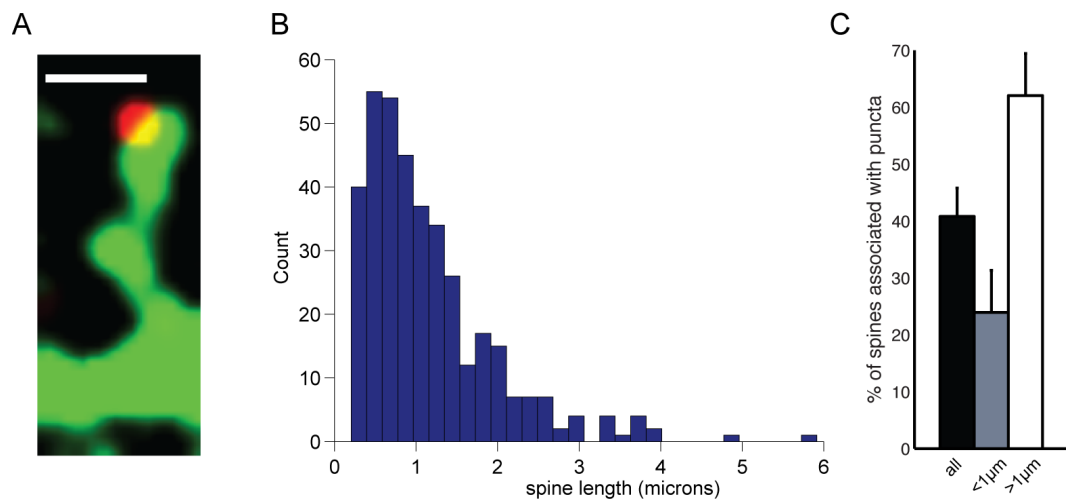
Figure 33 Connexin 36 labelling in spines. A) Dendritic spine (green), with associated red Cx36 immunopunctum (scale bar: 1 μm) B) Histogram of spine lengths in imaged region. C) Percentage of spines associated with an immunopunctum (n=375 spines) (black bar: all spines, grey bar: all spines smaller than one micron, white bar: spines longer than one micron).

Interactions between dendrites and somata

I had some indication from my paired recordings that dendrites from one

neuron seemed to occasionally come in close proximity to the other cell's

soma. I decided to study this systematically by combining labelling of single

recorded neurons with Nissl staining. I recorded from single neurons with

0.5% biocytin in the internal solution, and then fixed the slices and designed

a protocol combining streptavidin-Alexa488 staining with Neurotrace Red (Invitrogen), a fluorescent Nissl stain. I processed 10 slices in this manner.

I found that the inferior olive contained mainly flat oval shaped somata with a long axis of between 20-30 μm in length (Figure 34), although there was a very small proportion (<1%) of smaller round somata, probably corresponding to the interneurons previously reported (Walberg and Ottersen, 1989).
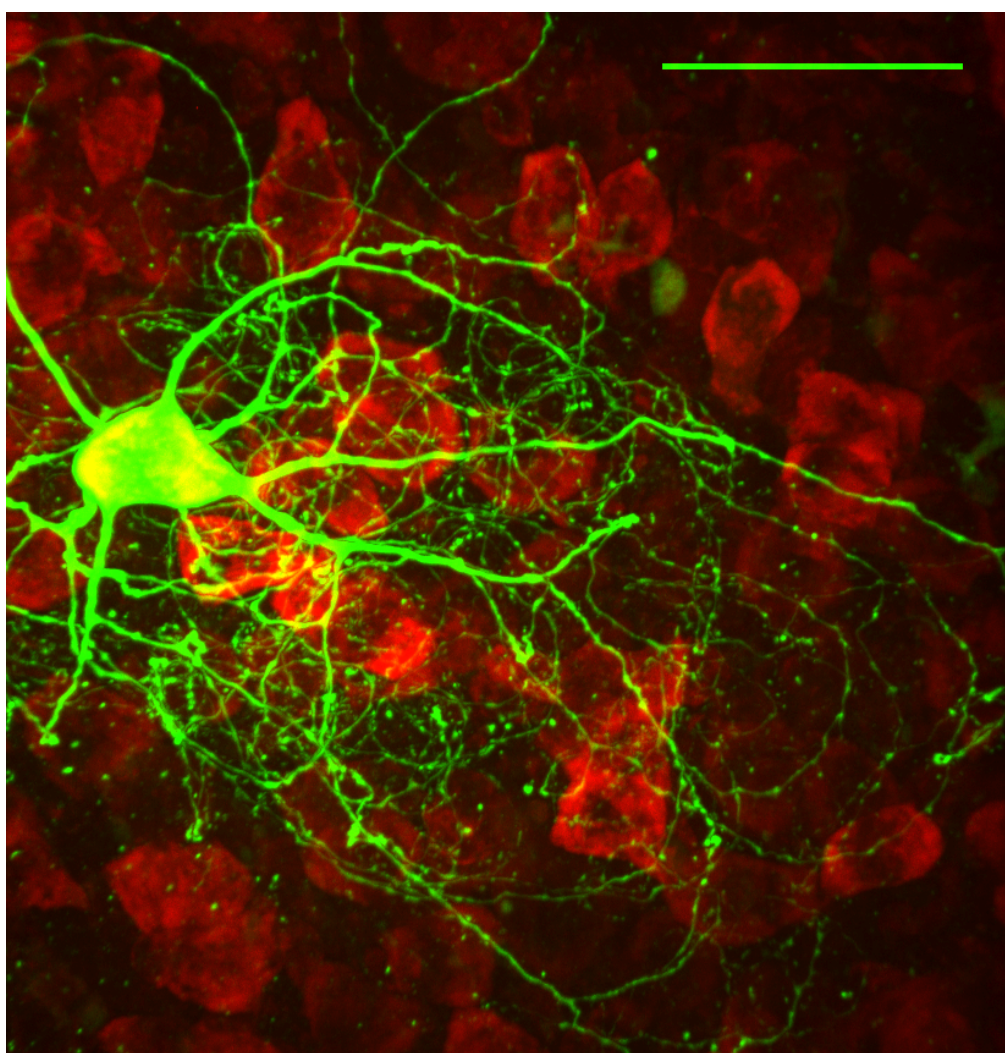
Figure 34 Single labelled neuron filled with biocytin combined with a fluorescent Nissl stain (maximum intensity projection, scale bar: 50 μm)

I found that the dendritic tree of the filled neuron made frequent (putative) contacts with the neighbouring somata. These contacts were mainly made by

terminal dendrites and came in several configurations (Figure 35). In the first type of contacts, the terminal tip of a dendrite appeared to make a simple contact with a neuronal soma.

In the second type, the terminal dendritic whorls described above closely followed the contour of one to three neighbouring somata. Importantly, not all whorls made such contacts with somata (Figure 36).
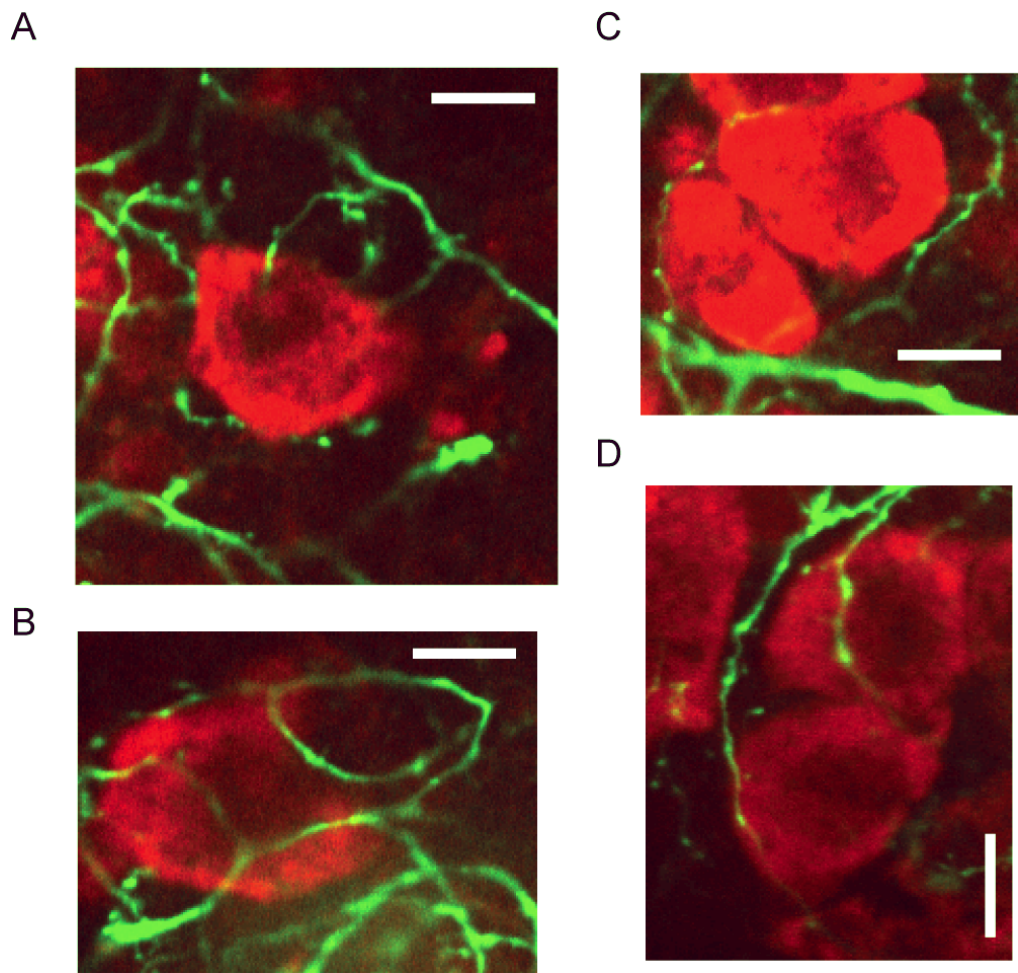
Figure 35 Different types of putative dendrosomatic contacts in the olive. A) Collection of terminal dendrites that fold around an olivary soma in a nest-like fashion. B) Two terminal dendritic whorls apposed to a soma. C) A dendritic whorl wrapped tightly around the upper contour of two somata. D) Two somata contacted by finger-like terminal dendrites. (Scale bar: 10µm)

Another type of configuration consisted of several terminal dendrites from the labelled neuron arranged together in a tangled, nest-like network. Neurons could sometimes be found within such a nest, and the dendrites appeared to contact the soma.
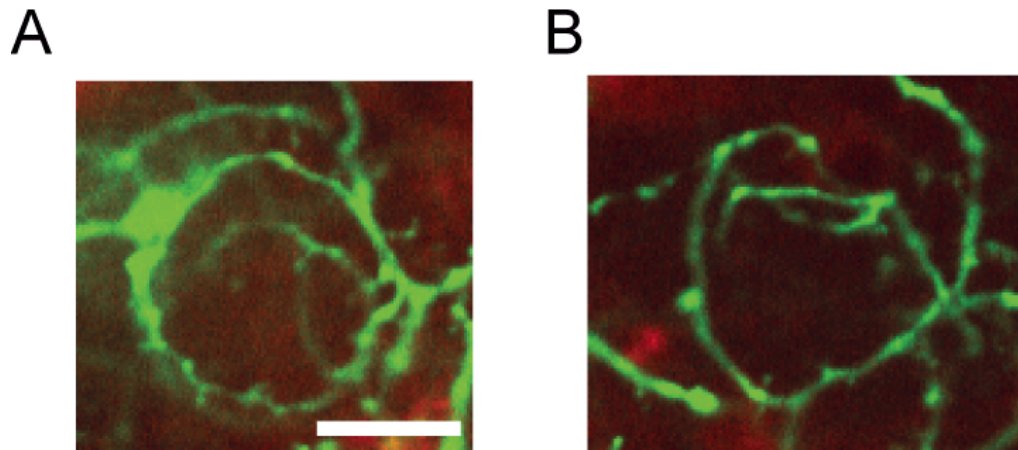
Figure 36 Two dendritic whorls in Nissl-stained tissue containing no stained neurons. Scale bar: 10µm

Oligodendrocytes and inferior olive neurons.

An early study of the inferior olive using Golgi staining showed that olivary dendrites made complex contacts with smaller, round cells whose soma stained orange (Scheibel and Scheibel, 1955). On the basis of their size (7-10 µm diameter), the Scheibels concluded that this was consistent with cells being oligodendrocytes, although this could not be confirmed ultrastructurally (Gwyn et al., 1977), and there have been suggestions that the cells might be interneurons (Armstrong, 1974).

To address this directly, I performed an immunostaining for oligodendrocytes using the Olig2 marker in 7 slices where single neurons had been filled with 0.5% biocytin. I found round cell bodies (7-10 µm diameter) were immunopositive for the marker (Figure 37).
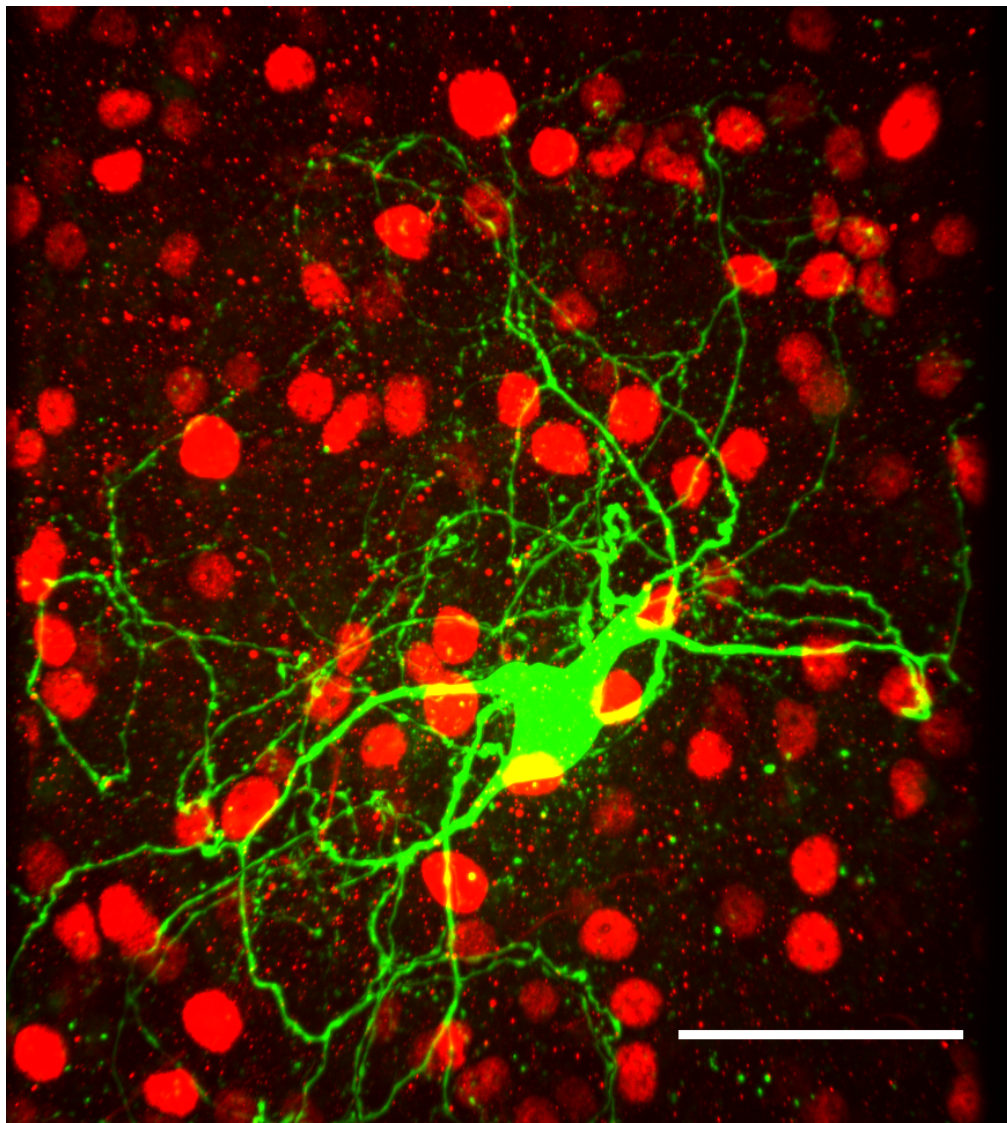
Figure 37 Slice containing a biocytin filled neuron (green) and Olig2 positive cells (red) (maximum intensity projection, scale bar: 50 μm).

While I didn't find contacts of the most complex type seen by the Scheibels (Scheibel and Scheibel, 1955), I found that the dendrites of the filled neurons made occasional contacts with the immunopositive glial cells. The contacts were usually made either by spinous processes from terminal dendrites, although occasionally an immunopositive cell could be found apposed to the branchpoint of a dendritic fork, as also seen by the Scheibels.
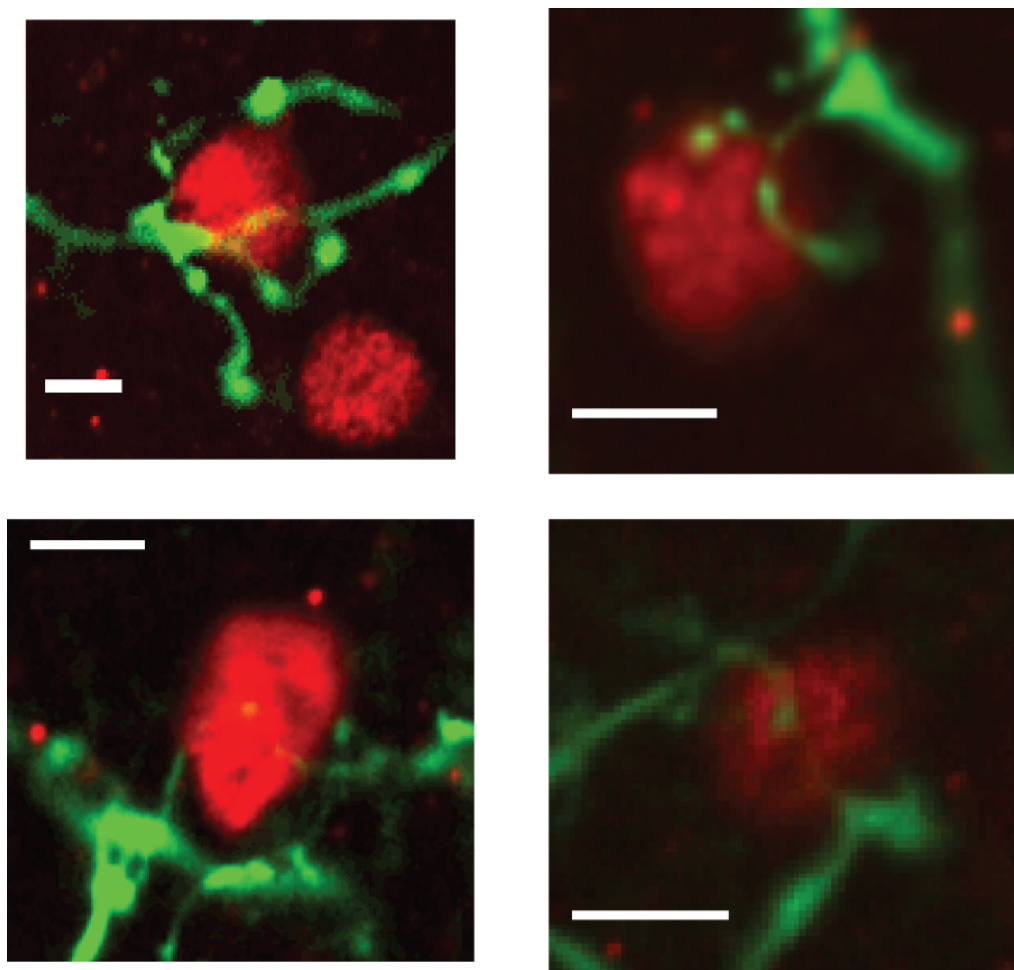
Figure 38 Close up of putative contacts between olivary neurons and oligodendrocytes (scale bar: 5 μm).

Discussion

Coupling in the olive

In accordance with previous studies, (Devor and Yarom, 2002b; Hoge et al., 2011), I have shown that the coupling in the olive is widespread but weak. While subthreshold currents are readily transmitted between cells, the low-pass properties of the coupling filter away the fast spikes. This is contrast to other electrically coupled systems, where fast spikes are transferred as spikelets to neighbouring cells. The ADP and rebound currents are filtered

less and could contribute directly to synchronous firing in the olive. Given the low coupling coefficients, it is surprising how efficacious the gap junctions are at synchronizing the subthreshold oscillations (Leznik and Llinas, 2005; Long et al., 2002; Placantonakis et al., 2006).

Spines and the olive

There has been speculation that the spines of olivary neurons allow the synchronization of synaptic input by gap junctions (Kistler and De Zeeuw, 2005). This model requires high (higher than 1 GOhm) resistance spine necks so that the coupled spines can be considered a compartment apart from the dendritic shafts to which they are attached. While it is possible that my staining technique undersamples long spines - olivary neurons are notoriously difficult to stain (Ramon y Cajal, 1911; Ruigrok et al., 1990a) - my data suggests that the majority of spine necks are in fact short, but that there is a large variation. I have shown that both short and long spines can have associated connexin 36 immunopuncta, so that it is probable that both are involved in gap junctions. A recent study examining cx36 immunopuncta found a similar staining pattern to ours, but could not relate this to the dendritic spines since they used viral transfection of Green Fluorescent Protein (GFP) to label the cells, and this did not label the spines (Placantonakis et al., 2006).

The heterogeneity in spine morphologies is puzzling and could perhaps reflect a plastic process (De Zeeuw et al., 2011). In the next chapter I will explore in more depth what this heterogeneity signifies for olivary function.

In the meantime I note that the spine necks could contribute significantly to making the intercellular coupling so weak.

Olivary dendritic contacts

I have shown that olivary dendrites make putative contacts with several elements of the neuropil, namely other olivary dendrites and somas, as well as with oligodendrocytes. While, to my knowledge, the association between dendritic whorls and somata has not been described before, an early ultrastructural study found casual appositions between dendrites and somata in the olive (Sotelo et al., 1974), but failed to find functional specializations at these locations. The authors considered and rejected the possibility that the function of these contacts was to facilitate ephaptic communication. However, given how widespread such contacts are in olivary neurons, and the recent finding that ephaptic communication can play a role in cortical neurons (Anastassiou et al., 2011), I think that this hypothesis needs to be reassessed in the olive.

Dendrodendritic contacts between olivary neurons have been described before at the ultrastructural level (Gwyn et al., 1977; Sotelo and Llinas, 1972). In contrast to the somatic contacts, the dendritic appositions have been shown to be associated with gap junctions. The fact that I found Cx36 immunopuncta associated with dendritic shafts is a confirmation of this. However, much to my chagrin, I do not think it is reliable to infer merely from a dendritic apposition that a gap junction is present, so that new methods will need to be developed to detect the position of a gap junction

during a recording, possibly involving dye coupling or a fluorescent tagging of the connexin molecule.

Finally, I believe my data supports the Scheibels' (Scheibel and Scheibel, 1955) supposition that oligodendrocytes can be contacted by dendritic elements. However, further study is needed to determine whether these putative contacts have a correlate at the ultrastructural level, and what purpose they could serve functionally.

Chapter 4: Modulation of olivary coupling by inhibition

Introduction

The spines of olivary dendrites are arranged in a glomerulus where they form gap junctions (de Zeeuw et al., 1989; Sotelo et al., 1974). The spines receive inhibitory and excitatory synapses at this location (de Zeeuw et al., 1990a). The possible interaction between the chemical and electrical synapses in the glomerulus has been the source of intense speculation and investigation. The inhibitory connection in particular has aroused interest, since it arises in the deep cerebellar nuclei, which, via the olivocerebellar loop, is modulated by the IO itself (De Zeeuw et al., 1998).

The most popular theory is that the main function of the inhibitory connection is to uncouple olivary neurons by shunting the inter-cellular current between them. This mechanism was first proposed and demonstrated in the buccal ganglion of the teleost fish (Spira and Bennett, 1972) and then later suggested for the inferior olive (Llinas, 1974). The most compelling evidence for this shunting hypothesis comes from an elegant set of studies showing that blocking GABA receptors in the IO increases complex spike synchrony in the cerebellar cortex (Lang, 2002; Lang et al., 1996). Lesioning the dentate nucleus – a source of inhibitory fibres to the IO - also increases synchrony (Lang et al., 1996). Most recently, it was shown *in vivo* that decreasing simple spiking in Purkinje cells in a patch of cerebellum also decreases complex spike synchrony in that patch, presumably by decreasing the DCN mediated inhibition onto the IO (Marshall and Lang, 2009). In slice,

local puffing of GABA in the neuropil suppresses subthreshold oscillations in olivary neurons (Devor and Yarom, 2000). This indirect evidence is held by some to vindicate the shunting hypothesis (Jacobson et al., 2008), despite objections that the main role of inhibition mediated by the deep cerebellar nuclei must be other than just regulating olivary synchrony (Bengtsson and Hesslow, 2006).

Furthermore, the anatomical picture is more complicated than the simple caricature presented above. First of all, while gap junctions do form between spines, they are also present on dendritic shafts (as my staining from the last chapter suggests; but see also (Gwyn et al., 1983; Sotelo et al., 1974)). It is unclear what the relative importance of these locations is. Moreover, while every spine receives inhibitory input, there is also inhibitory input at the soma, and on dendritic shafts (Devor et al., 2001). In this chapter, I will combine pharmacological experiments with theoretical arguments and modelling to assess the shunting hypothesis.

Results

Inhibition can decrease synchrony without affecting coupling

The experiments described above (Lang, 2002; Lang et al., 1996) have shown that complex spiking synchrony is increased by blocking inhibition at the level of the IO. Does this provide compelling evidence to support the shunting hypothesis?

I built a simple coupled two-neuron model to test this conclusion (Figure 39). The neurons were modelled as indentical integrate-and-fire cells. Both cells were injected with uncorrelated white noise current to generate spontaneous

spiking. The cells were connected by a conductance to mimic electrotonic coupling. As expected, increasing the coupling conductance caused spiking synchrony and the zero-lag crosscorrelation coefficient of the subthreshold membrane traces to increase (Figure 39C).

For a fixed coupling conductance (set to 50% of the input conductance of the uncoupled cells), the cells were then both injected with a negative current to represent subtractive (i.e. non-shunting) inhibition. As the amplitude of inhibition was increased, spike synchrony decreased. However, the cross correlation between the subthreshold membrane potentials of the cells remained constant (Figure 39D). In other words, the cells were coupled, but desynchronized at the level of spiking. Note that I used the same measure of synchrony as is commonly used in the field, namely the normalized cross-correlation coefficient of the spike bins, which is insensitive to the mean firing rate of the cells (see methods chapter for details). It is also easy to construct a converse example, namely two cells which are uncoupled, but synchronized, if they receive common synaptic input driving their spiking.

As this simulation makes clear, the experiments showing modulations in complex spike synchrony (e.g. (Lang, 2002; Lang et al., 1996; Schultz et al., 2009; Welsh et al., 1995)) are at best imperfect guides to the effective connectivity of the olivary network.
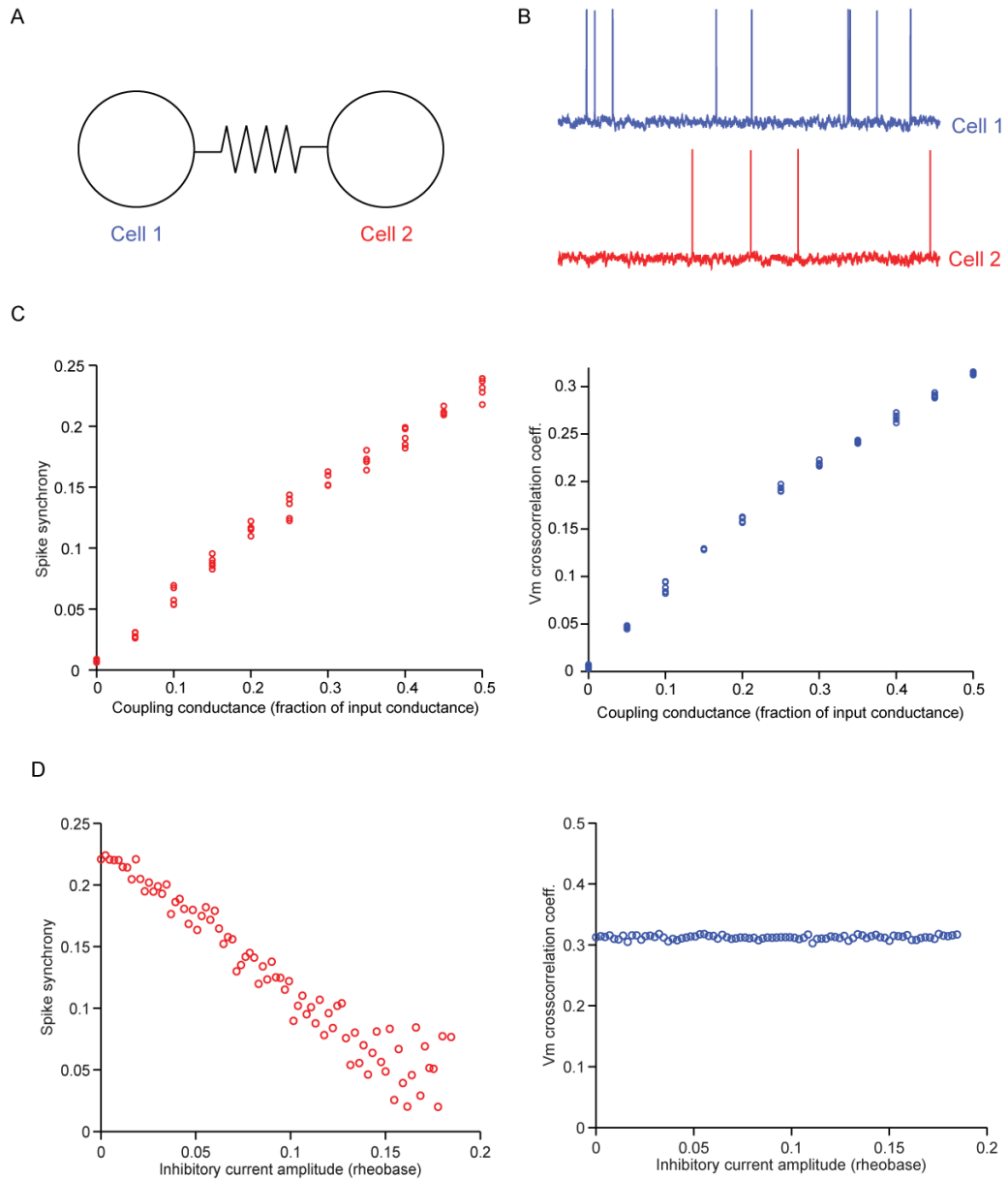
Figure 39 A simple model of synchrony and coupling. A) Two identical integrate and fire neurons are reciprocally connected by a resistor and are each injected with a different subthreshold current (white noise with variance 1.5% of rheobase). **B)** Sample spiking patterns from both cells in response to white noise current injection. **C)** Increasing the coupling between the cells increases the cross-correlation of their membrane voltage (right panel) and the normalized synchrony of their spike output (left panel) **D)** Steady state subtractive inhibition is added to both cells with the coupling conductance fixed at 50% of the input conductance. The spike synchrony goes down (left panel) while the membrane potential cross-correlation remains constant.

GABA-A receptor activation decreases coupling between olivary neurons

To directly test the hypothesis that inhibitory input can uncouple olivary neurons, I obtained paired recordings from coupled olivary neurons, using negative current pulses (-800pA, 200-300ms) to monitor their electrotonic coupling for a baseline period of 2-3 minutes before washing in muscimol, an agonist for the GABA-A receptor. I recorded from 8 pairs, divided in two groups of 4 pairs treated with 10 and 20 μM muscimol (Figure 40).

I collected baseline properties for both groups. The coupling coefficients were 0.015±0.005 and 0.014±0.006, the coupling conductances were 424±100pS and 303±105pS, the resting membrane voltages were -58±2mV and -54±2mV, and the input resistances were 43±5MΩ.

As expected from activation of GABAergic synapses, after wash-in of muscimol, the cells hyperpolarized (by 6±2mV (P=0.03), and 5±2mV (P=0.018)), and the input resistance reduced by 6±8% and 6.5±7.5% (although this reduction was statistically not significant - P=0.39 and P=0.40 respectively). The coupling coefficients dropped in both groups after wash-in of muscimol by 47±14% (10 μM muscimol, P=0.03) and 68±11% (20 μM muscimol, P=0.005), while the coupling conductances dropped by 45±11% (P=0.017) and 63±15% (P=0.015) respectively.
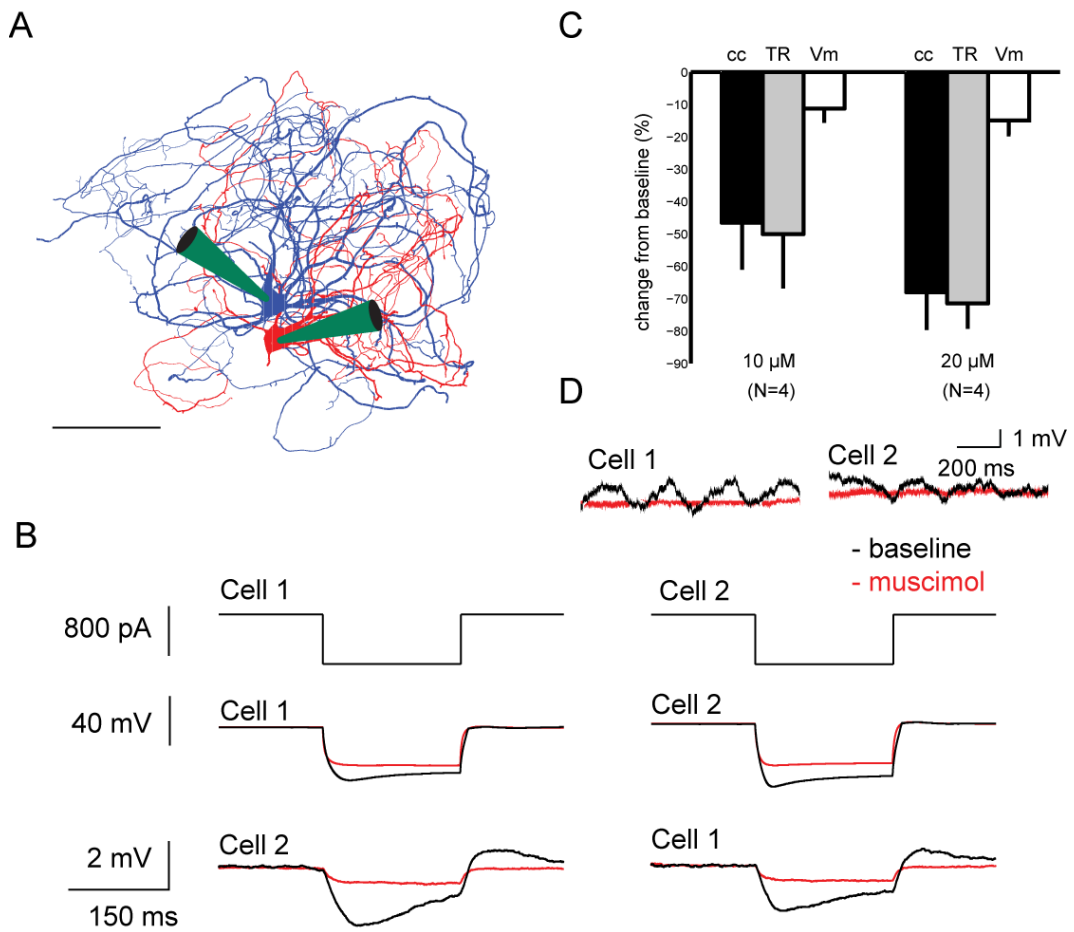
Figure 40 Pharmacological uncoupling of olivary neurons by GABA-A receptor activation. A) Paired recordings were obtained from olivary neurons (scale bar: 40μm). B) Coupling was assessed by injecting negative current pulses in both cells. Traces before (black) and after (red) bath application of 10 μM muscimol. C) Summary data for 10 μM and 20 μM muscimol cc: coupling coefficient, TR (see Appendix for definition): transfer resistance Vm: membrane voltage. D) Synchronized subthreshold oscillation in another pair before (black trace) and after wash-in of muscimol (red trace).

Note that this decrease cannot simply be accounted for by the reduction of input resistance as seen at the soma, since a purely somatic reduction in input resistance would not affect the coupling coefficient - it would reduce both the prejunctional and postjunctional voltage deflection in response to the test pulse in equal proportion. While the subthreshold oscillations were

not stable enough to study in most pairs, one pair was stably oscillating at 2Hz prior to wash-in of muscimol (Figure 40D). The oscillation was undetectable after muscimol was washed-in.

While these pharmacological experiments provide the first direct evidence in favour of the shunting hypothesis, the global activation of GABA-A receptors means that the effect could be unspecific or unphysiological.

I therefore attempted to support these results with more targeted experiments. As discussed in the last chapter, I do not think the morphology of the cells alone is sufficient to allow the localization of gap junctions connecting two pairs, precluding the option of puffing, iontophoresis or uncaging, each of which would constitute a more refined experiment to the one presented.

Using synaptic stimulation, I was able to evoke inhibitory events similar to those seen by a recent report (Best and Regehr, 2009), however only in voltage-clamp with a high-chloride cesium based internal (see Figure 41). The dubious space-clamp and the uncertainty about the location of the synapses stimulated (a factor I will show in the next sections to be of crucial importance) make this experiment unsuited to test the hypothesis. In the rest of the chapter, I will employ theoretical and modelling arguments to better understand synaptic shunting of coupling in olivary neurons.
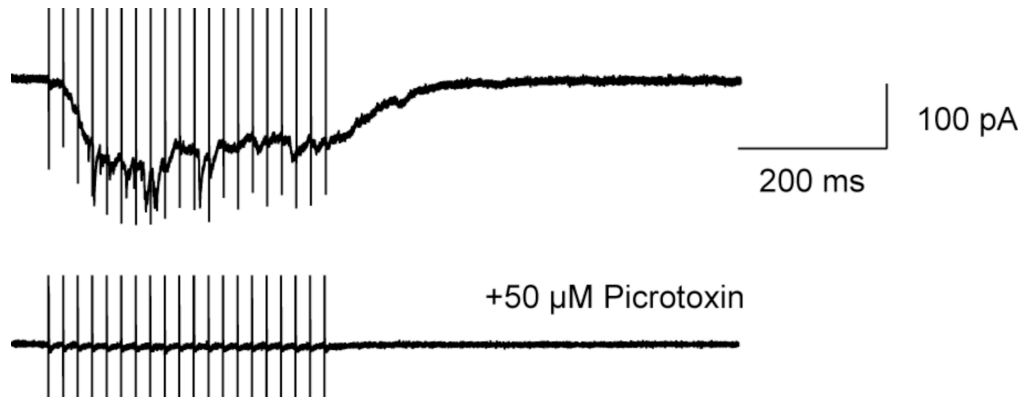
Figure 41 Synaptic inhibition in the olive. Top trace: Evoked synaptic currents in the presence of 100 mM kynurenic acid. The cell was held at -60 mV and the synapses stimulated at 50 Hz. Note that the currents are inwards because I used an internal solution with a high-chloride reversal potential. Bottom trace: The currents are blocked by application of 50 µM picrotoxin.

A simple model of synaptic uncoupling of neurons
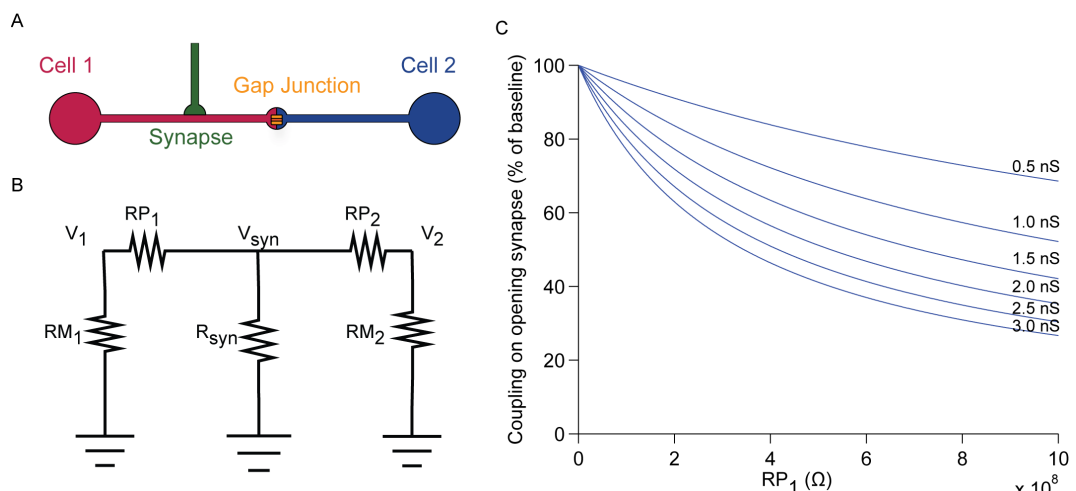
Figure 42 A simple model of synaptic uncoupling of electrically coupled cells. A) A cell is connected to another cell via a gap junction at the tip of their dendrites. A synapse is placed along the dendritic path B) Equivalent circuit C) Relative coupling conductance for different strengths of the shunting synapse as a function of the path resistance up to the shunting synapse (with RP2=10 GΩ, representing a typical gap junction resistance).

114

To provide a quantitative description of synaptic uncoupling of olivary neurons, I first consider a simple model of a coupled pair of neurons (Figure 42). The neurons are each represented by a resistor (RM_1 and RM_2), and are connected via two resistors (RP_1 and RP_2) between which is located the shunting synapse R_{syn}. Note that the sum of RP_1 and RP_2 represents the whole of the resistance of the dendritic path and gap junction connecting the two cells. One can calculate two measures of coupling as a function of the strength of the shunting synapse (For derivations of these formulae, see Appendix 2 of this chapter):

$$cc_1(g_{syn}) = ((\frac{RP_2 + RM_2}{RM_2})(1 + g_{syn} \times RP_1 + \frac{RP_1}{RP_2}) - \frac{RP_1}{RP_2})^{-1} \qquad (1)$$

$$g_c(g_{syn}) = (RP_1 + RP_2 + g_{syn} \times RP_1 \times RP_2)^{-1} \qquad (2)$$

I continue the analysis with the latter measure (Bennett, 1966). One can compute the relative change in coupling when the synapse is active as follows.

$$\frac{g_c(g_{syn})}{g_c(0)} = (1 + g_{syn} \frac{RP_1 \times RP_2}{RP_1 + RP_2})^{-1} \qquad (3)$$

This expression decreases with increasing RP_1, RP_2 and g_{syn}, showing that the path resistances and the shunting synaptic strength all contribute to the efficacy of synaptic uncoupling.

The question arises where the synapse should be placed in order to get the most uncoupling. Setting

$$RP_1 = \alpha \times RP_{tot} \text{ and } RP_2 = (1-\alpha) \times RP_{tot}$$

where $RP_{tot} = RP_1 + RP_2$ and $\alpha \in [0,1]$

(3) becomes:

$$\frac{g_c(g_{syn})}{g_c(0)} = (1 + g_{syn}RP_{tot}\alpha(1-\alpha))^{-1} \qquad\qquad (4)$$

This expression has a minimum at $\alpha = 0.5$. In other words, the best place for synaptic input to uncouple cells is the point along the path that equalizes RP_1 and RP_2. Surprisingly, this is not necessarily in the vicinity of the gap junction.

 I found that if I made the dendritic resistance symmetric on either side of the gap junction (Figure 43), then the best location was next to the gap junction. However, if the dendrites didn't taper, I found the location dependence to be relatively shallow (Figure 43A), echoing the "on-the-path" theorem for the interaction between excitatory and inhibitory synapses (Koch et al., 1982, 1983). If the dendrites taper, so that the path resistance increases supralinearly with distance along the dendrite, the location dependence is made considerably sharper (Figure 43B). In general, when dendritic paths are asymmetric, the optimal position will be along the dendrite that accounts for most of the total path resistance (Figure 43C).
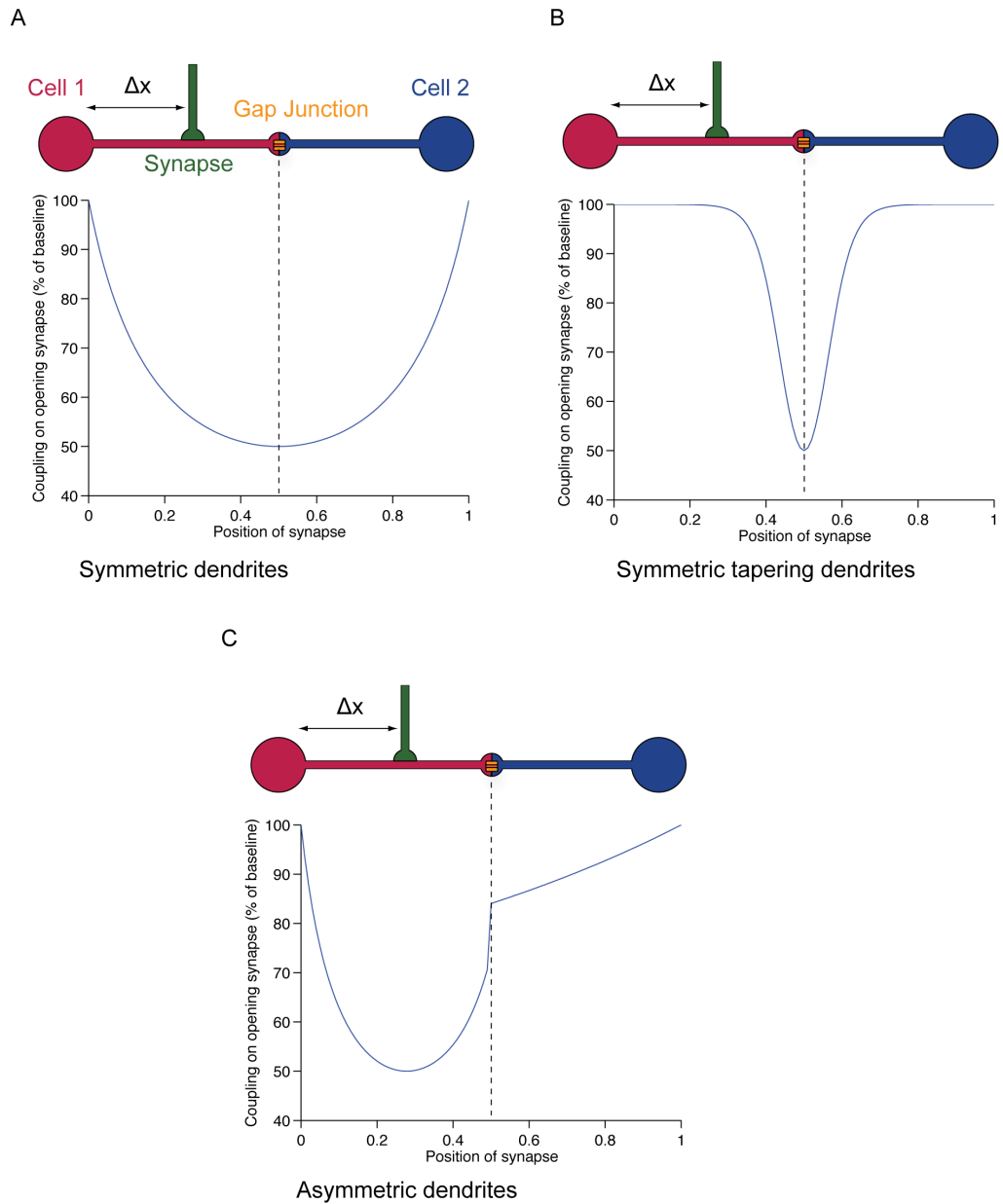
Figure 43 Optimal location of chemical synapse to uncouple cells depends on dendritic morphology. A) Both dendrites are symmetric cables B) Both dendrites are symmetric, but their diameters reduce towards the tips C) The left dendrite is a cable with a smaller diameter than the right diameter. In these examples RP_{tot} is set to 2 GΩ and g_{syn} to 2 nS.

To get an impression of the magnitude of the effect with physiological parameters (Figure 42B), I first set $RP_1 = R_{dendrite1} + R_{spine1}$ and $RP_2 = R_{dendrite2} + R_{spine2} + (g_{GJ})^{-1}$. This second expression is dominated by $(g_{GJ})^{-1}$

since the values reported in the literature are in the 10 GΩ range (Hoge et al., 2011; Srinivas et al., 1999; Vervaeke et al., 2010). The first expression depends critically on the spine neck resistance - a parameter that has been notoriously difficult to pin down (Araya et al., 2006; Bloodgood and Sabatini, 2005; Grunditz et al., 2008; Palmer and Stuart, 2009; Svoboda et al., 1996). Depending on the reports, the spine neck resistance is said to vary from around 5 MΩ to 5 GΩ - three orders of magnitude. As I have shown in the previous chapter, the dendritic spines of rat IO neurons involved in gap junctions have very heterogeneous morphologies, and it is therefore likely that their resistance is equally variable. In the cat, olivary neurons have remarkably long spines and therefore probably resistances on the upper end of the estimates above (de Zeeuw et al., 1990b).

Recently, the DCN to IO synapse has been characterized (Best and Regehr, 2009). These authors recorded synaptic currents in rat olivary neurons in voltage clamp, and show traces from a cell with mIPSCs ranging from 20 to 70pA with a driving force of 70mV, which corresponds to a g_{syn} of 0.2 to 1nS. They also show that the synapse facilitates considerably with repeated stimulation. Furthermore, it is quite likely that, because of space clamp issues, the conductance is underestimated, so that it is reasonable to assume an upper bound of 3 nS for this synapse.

I note a further feature of the model: A nonzero E_{rev} for the synapse would not affect the junctional conductance between the cells, but merely add an offset to the somatic voltages (this can be seen in the Y-Δ transform

employed to derive the formula). As a consequence, it is equally valid for inhibitory and excitatory synapses.

Input resistance decrease due to synaptic activation

Apart from decreasing the coupling conductance, activating the synapse will also cause the input resistance as viewed from both somas to change. If R_{11} and R_{22} are the input resistances of the cells, then we have

$$R_{11} = \frac{R_a(R_c + R_b)}{R_a + R_c + R_b}$$

$$R_{22} = \frac{R_b(R_c + R_a)}{R_a + R_c + R_b}$$

Where R_c is as above and

$$R_a = \frac{R_\alpha \times RM_1}{R_\alpha + RM_1}$$

$$R_b = \frac{R_\beta \times RM_2}{R_\beta + RM_2}$$

$$R_\beta = \frac{R_{syn} \times RP_1 + R_{syn} \times RP_2 + RP_1 \times RP_2}{RP_1}$$

$$R_\alpha = \frac{R_{syn} \times RP_1 + R_{syn} \times RP_2 + RP_1 \times RP_2}{RP_2}$$

We plot (Figure 44) how the input resistance in the cell changes as a function of increasing RP1 (in other words, as the synapse is placed more distally), with physiological parameters (RM$_1$=RM$_2$=50MΩ, RP$_2$=10GΩ). Because the gap junction has a very high resistance, the postjunctional cell does not see the synaptic conductance. The prejunctional cell sees a subtle change in input resistance, especially when the synapse is proximal. In other words, the synaptic shunt will cause a symmetric decrease in coupling conductance, and an asymmetric decrease in input resistance (and therefore also the coupling

coefficient). The extreme example of this is a synapse at one of the somas, which will not affect the coupling conductance at all, but will change the input resistance of the cell.
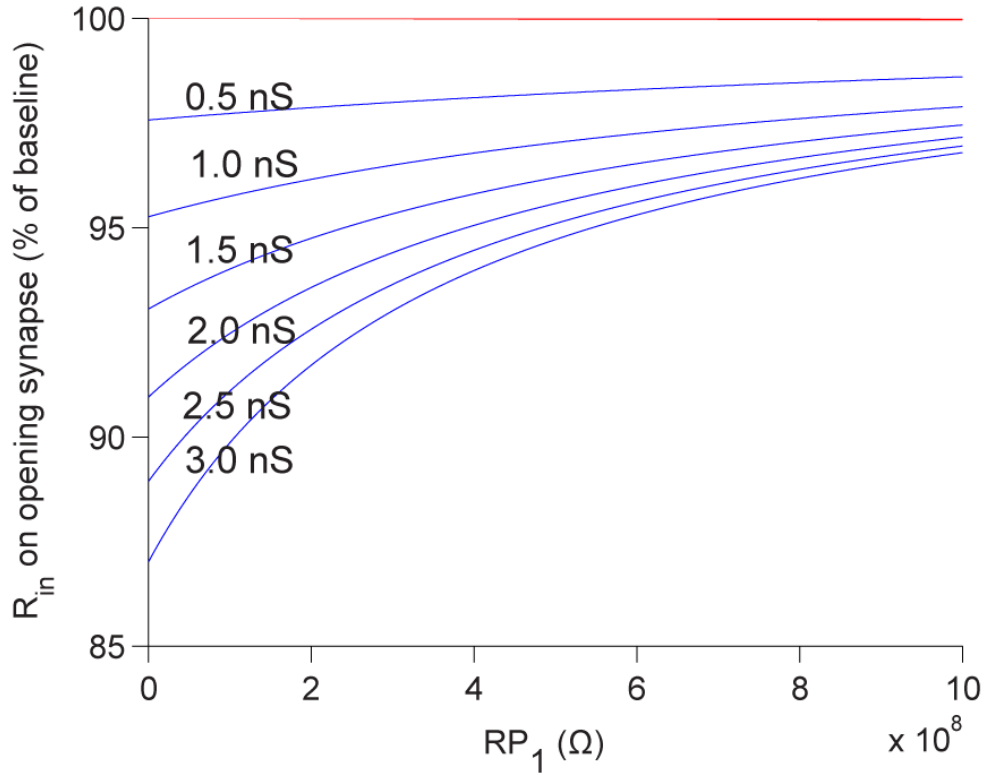
Figure 44 Input resistance decrease due to synaptic activation: The input resistance of the prejunctional (blue traces) and postjunctional (red traces) cells is plotted as a function of the shunting synapse. Note that the postjunctional cell's input resistance hardly changes ($RM_1=RM_2=50M\Omega$, $RP_2=10G\Omega$).

The effect of multiple gap junctions

In general, the two cells will be connected by multiple gap junctions along several dendritic paths. If one assumes that each gap junction has an associated synapse and that they are on parallel paths, the junctional conductance between the cells then becomes

$$g_c(g_{syn1},...,g_{synN}) = \sum_{1}^{N}(RP_{1,i} + RP_{2,i} + g_{syni} \times RP_{1,i} \times RP_{2,i})^{-1}$$

120

Where N is the number of gap junctions.

To simplify the analysis, I assume that all the paths have the same resistance $RP_{1,i}=RP_{2,i}=RP$ and that all the synapses are either on or off, and have the same maximal conductance g_{syn}. One can then express the junctional conductance between the cells as a function of the proportion synapses activated $\eta = \dfrac{n}{N}$:

$$\frac{g_c(\eta)}{g_c(0)} = \frac{(2 + g_{syn} \times RP) - \eta \times g_{syn} \times RP}{(2 + g_{syn} \times RP)}$$
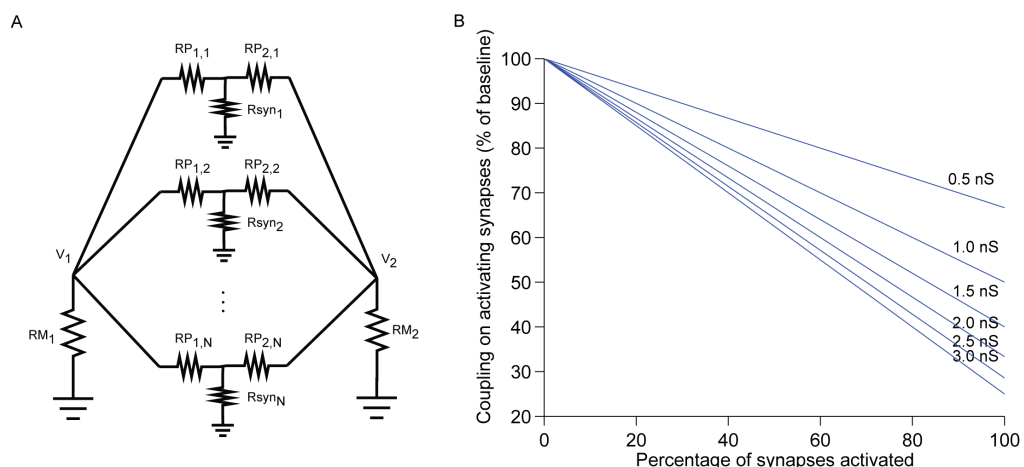
Figure 45 Uncoupling with multiple parallel paths coupling cells A) Circuit diagram: Two cells are connected by N gap junctions associated to as many shunting synapses B) Coupling conductance as a function of percentage of synapses activated when the paths are identical for synapses of different magnitude. (RP$_{1,i}$=RP$_{2,i}$=2GΩ; g$_{syn1}$=g$_{syn2}$=2 nS).

This expression is linear in η, which shows that the amount of uncoupling achieved is in direct proportion to the number of synapses activated (Figure 45). Therefore, for connected cells with many parallel paths between them, synchronous inhibitory input at the relevant glomeruli may be required to uncouple the cells in a significant way.

Transient analysis

The previous sections dealt with steady state properties of the cells. I now extend the model to understand how time varying signals are transmitted in the network. I therefore have to take into account the capacitance of the cells, C_1 and C_2.
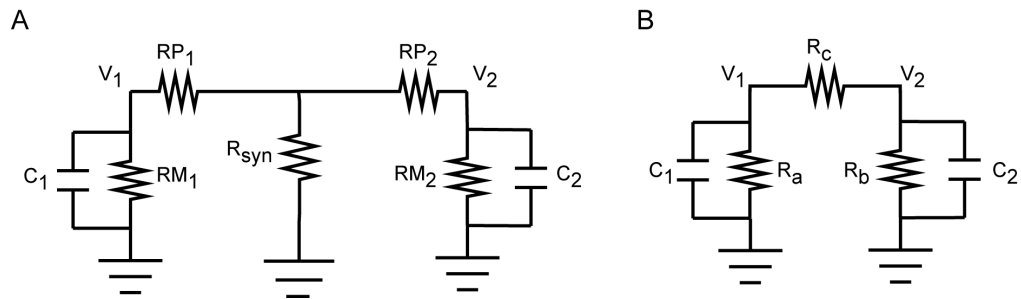
Figure 46 Simple model with transient properties A) the simple model is modified to account for capacitive effects. B) Same circuit after Y-Δ transformation.

Let's assume the first cell's voltage is clamped, and that the output is measured at the second cell.

Using Kirchhoff's laws, one find the equation for this network is

$$\frac{V_1 - V_2}{R_c} = \frac{V_2}{R_b} + C_2 \times \frac{dV_2}{dt}$$

(5)

where

$$R_c = \frac{R_{syn} \times RP_1 + R_{syn} \times RP_2 + RP_1 \times RP_2}{R_{syn}}$$

$$R_b = \frac{R_\beta RM_2}{R_\beta + RM_2}$$

$$R_\beta = \frac{R_{syn} \times RP_1 + R_{syn} \times RP_2 + RP_1 \times RP_2}{RP_1}$$

then the solution to equation 5 is given by

$$V_2(t) = \exp(-\int_0^t \tau^{-1}d\theta) \times \int_0^t \frac{V_1}{R_c C_2} \times \exp(\int_0^\sigma \tau d\theta)d\sigma$$

(6)

where

$$\tau(t) = \frac{R_b R_c C_2}{R_b + R_c}$$

(7)

can be recognized as an instantaneous time constant. It sets the time in which the second neuron integrates signals from the first neuron. Equation 6 reveals that, for time varying signals, the shunting synapse can change both the magnitude and temporal window of coupling.
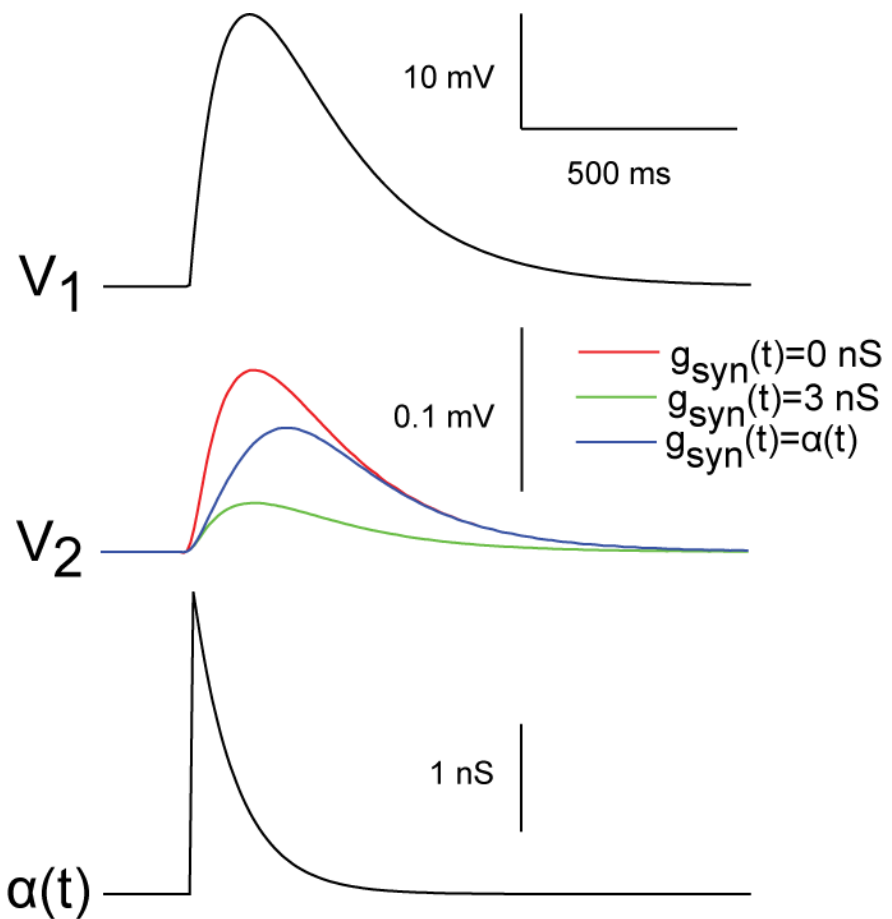
Figure 47 Dynamic effects of synaptic uncoupling. The first cell is clamped to have biexponential voltage waveform (top trace). The response in second cell is shown when the synapse is off, tonically on, or transient (red, green and blue middle traces respectively). The synaptic transient used is an alpha function (bottom trace). RP_1 is set to 1 GΩ, RP2=10 GΩ.

As can be seen in Figure 47, the effect of shunting a prejunctional voltage with a time varying synapse can have the effect of introducing a phase delay as well as reducing the amplitude of the coupled current. If both the somatic voltage and synaptic conductance were oscillating, it is possible to get amplitude modulated oscillations (Figure 48), which is a pattern occurring spontaneously in olivary neurons (Devor and Yarom, 2002c).
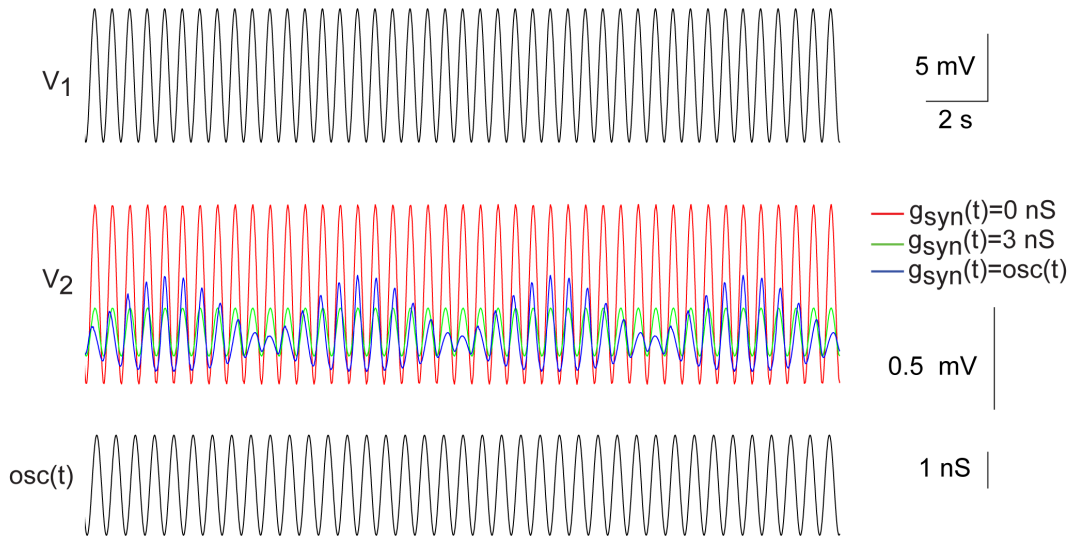
Figure 48 Modulation of oscillations by inhibition: V1 is a sinusoid with a frequency of 10 Hz (Top trace). When the shunting synapse is an 11 Hz sinusoid (bottom trace), the coupled cell sees an amplitude-modulated sinusoid (middle trace). RP$_1$ is set to 1 GΩ, RP2=10 GΩ.

Stochastic properties of the coupling conductance

Best and Regehr (Best and Regehr, 2009) have shown that the release properties of the DCN-IO synapse are quite remarkable: when stimulated, the synapse has practically no synchronous component, but instead a sustained increase in asynchronous release probability. The authors interpreted this as being ideal for shunting intercellular currents, because when the synaptic currents are averaged over trials, they give the impression of providing a sustained conductance, in a similar way to a tonic synapse.

However, in actual fact, such asynchronous release means that the shunting conductance is extremely variable from trial to trial. In models of spiking neurons, the conductance distribution can drastically affect information processing (Richardson and Gerstner, 2005; Volman et al., 2010). To capture this, one can model the synaptic conductance as a stochastic process. As a

consequence, the coupling conductance becomes a derived stochastic variable, and equation (5) becomes a stochastic differential equation

In response to repeated high-frequency stimulation, (a regime that GABAergic DCN neurons seem to operate in (Uusisaari et al., 2007)), the DCN-IO synapse releases at a constant sustained rate (Best and Regehr, 2009). I therefore modelled the occurrence of synaptic events as a Poisson process. Each synaptic event was modelled as a biexponential conductance with a rise time of 0.6ms and a decay time of 6 ms, in accordance with the miniature EPSCs shown in (Best and Regehr, 2009), using release rates in the 0-100Hz range (Figure 49).

I found that the statistical properties of the coupling conductance changed drastically as a function of the synaptic event rate (Figure 50). For low frequencies (<30 Hz), the coupling conductance was sharply peaked at the maximum conductance (corresponding to the situation where the shunting synapse is silent), with a uniform tail distribution. For higher frequencies, a peak appears in the left of conductance distribution with a right skew. The peak increases in importance with the higher frequencies. The mean and variance of the distribution are shown for different frequencies in Figure 51.

One can derive a functional form for the coupling conductance at high event frequencies: It has been shown (Destexhe et al., 2001; Lansky and Lanska, 1987) that a Gaussian model for fluctuating synaptic conductances is adequate to capture the dynamics of real synaptic conductances when event

frequencies are high enough (although see (Richardson and Gerstner, 2006)).

In other words g_{syn} is a stationary stochastic process with density function:

$$P(g_{syn}) = \frac{1}{\sqrt{2\pi\sigma_{syn}^2}}\exp(-\frac{(g_{syn} - \overline{g}_{syn})^2}{2\sigma_{syn}^2})$$

(8)

Where $\overline{g}_{syn}$ is the mean conductance, σ_{syn} is its variance.

Then one can compute the density of the coupling conductance by a change of variable with equation 2, g_c is also a stationary stochastic process with the following density equation:

$$P(g_c) = \frac{1}{g_c^2\sqrt{2\pi \times RP_1^2 \times RP_2^2 \times \sigma_{syn}^2}}\exp\left(-\frac{\left(\frac{1}{g_c} - (\overline{g}_{syn} \times RP_1 \times RP_2 + RP_1 + RP_2)\right)^2}{2 \times RP_1^2 \times RP_2^2 \times \sigma_{syn}^2}\right)$$

(9)

In Figure 50D, the coupling conductance distribution is plotted for a shunting event frequency of 100Hz. Equation 9 gives a good fit to this right-skewed peaked density . The fact that a single peaked distribution is only a good fit at high synaptic event frequencies indicates that it is only at these frequencies that the shunting is comparable to a tonic conductance.
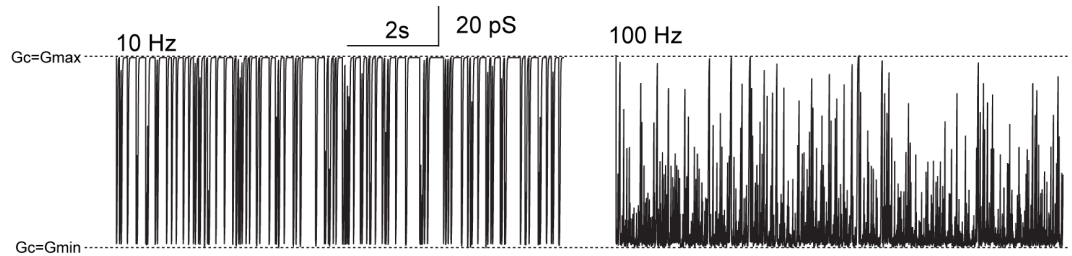
Figure 49 Time course of coupling conductance between two cells with a Poisson train of shunting events into the chemical synapse: the statistical properties of the conductance change markedly between low (10 Hz, left trace) and high event frequency (100 Hz, right trace) ($RP_1=0.2G\Omega$; $RP_2=10G\Omega$; $g_{syn}=1$ nS).
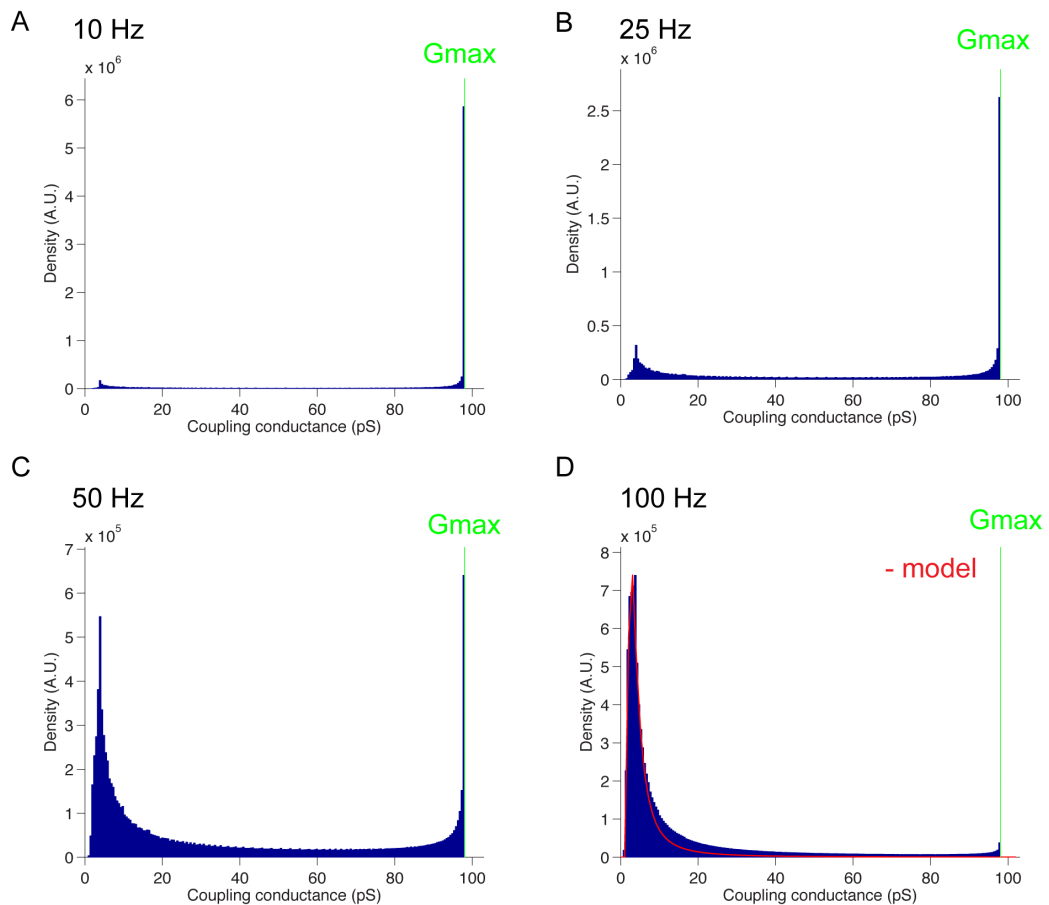
Figure 50 Coupling conductance distributions for four synaptic event frequencies: A) 10 Hz, B) 25 Hz , C) 50 Hz D) 100 Hz. For the 100 Hz condition I have plotted the distribution predicted in the text by the Gaussian synaptic conductance model (red trace). ($RP_1=0.2G\Omega$; $RP_2=10G\Omega$; $g_{syn}=1$ nS).

A   B
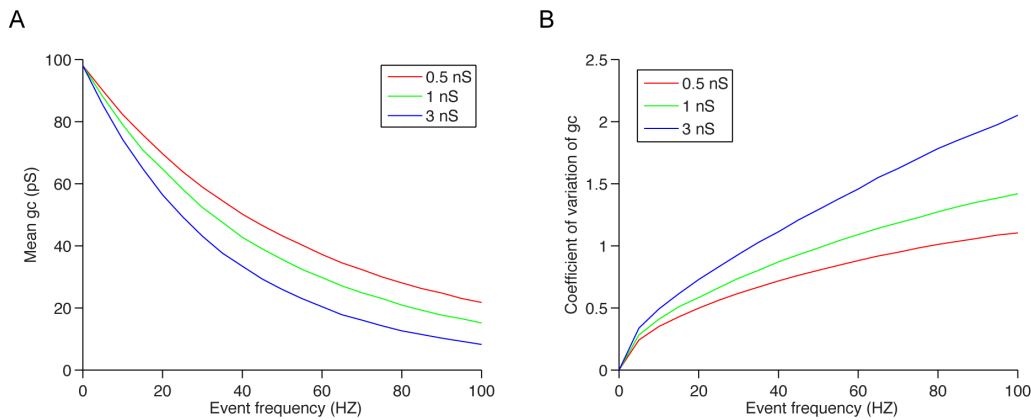
Figure 51 Statistical properties of the coupling between two cells as a function of the shunting event frequency A) Mean and B) Coefficient of variation of coupling conductance distribution for increasing frequencies of shunting events with a Poisson model (RP$_1$=0.2GΩ; RP$_2$=10GΩ; g$_{syn}$=1 nS).

Compartment model from neuronal reconstruction

The simple models I have just discussed have revealed some general principles of uncoupling by inhibition. It is however important to validate them with realistic morphologies. To this end, I reconstructed an olivary neuron that was filled with an intracellular dye (AlexaFluor 488, 200µM) and imaged on a two-photon laser-scanning microscope. The neuron was of the curly morphology (see introductory chapter). Following (Roth and Hausser, 2001), I injected short pulses (1ms, 600 pA) in current clamp and recorded the resulting voltage trace. I loaded the morphology into the Neuron simulation environment (Hines and Carnevale, 2001), and fit the intrinsic parameters of the cell to reproduce the transient obtained in the experiment (Figure 52). The procedure converged on specific capacitance of 0.79 µF/cm2, and membrane resistance of 4583Ω.cm^2 and an axial resistivity of 140 Ω·cm.
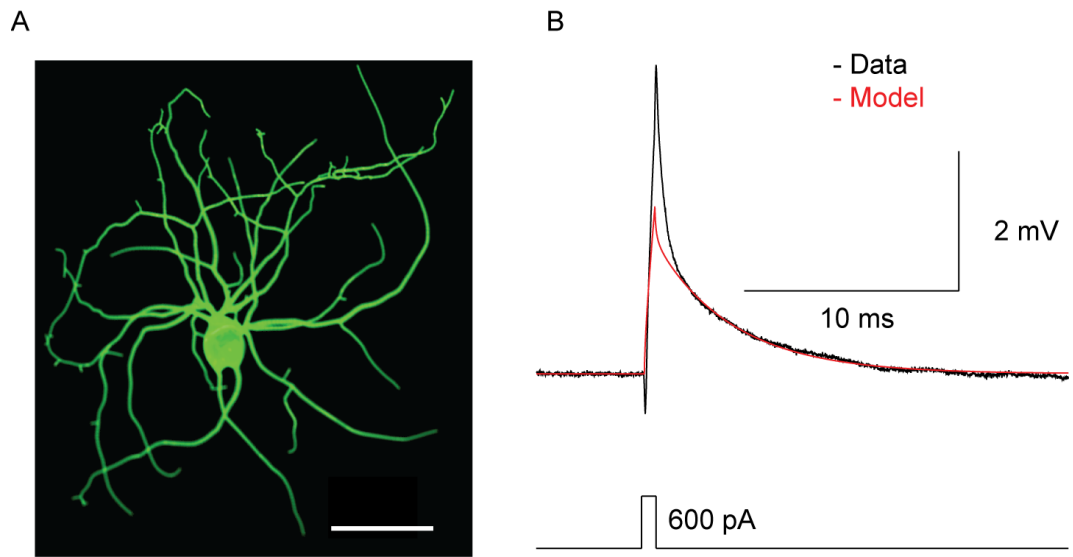
Figure 52 A compartment model from a filled olivary A) Three dimensional rendering of reconstructed olivary neuron (scale bar 50μm) B) The model parameters were optimized to fit the response to a current pulse (0.5 ms, 650 pA, average of 25 traces).

Inhibitory uncoupling with single synapses

I modelled coupling in olivary neurons by connecting two neurons by a gap junction on a dendritic spine (consisting of a head and neck compartment of varying diameter) (Figure 53). The gap junction was modelled as a simple conductance of 100 pS. The inhibitory synapses were modelled as steady state conductance increases at different locations in the compartment model. I measured the coupling by injecting current in one cell's soma and recording the postjunctional voltage deflection, and then calculating the coupling conductance according to equation 2.
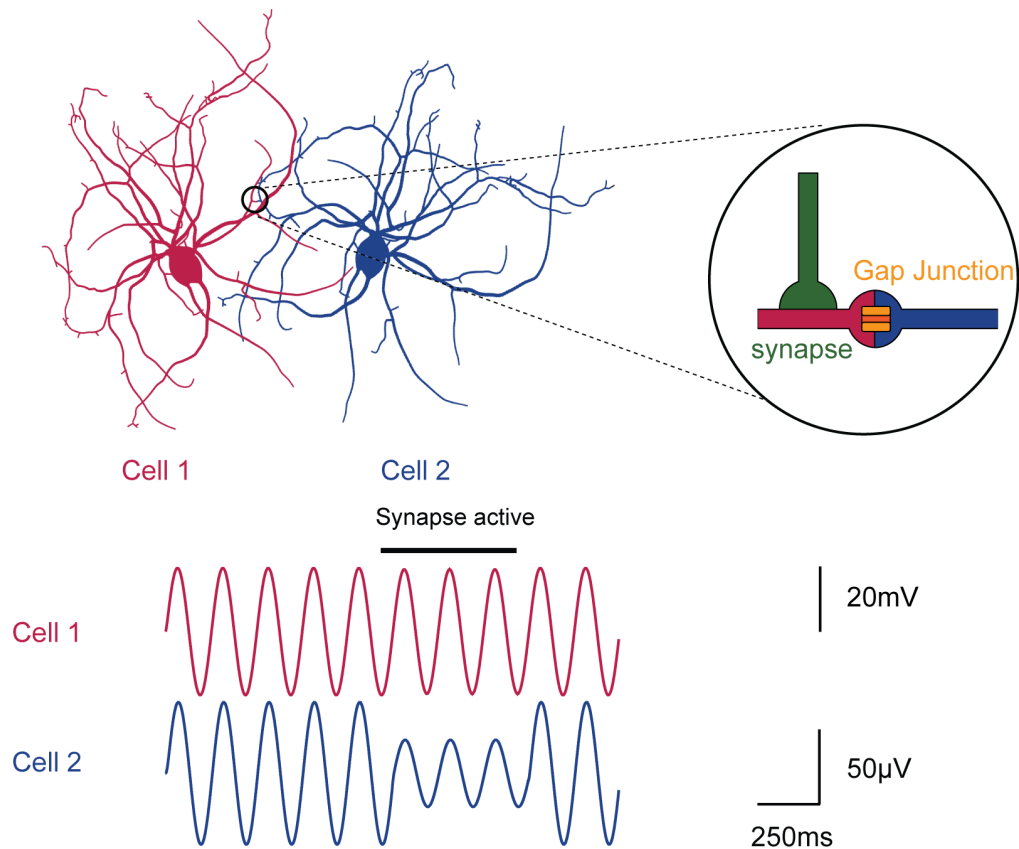
Figure 53 Coupled compartment model of olivary neurons: a gap junction couples the two neurons. A chemical synapse is placed in close vicinity to the gap junction. A sinusoidal current is injected in the first cell and recorded in the second cell. When the chemical synapse is activated, the coupled oscillation is attenuated.

I found I was able to obtain a significant reduction (0-40%) in the coupling conductance by activating single inhibitory synapses in the 1-3 nS range.

I varied the location of the inhibitory synapse. As predicted from the simple model above, I found that the optimal location for uncoupling the cells was close to the gap junction (Figure 54)
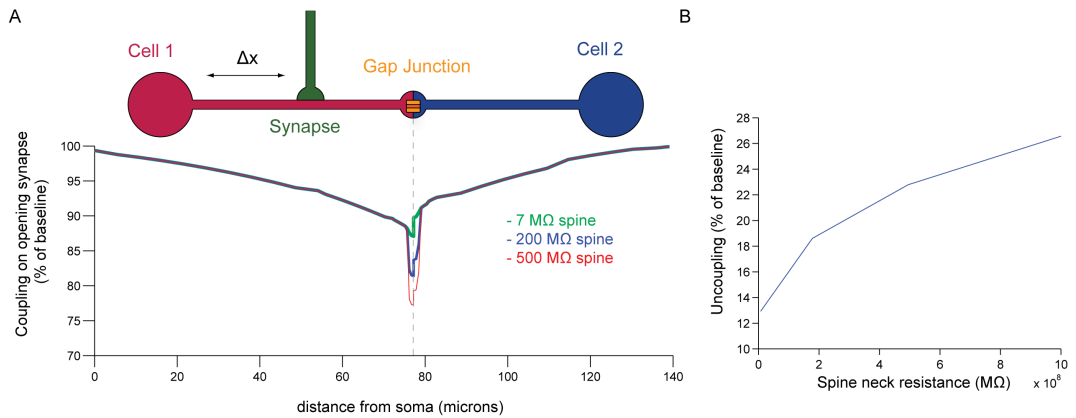
Figure 54 Location dependence of uncoupling in the detailed compartmental model. A) The synapse (3nS conductance) is moved along the path connecting the two neurons. The gap junction is placed between two spines. The relative coupling is plotted as a function of synapse placement for spines of different neck resistance. Note that the spine neck resistance affects both the magnitude (B) and compartmentalization of the uncoupling

I found that, particularly for proximal gap junctions, the spine neck resistance could significantly affect the uncoupling achieved.

To test the specificity of the synapse for the uncoupling, I moved the synapse around the cells (with spine neck resistances set to 200 MΩ) and for each point in the cell plotted the amount of uncoupling achieved by activating the synapse. I found that for low conductances, only on-path synapses were effective in shunting the intercellular current (Figure 55). When I made the synapse stronger, off-path synapses could suck in a significant proportion of the intercellular current, showing that inhibition on the shaft of the dendrite could be effective if only it is strong enough.
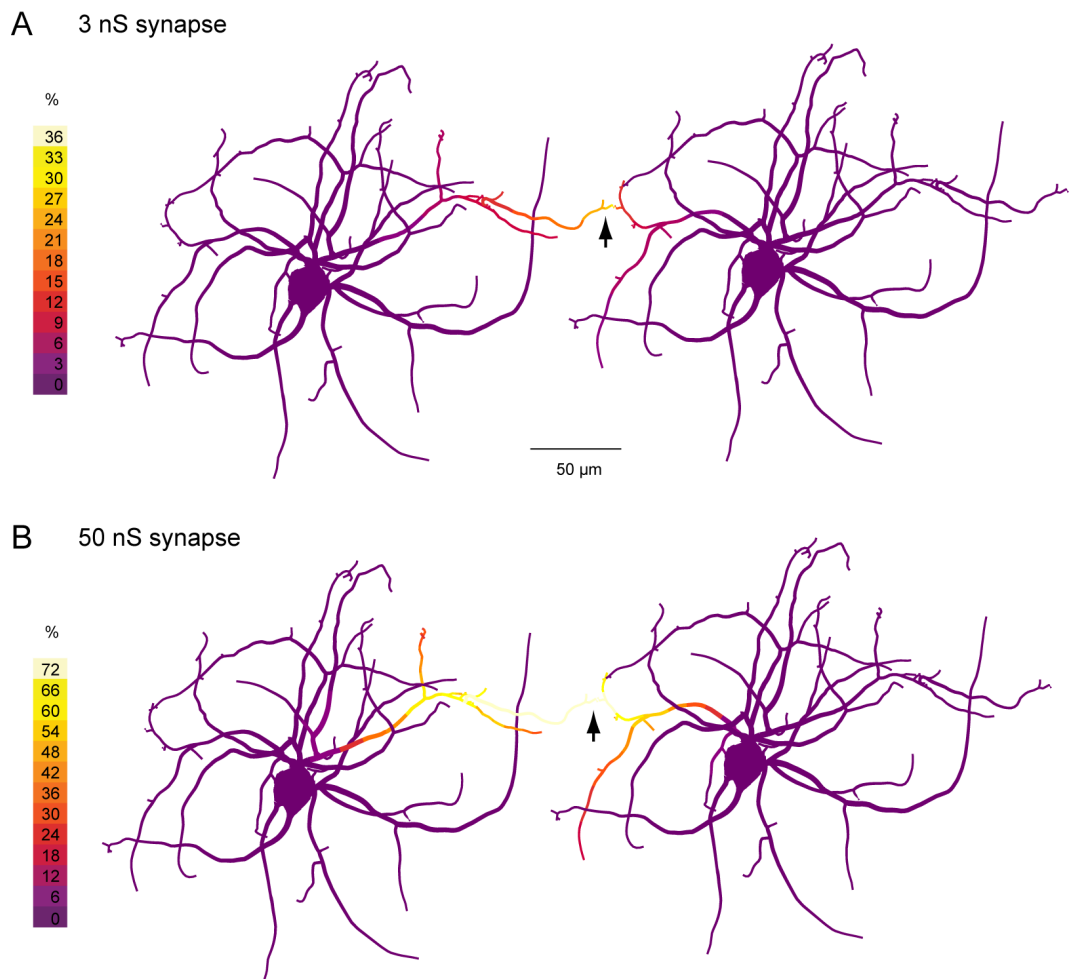
Figure 55 Uncoupling by single synapse: A gap junction links two spines (200 MΩ spine neck resistance) between the two neurons (arrow), and a chemical synapse (3 nS) is moved around the dendritic tree. The colour displays the relative amount of uncoupling (as assessed by the coupling conductance) achieved by activating the synapse. Note that the effect is well compartmentalized for low conductances.

Somatic inhibition was never effective in uncoupling the cells (even with a 200 nS synapse). The reason for this is that the coupling conductance formula corrects for the local input resistance at the site where the coupling is measured. A somatic shunt will act mainly to reduce this input resistance and therefore not affect the coupling conductance (but note it will affect the coupling coefficient markedly in the direction from the non-shunted neuron to the shunted neuron).
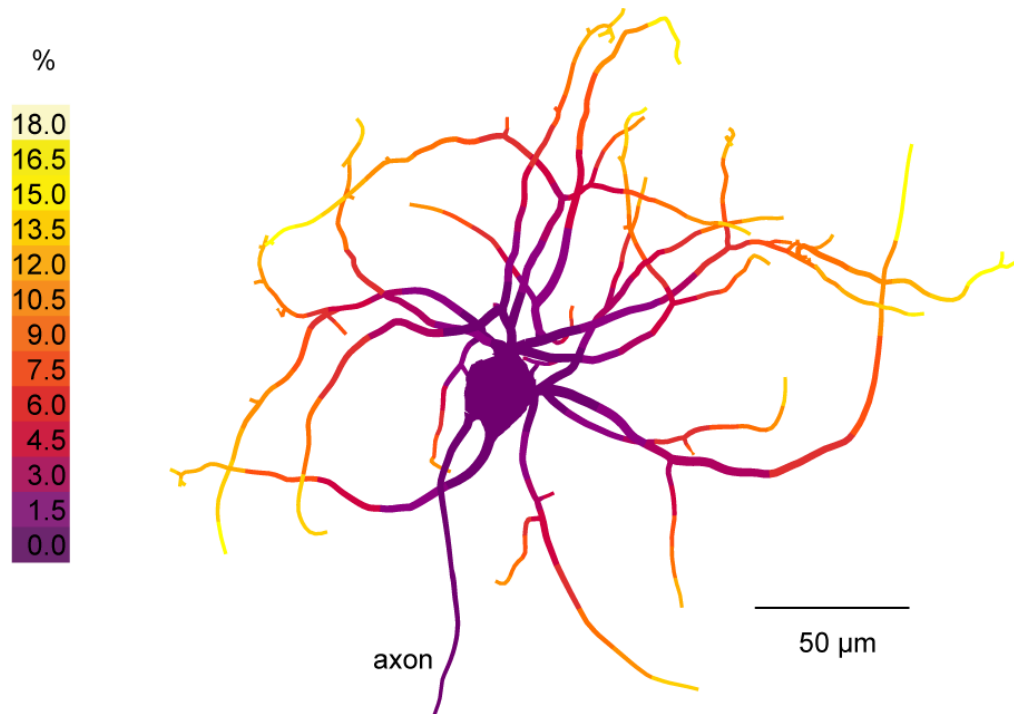
Figure 56 Distal gap junctions are more effectively uncoupled: a spine (200 MΩ spine neck resistance) containing a gap junction and a 3 nS synapse is moved around the cell. The gap junction links the neuron to a spine with (200 MΩ spine neck resistance) on a fixed location on another neuron (not shown). The colour displays the amount of uncoupling evoked by activating the synapse. Note that in proximal locations, the synapse has a negligible effect on the coupling, whereas it can significantly uncouple distal gap junctions.

Finally, I investigated if the location of the gap junction itself could affect the efficacy of uncoupling (Figure 56). I connected two neurons with a gap junction between two spines (200 MΩ spine neck resistance) in their dendritic tree. One of the spines was innervated by a synapse (3 nS conductance). I next moved the whole spine (containing gap junction and synapse) around the neuron, and compared the coupling when the synapse was activated to when it was silent, without changing other parameters in the model. I found that when the spine was in the proximal tree, hardly any uncoupling was achieved on stimulating the synapse, whereas when it was distally placed, the coupling could be significantly modulated.

Effect of uncoupling on synchrony of oscillations

So far we have looked at the passive properties of olivary neurons and found the determinants and range of uncoupling achievable by synaptic activation. We have found that unless the morphological conditions are right, the uncoupling achievable will be low. This raises the question: How much uncoupling is necessary to affect synchronisation between olivary neurons? (Manor et al., 1997) have developed an experimentally validated one-compartment model of olivary neurons with two active conductances, a low-threshold calcium channel and a leak conductance. They found that varying the channels densities (termed g_T and g_L respectively) can create neurons behaving in four qualitatively different ways (stable, bistable, conditionally oscillating, spontaneously oscillating), and that coupling cells that would not oscillate on their own can cause a network oscillation to appear.

We performed a simulation in MatLab (Mathworks) based on this model by connecting by a coupling conductance two model cells with different channel densities. We made the initial coupling conductance 1% of the input conductance of the cell, which is in the range of the low coupling conductances we have shown in chapter 2. We initialised the model with channel densities in a region of parameter space containing the conditionally oscillating and spontaneously oscillating cells (g_T between 0.25 and 0.5 ms/cm^2, g_L between 0.1 and 0.25 ms/cm^2). We ran the simulation 10000 times with different parameters, sampling the parameter space uniformly. Out of these 10000 runs, we selected the 1578 parameters sets that showed cells with synchronised oscillations (defined as a zero-lag normalised crosscorrelation coefficient of the membrane voltages larger than 0.9) larger

than 0.2 mV (see Figure 57A). For each of these oscillating parameters sets, we then ran the simulation again, but with a modification: two seconds into the simulation, we reduced the coupling conductance by a certain amount, and crosscorrelated the voltage of the two cells afterwards to measure how much the cells were desynchronised (again measured by the zero-lag crosscorrelation coefficient 3 seconds after uncoupling, see Figure 57). We found that the relation between synchronization and uncoupling was extremely nonlinear, and that generally speaking, it was necessary to uncouple the cells substantially (>50%) before the cells desynchronized (Figure 57B).
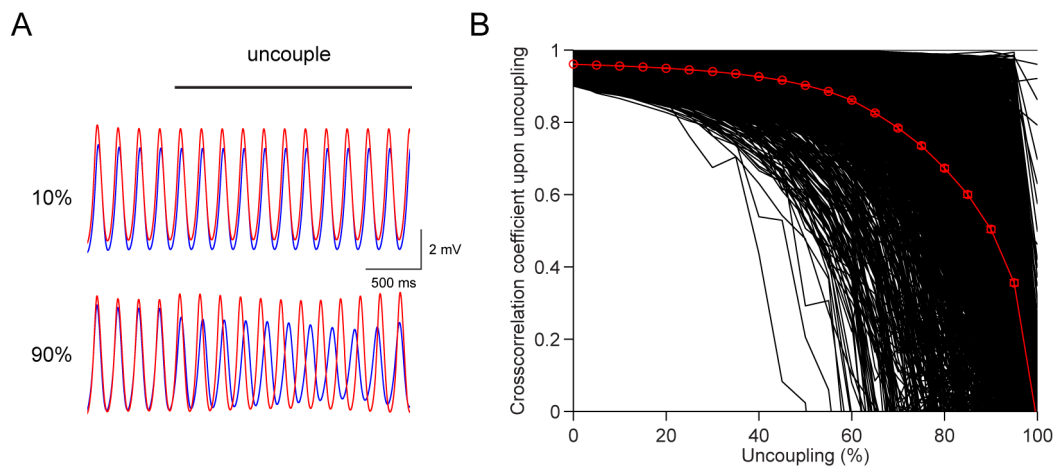
Figure 57 Uncoupling of oscillations in an active model. A) Two coupled cells (red and blue) with different channel densities (for cell 1: g_L=0.15 mS/cm^2 and g_T=0.35 mS/cm^2; for cell 2: g_L=0.153 mS/cm^2 and g_T=0.38 mS/cm^2) show synchronized oscillations. After the coupling conductance is uncoupled by 10% (top trace), the oscillations are still synchronized. When the uncoupling is 90%, the oscillations desynchronize (bottom trace). B) Plot of the zero-lag cross-correlation coefficient of the cells after uncoupling in 1578 runs (black traces) of the model which were initially displaying synchronized oscillations larger than 0.2 mV. The red trace shows the average relation across the parameter space.

Discussion

Cell morphology and the shunting hypothesis

I have presented a simple model from which I have derived some general principles about fast synaptic modulation of gap junction coupled neurons in general, and olivary neurons in particular. I have shown that the efficacy of uncoupling depends on three parameters: the two path resistances leading to the synapse and the strength of the inhibitory synapse. When the gap junction is of high resistance, then the path resistance on the proximal side of the synapse is the most critical parameter. In their seminal study of cat retinal ganglions, Koch and colleagues showed that inhibition is only effective in vetoing excitation when the conductance is approximately 50 nS (Koch et al., 1983), however I found smaller conductances are effective when the path resistances were high enough.

I have also shown that the optimal location for a synapse to accomplish uncoupling depends critically on the morphology of the cell. In the case where the dendritic paths leading to the gap junctions are symmetric, this location will be next to the gap junction, but that for more general morphologies, the optimal location may be elsewhere. With relation to olivary neurons, I have shown that the spine neck resistance of the spine on which the inhibitory input is present is critical in determining how efficacious the uncoupling is. In the previous chapter I have shown that spine

morphology varies considerably within olivary neurons, so that is also likely that the spine resistance varies considerably[1].

I have studied the case when the coupling between two cells is distributed among several gap junctions, and found that when the paths are identical, then the amount of uncoupling is directly proportional to the proportion of synapses activated. I have shown that when the synaptic input is time varying, the synapse can interfere with the shape of intercellular waveforms and produce phase and amplitude modulations. Furthermore, I studied the effect of asynchronous release on the distribution of the coupling conductance.

Relation to other models of the olive

There have been many previous attempts at modelling inferior olive neurons, mainly at the network level. Leznik et al. (2002) used a lattice of idealized single compartment neurons which are modelled as noisy coupled oscillators, and show that activity tends to occur in clusters, the size of which can be regulated by the magnitude of coupling between cells. There have been several models based on Van-der-Pol oscillators, a canonical model for non-linear oscillation (Kazantsev et al., 2003, 2004; Lee and Singh, 2011; Velarde et al., 2002). In these models, a low-frequency oscillator is used to represent the subthreshold oscillation, and on top of this is superimposed a spiking mechanism. (Katori et al., 2010; Leznik et al., 2002) use a Hodgkin-Huxley conductance based approach and reproduce patterns of complex

---

[1] Since the spine length we have measured can go from 0.5 to 6 microns. Assuming a spine neck diameter of 200 nm, and the axial resistance we found (140 $\Omega \cdot$cm), this gives a range of around 50-600MΩ.

spike synchrony comparable to those obtained from multielectrode recordings. (Schweighofer et al., 1999, Schweighofer et al., 2004) show synchronous oscillations in a network of two-compartment model of olivary neurons which I discussed in the first results chapter of this thesis.

Finally, an important modelling study we have used in this chapter (Manor et al., 1997) found that low amplitude oscillations could arise in coupled neurons with a voltage-gated conductance with similar properties to the low-threshold calcium channel, even if the neurons don't oscillate when uncoupled.

While these models show that interesting spatiotemporal patterns of activity can arise in simulations inspired by olivary cells, they either do not explicitly make reference to or incorporate the physiological details of the shunting synapse, but rather assume that it can sufficiently uncouple neurons. Our findings should help future studies to more carefully calibrate the magnitude of the uncoupling that can be expected.

Finally, there have been many models studying the interaction between chemical and electrical synapses. (Pfeuty et al., 2005) study networks of neurons connected both gap junctions and inhibitory synapses and find that electrical and chemical transmission can have antagonistic or synergistic effects on network synchrony depending on the intrinsic properties of the cells. A study on hippocampal interneurons (Bartos et al., 2002) found that inhibitory transmission in these networks can induce oscillations in the gamma range. In the cerebellum, (Simoes de Souza and De Schutter, 2011) suggest that the main role of gap junctions in cerebellar Golgi cell networks is to stabilize the oscillations created by synaptic interactions between these

cells and the granule cells. The inferior olive stands apart from these networks in that the horizontal interactions between neurons are all via gap junctions, and all the chemical synapses originate outside of the nucleus. However, our theoretical results do not make special reference to the properties of the olive and should therefore be of relevance to these other systems.

Critical appraisal of the shunting hypothesis

The original inspiration for the shunting hypothesis was the uncoupling of G and M cells in the buccal ganglion of the teleost fish achieved by stimulation of pharyngeal nerve afferents (Spira and Bennett, 1972; Spira et al., 1980). These studies, which also make use of a simple model analogous to ours, found that upon electrically stimulating the afferents with a volley of pulses, the coupling between the cells could transiently almost be abolished. However, the synaptic volley also reduced the input resistance of the cells considerably (by >50%). This suggests that the magnitude of the chemical synaptic conductance activated must be large.

The original rationale for assuming that the same mechanism applied to the inferior olive was because of the existence of chemical synapses in close proximity to gap junctions in the olivary glomerulus (Sotelo and Llinas, 1972). Such chemical synapses have been called "strategically placed". However, if the recent characterization of the DCN-IO synapse (Best and Regehr, 2009) is accurate, then individual synapses are weak and our results suggest that they will only be able to significantly uncouple neurons under quite special conditions, namely that the path leading up to the chemical

synapse has a high path resistance (> 300 MΩ). Such resistances are only likely to be present at distal sites, or at very long spines. For gap junctions in other locations, it would be more effective to activate several synapses on a dendritic shaft on the path to the gap junction rather than a single "strategically placed" one.

I have also argued that spiking data alone is not sufficient to really test the shunting hypothesis, since spike desynchronisation can also occur as a consequence of hyperpolarisation and changes in input resistance (as opposed to coupling conductance). The ultimate test of whether dynamic changes in coupling are employed for coding in the olivocerebellar system would be to observe such changes directly by obtaining paired intracellular recordings from olivary neurons in-vivo, preferably, during a task. The daunting technical hurdles this experiment poses means that we may be resigned to more indirect experimental means for the foreseeable future.

Beyond shunting: possible interactions between synapses and electrical coupling

In this chapter I have considered the pure conductance effects of the chemical synapses and the gap junctional coupling. It is important to consider other possible interactions. In the first instance, it is unlikely that the local voltage modified by the synapse affects the gap junction very much since connexin 36 has a shallow voltage dependence (Mann-Metzer and Yarom, 1999; Srinivas et al., 1999). However, it could be possible that other on-path voltage-gated channels (such as Ih) have their conductance modulated by the synaptically induced voltage change and modify the

coupling. (Mann-Metzer and Yarom, 1999) found that intrinsic properties contributed significantly to the coupling between interneurons, and (Devor and Yarom, 2002b) showed in IO neurons that somatic depolarisation decreased their coupling.

Secondly, it is known that connexins are pH sensitive, and that synaptic input can affect pH. Recently, it has been shown that localized pH transients (Willoughby and Schwiening, 2002) can occur within a cell, and it is therefore theoretically possible that if this pH shift is adjacent to a gap junction, the coupling between cells could be affected. In the case of connexin36 (Gonzalez-Nieto et al., 2008) (as opposed to all the other connexins for which this has been studied (Connors and Long, 2004)), acidification increases coupling slightly. There is some evidence that GABAergic input lowers cytoplasmic pH (Kaila and Voipio, 1987) and therefore one would predict that this would tend to increase coupling.

Finally, there remains the possibility that synapses modulate gap junctional coupling by the activation of intracellular signalling cascades leading to plasticity. In other systems (Hatton, 1998), it has been shown that synapses interact with gap junctions in several ways. In the retina dopaminergic input can modulate the coupling between amacrine cells, so that the retina can change the effective range of spatial integration necessary in photopic and scotopic conditions. In the Mauthner cells of the goldfish, glutamatergic synapses located next to gap junctions have been shown modulate the electrical coupling coming from an (Cachope et al., 2007; Pereda et al., 2003; Smith and Pereda, 2003). Since the olivary spines are innervated by

glutamatergic input which express NMDA receptors (Hoge et al., 2011), it is possible that a similar mechanism occurs between IO cells.

Appendix 1: Definitions

V_1 (I_1) and V_2 (I_2) are the transmembrane voltages (currents) at the somas of the cells in the pair, while V_{syn} is the voltage at the synapse.

$g_{syn}=(R_{syn})^{-1}$ is the conductance of the shunting synapse

RP_1 and RP_2 are the resistance along the path from the first soma to the shunting synapse, and from the synapse to the second soma respectively.

RM_1 and RM_2 are the input resistances of the cells when not connected to each other, while R_{11} and R_{22} are the input resistances when the cells are connected.

$TR_1=(V_2/I_1)$ is the transfer resistance between cell1 and cell2. If the cells have only linear elements, we have $TR_1=TR_2$ i.e. the transfer resistances are symmetric.

$cc_1=(V_2/V_1)$ and $cc_2=(V_1/V_2)$ are the coupling coefficients. Note that in general cc_1 is not equal cc_2.

The junctional conductance (Bennett, 1966) between the cells, which is a popular measure of coupling, is given by:

$$g_c = (R_c)^{-1} = (\frac{R_{11} \times R_{22} - TR^2}{TR})^{-1}$$

g_{GJ} is the conductance of a single gap junction.

Appendix 2: Derivations

<u>Equation 1:</u>

By Kirchoff's current law, we have

$$\frac{V_1 - V_{syn}}{RP_1} = \frac{V_{syn}}{R_{syn}} + \frac{V_{syn} - V_2}{RP_2} \qquad (3)$$

and furthermore, spotting a voltage divider circuit, we can see that

$$V_{syn} = \frac{RP_2 + RM_2}{RM_2} \times V_2 \qquad (4)$$
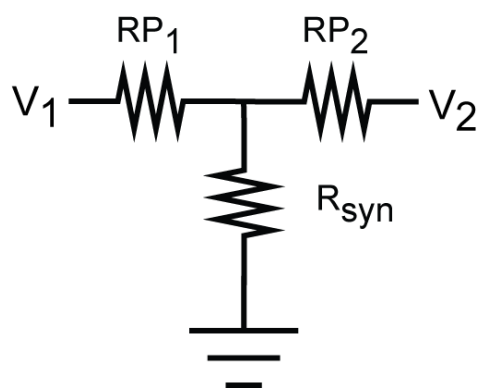
We substitute (4) into (3) and rearrange to obtain

$$cc_1 = \frac{V_2}{V_1} = ((\frac{RP_2 + RM_2}{RM_2}) \times (1 + \frac{RP_1}{R_{syn}} + \frac{RP_1}{RP_2}) - \frac{RP_1}{RP_2})^{-1}$$

By symmetry cc_2 can be obtained by exchanging the indices in this expression.

<u>Equation 2:</u>
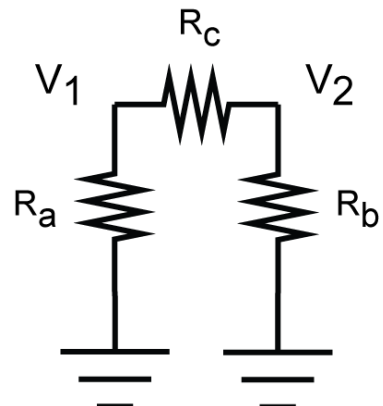
Figure 58 Y-Δ transform: the dendritic path with the shunting synapse (A) is equivalent to circuit with a single resistor - with higher resistance – on the path.

The shunting circuit in my simple model (Figure 58 A) is in Y configuration To find the effective resistance of the whole path between the cells, I perform a Y-Δ transform (Bennett, 1966) of the shunt circuit. The coupling resistance R_c is then apparent as the horizontal leg of the Δ. Kennelly's theorem (Kennelly, 1899) tells us:

$$R_c = \frac{RP_1 \times RP_2 + RP_1 \times R_{syn} + RP_2 \times R_{syn}}{R_{syn}}$$

From which equation 2 trivially follows.

Materials and methods

Slice Preparation

Sagittal and coronal brain slices of the inferior olive (250 or 300 μm) and sagittal slices of the cerebellar vermis (250 μm) were prepared from Sprague Dawley (P18–P25) rats in accordance with national and institutional guidelines. Rats were anesthetized with isoflurane and subsequently decapitated. The brain was removed and submerged in ice-cold artificial cerebrospinal fluid (ACSF) bubbled with carbogen (95% O2, 5% CO2). For inferior olive slices, the slicing ACSF contained (in mM) 250 sucrose, 25 $NaHCO_3$, 10 glucose, 5 KCl, 1.25 NaH_2PO_4, 0.5 $CaCl_2$, 3.5 $MgCl_2$; and for cerebellar slices, the slicing ACSF contained (in mM) 125 NaCl, 25 NaHCO3, 25 glucose, 2.5 KCl, 1.25 NaH_2PO_4, 1 $CaCl_2$, 4 $MgCl_2$. The brain was cut parallel to the plane of slicing, and cyanoacrylate adhesive was used to fix the brain to the platform of a Leica VT-1000 vibratome. Slices were transferred to a holding chamber and incubated for 30 min at 34°C in standard ACSF containing (in mM) 125 NaCl, 25 $NaHCO_3$, 25 glucose, 2.5 KCl, 1.25 NaH_2PO_4, 2 $CaCl_2$, 1 $MgCl_2$. Slices were then kept at room temperature until they were transferred to a recording chamber and continuously superfused with oxygenated standard ACSF (same composition as above, except olivary experiments were done with 5 mM KCl).

Slice Electrophysiology

Patch pipettes were pulled from borosilicate glass on a PC-10 puller (Narishige, Japan) to a resistance of 5 MΩ for somatic recordings, 5–10 MΩ for axonal recordings. For the olive experiments, the internal solution contained (in mM) 130 $KMeSO_4$, 7 KCl, 0.1 EGTA, 2 Na_2ATP, 2 MgATP, 0.3 Na_2GTP, 0.5% biocytin, pH 7.3. For Purkinje cell experiments, the internal solution contained (in mM) 130 K-methanesulfonate, 7 KCl, 0.05 EGTA, 2 Na_2ATP, 2 MgATP, 0.5 Na_2GTP, pH 7.3. Patch-clamp recordings were made using a Multiclamp 700A amplifier (Axon Instruments, Union City, CA). All recordings were made at 33°C ± 1°C.

Axonal recordings

Neurons were identified using an upright microscope (BX51; Olympus Optical, Southall, UK or Axioskop; Zeiss, Oberkochen, Germany) under infrared oblique illumination or infrared DIC optics, using either a high-resolution cooled CCD camera (Imago QE; T.I.L.L. Photonics, Martinsried, Germany) or a standard CCD camera (VX-55; T.I.L.L. Photonics). To aid visualization of the axon of olivary neurons, 90 μM AlexaFluor 488 (Molecular Probes, Eugene, OR) was included in the internal solution. Fluorescence excitation was minimized by using brief exposures (80 ms, 2–5 Hz) timed with a monochromator (Polychrome IV; T.I.L.L. Photonics). Cell-attached recordings (seal resistance 50–400 MΩ) were made from the axon and from axon "blebs" forming at the cut ends of axons (mean distance 92 ± 12 μm from the soma) (Khaliq and Raman, 2005; Kole et al., 2007; Monsivais

et al., 2005; Shu et al., 2006); whole-cell axonal recordings were made only from blebs. Synaptic input was activated using ACSF-filled patch pipettes.

Purkinje cell plasticity experiments

Long-term plasticity experiments were performed in current-clamp mode without holding current (i.e., allowing spontaneous spiking) in the presence of SR95531 [2-(3-carboxypropyl)-3-amino-6-(4-methoxyphenyl)pyridazinium bromide; 10 μM]. PF synaptic strength was monitored every 10 s at −65 mV during 500 ms hyperpolarizing current pulses using two stimuli separated by 10 ms, measuring the slope of the EPSP in response to the second stimulus as an index of synaptic efficacy. Long-term plasticity induction was carried out (during spontaneous spiking without holding current) using a burst of five PF stimuli at 100 Hz followed by a single or multiple climbing fibre stimuli (40 ms from onset of first PF stimulus), repeated 25 times at 0.5 Hz.

Synaptic suppression of excitation (SSE) experiments were carried out in current-clamp mode at −65 mV using standard ACSF. PF EPSPs were measured every 2 s using a single PF stimulus. SSE induction was performed using a burst of four to six (one below threshold—defined as the number of PF stimuli causing >20% depression of EPSP amplitude on their own) PF stimuli at 100 Hz together with a single or multiple climbing fibre stimuli (50 ms from onset of the first PF stimulus). Multiple climbing fibre stimuli were delivered as a burst of three or five at 400 Hz. SSE inductions were separated

by a recovery period of at least 90 s, and the different induction protocols were interleaved within a recording.

Olivary paired recordings

Two olivary somata separated by less than 50 μm were identified using Infrared-DIC optics and patched. Coupling was assessed in current-clamp mode by injecting negative current pulses alternately (from 400 to 800pA) in both cells and measuring the steady state pre and postjunctional voltage deflection. I used three different measures of coupling. The transfer resistance (TR) was calculated as the size of the postjunctional response divided by the amplitude of current injection on the prejunctional side. The coupling coefficient (cc) was calculated as the ratio of the postjunctional voltage deflection by the prejunctional voltage. Following (Bennett, 1966), the junctional conductance was calculated as follows:

$$g_c = (R_c)^{-1} = (\frac{R_{11} \times R_{22} - TR^2}{TR})^{-1}$$

Where

R_{11} and R_{22} are the input resistances of the first and second cells respectively.

Data Acquisition and Analysis

Data were low-pass filtered at 3–10 kHz and acquired at 20–100 kHz using an ITC-18 board (Instrutech, Port Washington, NY) in conjunction with AxoGraph (AxoGraph Scientific, Australia) software. Analysis was carried out using custom-written software for MatLab (MathWorks, Natick, MA) and Igor Pro (Wavemetrics, Lake Oswego, Oregon). All data are reported as mean ±

SEM unless otherwise indicated. Differences between groups were tested for statistical significance using Student's t test. For whole-cell axonal recordings, the attenuation of the ADP and AHP was calculated by dividing the voltage of the ADP and AHP plateau (measured from rest) in the axon by the corresponding voltages measured at the soma and subtracting the resulting number from 1.

Calcium imaging

Calcium transients during olivary spiking were imaged using a two-photon laser-scanning microscope (Prairie Technologies) with a pulsed titanium-sapphire laser (Spectra-Physics MaiTai) exciting at 810nm. Cells were filled with an intracellular solution as for the normal olivary recordings (see above), but with no calcium buffer, and further containing 200 µM Oregon-Green Bapta 1 for at least 15 minutes before imaging. Line scans where acquired at 500 Hz, whereas frame scans were obtained at 1-20 Hz .

Three compartment modelling of olivary bursting

I adapted the inferior olive model from Schweighofer et al (Schweighofer et al., 1999). The original model consisted of a dendritic and somatic compartment each charged by a current consisting of the sum of ionic currents, and intercompartmental current. I reimplemented the model in MatLab (Verson 7.10, MathWorks) using the ode45 function. I added an axonal compartment, and coupled it to the soma. Therefore the dendritic

currents remained as in the original model, and the somatic and axonal currents were as follows:

$$I_{soma} = I_{ionic} + I_{leak} + I_{ds} + I_{as}$$
$$I_{axon} = I_{Na} + I_{Kdr} + I_{sa}$$

Where I_{as} is the current from soma to axon, I_{sa} is the current from soma to axon. I_{Na} and I_{Kdr} are axonal sodium and potassium channels. The remaining currents are described in the paper referenced above.

For the intercompartmental currents, we have:

$$I_{as} = \frac{g_{int\_axon}}{p_{sa}} \times (V_{soma} - V_{axon})$$

$$I_{as} = \frac{g_{int\_axon}}{1 - p_{sa}} \times (V_{soma} - V_{axon})$$

Where g_{int_axon} is the conductance between the compartments, and p_{sa} represents the proportion of the membrane area taken by the somatodendritic compartments with respect to the axonal compartment.

I set p_{sa}=0.9, and g_{int_axon} = 0.13 mS/cm^2

For the axonal channels, I used Hodgkin-Huxley type channels:

$$I_{Na} = m^3 h \times (V_{axon} - E_{rev})$$
$$I_{Kdr} = n^4 \times (V_{axon} - E_{rev})$$

The state variables m,n,h are updated using the standard expression for their derivative:

$$\frac{dx}{dt} = \frac{x_\infty(V) - x}{\tau_x(V)}$$

with

$$m_\infty(V) = \frac{\alpha_m(V+60)}{\alpha_m(V+60) + \beta_m(V+60)}$$

$$\tau_h(V) = \frac{1}{\alpha_m(V+60) + \beta_m(V+60)}$$

$$\alpha_m(V) = \frac{25 - V}{10 \times (\exp(\frac{(25-V)}{10}) - 1)}$$

$$\beta_m(V) = 4 \times \exp(-\frac{V}{18})$$

$$n_\infty(V) = \frac{\alpha_n(V+60)}{\alpha_n(V+60) + \beta_n(V+60)}$$

$$\tau_n(V) = \frac{1}{\alpha_n(V+60) + \beta_n(V+60)}$$

$$\alpha_n(V) = \frac{(10 - V)}{100 \times \exp(\frac{(10-V)}{10}) - 1}$$

$$\beta_n(V) = 0.125 \times \exp(-\frac{V}{80})$$

$$h_\infty(V) = \frac{\alpha_h(V+60)}{\alpha_h(V+60) + \beta_h(V+60)}$$

$$\tau_h(V) = \frac{1}{\alpha_h(V+60) + \beta_h(V+60)}$$

$$\alpha_h(V) = \frac{1}{\exp(\frac{(30-V)}{10}) + 1}$$

$$\beta_h(V) = \frac{1}{\exp(\frac{30-V}{10}) + 1}$$

Integrate and fire model

I constructed a simple integrate and fire model of two coupled neurons using the Runge-Kutta ODE solver in MatLab (Version 7.10, MathWorks). Each cell's membrane V_m was updated as follows:

$$\frac{dV_m}{dt} = -\frac{V_m}{R_m \times C_m} + \frac{1}{C_m}(I_{cell} + I_{coupled})$$

Where R_m and C_m are the input resistance and cell capacitance.

I_{cell} was modelled as white noise. $I_{coupled}$ is the coupling current between the cells, modelled as follows:

$$I_{coupled1} = g_c \times (V_{m2} - V_{m1})$$

Where g_c is the coupling conductance.

When the voltage crossed the threshold, a spike was output by the cell.

To measure spike synchrony between two cells, I binned the spike trains from both cells (with bin size 10 ms), thus obtaining two vectors $X_1[i]$ and $X_2[i]$ with N elements, each of which equal to one if the corresponding bin contained a spike and zero otherwise. Then the spike synchrony was measure with the same index used by authors studying climbing fibre synchrony (Marshall and Lang, 2009):

$$S = \frac{\sum_{i=1}^{N}(X_1[i] - \overline{X}_1) \times (X_2[i] - \overline{X}_2)}{\sqrt{\left(\sum_{i=1}^{N}(X_1[i] - \overline{X}_1)^2\right) \times \left(\sum_{i=1}^{N}(X_2[i] - \overline{X}_2)^2\right)}}$$

Where

$$\overline{X}_1 = \sum_{i=1}^{N}\frac{X_1[i]}{N}$$

$$\overline{X}_2 = \sum_{i=1}^{N}\frac{X_2[i]}{N}$$

correspond to the average spike rates of the neurons.

Compartmental model of olivary pairs

I used the Trees Toolbox (Cuntz et al., 2011) to reconstruct neuronal morphologies obtained by fluorescence imaging. Cylinders were manually fit to the somata and dendritic trees to capture the cable properties of the neurons. The morphologies were then exported as compartment models for the Neuron Simulation environment (Hines and Carnevale, 1997), and a hill-climbing algorithm was used to fit the intrinsic parameters (i.e., the specific

capacitance, membrane resistance, axial resistivity) of the cells (assuming they were uniform across the cell) to reproduce a transient response to a current pulse (Roth and Hausser, 2001).

Active model of oscillations

We reimplemented in MatLab (version 7.10, Mathworks) a Hodgkin-Huxley like model of subthreshold oscillations in olivary neurons (Manor et al., 1997). While we refer the reader to the publication for the full specification of the model, in brief, each cell has one compartment and two active conductances: a low-threshold calcium channel, and a leak channel. The model is simulated by solving the differential equation:

$$\frac{dV_i}{dt} = -\frac{1}{C_m}(I_{ion}) + \sum_{j=1}^{N} g_{coupl(i,j)}(V_j - V_i)$$

Where V_i is the voltage of cell i, I_{ion} is the ionic current due to the two channels, and $g_{coupl(i,j)}$ is the coupling conductance between cell i and j. We used this model to look at oscillations between a pair. We used the ode45 function of MatLab to solve this equation for different parameters of the model (varying the densities of the active channel and the coupling conductance between the cells).

Immunohistochemistry

To gain information about the relationship between olivary neurons and other elements of the neuropil, I performed combined staining of single or pairs of olivary neurons with other markers. To this end, I first prepared the slices for electrophysiology as above, and filled a single cell or pair with an intracellular solution containing 0.5% biocytin. Slices were then fixed

155

overnight at 5 degrees in 5% paraformaldehyde in phosphate buffered saline (PBS). Staining procedures were performed in 24-well plates. After processing (see below) slices were placed on glass microscope slides, and coverslipped. Hard-set Vectashield mounting medium was used.

Combined biocytin–antibody (connexin 36, olig2) staining

Slices were washed in PBS (3x10min), and then permeabilised and blocked with 5% normal goat serum (10%), 0.3% Triton X-100 in 1X PBS for 2 hours at room temperature (RT). After another wash in PBS (3x10min), slices were incubated with the primary antibody in 5% normal goat serum (1%), 0.3% Triton X-100 in 1X PBS overnight at 5 degrees. Slices were then washed in PBS (3x10min) and repermeabilised in 0.05 % Triton in PBS (3x20 min). They were incubated with the secondary antibody and/or Streptavidin-Alexa488 in 5% normal goat serum, 0.3% Triton X-100 in 1XPBS for 2 hours at RT. Slices were then washed in PBS (3x10min, then 4x20 min). The last wash was performed in filtered PBS.

For connexin 36, the primary was polyclonal rabbit anti-connexin diluted 1:50 (Invitrogen catalogue number 364600). For oligodendrocyte staining, I used rabbit anti-olig2 diluted 1:700 from Millipore (AB9610). I used the same secondary for both stainings: goat-anti rabbit IgG conjugated to Alexa568 diluted 1:500 or 1:1000 (Invitrogen catalogue number 11036). Steptavidin-Alexa 488 was used in 1:2000 dilution.

Combined Biocytin-Nissl stain

I devised a combined biocytin and Nissl stain protocol to view the relationship between somata and single neurons from which recordings were obtained. I selected Neurotrace Red (Invitrogen) as my Nissl stain.

Slices were first washed in 1X PBS (3 times 10minutes), and permeabilised with 0.3% Triton X-100 in 1X PBS for 2 hours at room temperature, followed by another (3 times 10 minutes) washing step. Slices were then incubated with Streptavidin-Alexa488 (1:2000) in 1X PBS for 2 hours at room temperature. Another wash was performed in 1X PBS (3x10min), and the slices where repermeabilised with 0.1% Triton X-100 for 10mins. After washing (3x5mins), slices were incubated with Neurotrace Red (Invitrogen) for 20 minutes at room temperature. Slices were then washed in 0.1% Triton X-100 for 10min, and then in PBS for 2 times 5 minutes, and 1 times 2 hours. Slices were then mounted on glass slides and coverslipped, using hard-set Vectashield as a mounting medium.

Imaging

Microscopic slides were imaged on a spinning-disc confocal system (Perkin Elmer), using the 488 and 568 laser lines. The acquisition software was Volocity (Perkin Elmer). For the connexin staining, the 100x oil-immersion objective (NA 1.3) was used, because the immunopuncta were in the micron range. For other preparations, the 40x and 60x objectives were used.

Analysis of microscopic images

When the object of interest spanned more than one field of view, it was necessary to stitch together adjacent images. For this purpose I either used Volocity, the XUVtools software suite, or the stitch plugins from the ImageJ analysis software. Images used for spine analysis were deconvolved offline using the Huygens deconvolution package (SVI software), using a point-spread function calculated from the imaging parameters. For the detection of immunopuncta, I reimplemented a simple algorithm (Fish et al., 2008). This algorithm picks out puncta at different intensity thresholds and keeps only those that respect a size criterion. I set this to be between 0.2 and 0.8 cubic micron.

For spine analysis, I loaded image stacks into the Trees Toolbox, and traced individual spines, fitting cylindrical sections. I investigated colocalisation of spines and puncta by looking for overlapping pixels between the puncta detected with the algorithm described above and my traced spines. I defined a punctum as colocalized with a spine if they shared more than 3 pixels. To determine putative contacts in the reconstructions of coupled neurons, I reconstructed the dendritic tree with the Trees Toolbox, and looked for areas where the cylinders fit to two dendrites in close proximity overlapped. (See Figure 59 for a detailed explanation)
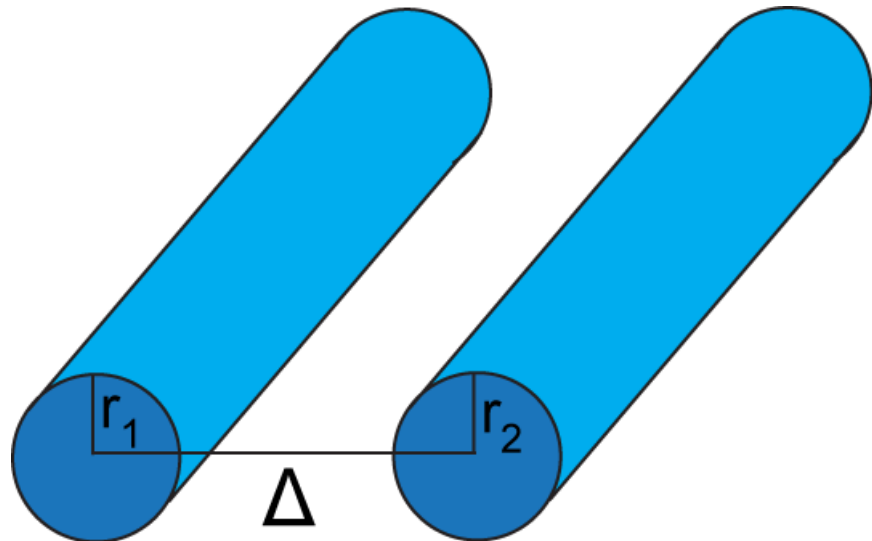
Figure 59 Detecting dendritic contacts: cylinders were locally fit to dendrites of diameters r1 and r2 in confocal stacks. The distance between the centres of the cylinders is Δ. If Δ<r1+r2, then the dendrites are classified as possibly touching. Note that Δ is calculated as the shortest distance between the line segments at the centres of the cylinders and so this method doesn't depend on the cylinders being parallel.

Chapter 5: General discussion

This thesis has covered several aspects of the anatomy and physiology of inferior olive neurons.

In Chapter 2, I showed that inferior olive neurons fire in short bursts, and these axonal bursts could encode information about the state of the olivary network. I characterised the bursts and built a simple compartment model to explain the mechanism behind their generation. I explored the functional consequences of this mode of firing by employing it in plasticity protocols.

In Chapter 3, I combined recordings from olivary neurons and (immuno)-histochemistry to study the coupling between olivary neurons. I found that the coupling is weak, and mediated by spines of very heterogeneous morphologies. I further showed that olivary neurons make many contacts with the dendrites and somas of other olivary cells, and possibly with oligodendrocytes of the neuropil.

In Chapter 4, I addressed a long-standing issue in olivary physiology: the role of inhibition in uncoupling neurons connected by gap junctions. I showed that activation of GABA-A receptors reduces the coupling between olivary neurons. Using a simplified model of synaptic uncoupling, I derived theoretically the best location for a shunting synapse to decouple neurons. With a realistic compartment model of olivary neurons, I showed that the best location for uncoupling is next to the gap junction. The model also

implies that the uncoupling is more effective in high resistance spines and in gap junctions in the distal dendritic tree.

Finally, I would like to suggest future experiments to advance our knowledge of olivary function.

From an anatomical viewpoint, it is important to determine if the olive consists of discrete clusters of coupled cells (as suggested by the dye coupling experiments of (Hoge et al., 2011)), or if it is a complete syncytium. Devor and Yarom (Devor and Yarom, 2002b) have suggested - also based on dye coupling - that the cells of two distinct morphologies (straight and curly) never contact each other, so that there are at least two olivary subnetworks; but whether there is a finer scale structure to the electrotonic network is not clear. The rise of high-throughput methods for obtaining ultrastructure from neural tissue (Chklovskii et al., 2010; Denk and Horstmann, 2004), combined with genetic labels for making gap junctions more readily visible by electron microscopy (Shu et al., 2011) mean that it should eventually be feasible to directly address the question by reconstructing a large section of olivary neuropil. In the long run, it will be interesting to know if there is structural plasticity of the coupled network and on what time scales such plasticity occurs. Such plasticity could occur at the level of spines, or the formation of and modulation of gap junction plaques.

One of the further remaining mysteries is how oscillations in the olivocerebellar system relate to movement. While there have been suggestions from climbing fibre recordings *in vivo* (Chorev et al., 2007;

Schultz et al., 2009; Welsh et al., 1995), I believe it is imperative to obtain whole cell recordings from olivary neurons during behaviour, since the spatiotemporal theory of cerebellar function requires that the patterns of firing be driven by subthreshold oscillations. As of writing, there is no direct evidence that sinusoidal subthreshold oscillations are engaged during movement. We also need a better understanding of what the triggers are for turning on and off the oscillations and how this relates to movement and learning.

Furthermore, it is necessary need to move from correlation of activity with movement to causal experiments. The last years have seen the advent of techniques (in particular, optogenetics) which allow the precise manipulation of defined elements of neuronal microcircuits (See for instance (Yizhar et al., 2011)). The next era of cerebellar research will take advantage of these techniques to stimulate the different components of the circuit. In the context of the olive, it would be informative to stimulate specific patterns of climbing fibres (perhaps using patterns that were observed during a specific behaviour) and see whether behaviours can be elicited reliably.

To provide a definite of test the learning theories of the cerebellum will eventually require techniques that read-out and modify individual synapses in a targeted way, as well as methods that prevent the expression of plasticity at this level of granularity. Only then will we be close to the goal of understanding the neuronal machine.

Bibliography

Albus, J. (1971). A theory of cerebellar function. Mathematical Biosciences *10*, 25-61.

Amitai, Y., Gibson, J.R., Beierlein, M., Patrick, S.L., Ho, A.M., Connors, B.W., and Golomb, D. (2002). The spatial dimensions of electrically coupled networks of interneurons in the neocortex. J Neurosci *22*, 4142-4152.

Anastassiou, C.A., Perin, R., Markram, H., and Koch, C. (2011). Ephaptic coupling of cortical neurons. Nat Neurosci *14*, 217-223.

Andersson, G., and Armstrong, D.M. (1987). Complex spikes in Purkinje cells in the lateral vermis (b zone) of the cat cerebellum during locomotion. J Physiol *385*, 107-134.

Andersson, G., and Oscarsson, O. (1978). Climbing fiber microzones in cerebellar vermis and their projection to different groups of cells in the lateral vestibular nucleus. Exp Brain Res *32*, 565-579.

Apps, R., Atkins, M.J., and Garwicz, M. (1997). Gating of cutaneous input to cerebellar climbing fibres during a reaching task in the cat. J Physiol *502 (Pt 1)*, 203-214.

Apps, R., and Garwicz, M. (2005). Anatomical and physiological foundations of cerebellar information processing. Nat Rev Neurosci *6*, 297-311.

Araya, R., Jiang, J., Eisenthal, K.B., and Yuste, R. (2006). The spine neck filters membrane potentials. Proc Natl Acad Sci U S A *103*, 17961-17966.

Armstrong, D.M. (1974). Functional significance of connections of the inferior olive. Physiol Rev *54*, 358-417.

Armstrong, D.M., Eccles, J.C., Harvey, R.J., and Matthews, P.B. (1968). Responses in the dorsal accessory olive of the cat to stimulation of hind limb afferents. JPhysiol *194*, 125-145.

Armstrong, D.M., Edgley, S.A., and Lidierth, M. (1988). Complex spikes in Purkinje cells of the paravermal part of the anterior lobe of the cat cerebellum during locomotion. J Physiol *400*, 405-414.

Armstrong, D.M., Harvey, R.J., and Schild, R.F. (1974). Topographical localization in the olivo-cerebellar projection: an electrophysiological study in the cat. J Comp Neurol *154*, 287-302.

Armstrong, D.M., and Rawson, J.A. (1979). Activity patterns of cerebellar cortical neurones and climbing fibre afferents in the awake cat. J Physiol *289*, 425-448.

Baker, R., Precht, W., and Llinas, R. (1972). Mossy and climbing fiber projections of extraocular muscle afferents to the cerebellum. Brain Res *38*, 440-445.

Bal, T., and McCormick, D.A. (1997). Synchronized oscillations in the inferior olive are controlled by the hyperpolarization-activated cation current I(h). J Neurophysiol *77*, 3145-3156.

Barmack, N.H. (2006). Inferior olive and oculomotor system. Prog Brain Res *151*, 269-291.

Barmack, N.H., and Simpson, J.I. (1980). Effects of microlesions of dorsal cap of inferior olive of rabbits on optokinetic and vestibuloocular reflexes. J Neurophysiol *43*, 182-206.

Barmack, N.H., and Yakhnitsa, V. (2011a). Microlesions of the inferior olive reduce vestibular modulation of Purkinje cell complex and simple spikes in mouse cerebellum. J Neurosci *31*, 9824-9835.

Barmack, N.H., and Yakhnitsa, V. (2011b). Topsy turvy: functions of climbing and mossy fibers in the vestibulo-cerebellum. Neuroscientist *17*, 221-236.

Barragan, L.A., Galindo-Morales, J.A., and Delhaye-Bouchaud, N. (1983). The microiontophoretic sensitivity of the inferior olivary nucleus to serotonin and related drugs. Proc West Pharmacol Soc *26*, 151-154.

Bartos, M., Vida, I., Frotscher, M., Meyer, A., Monyer, H., Geiger, J.R., and Jonas, P. (2002). Fast synaptic inhibition promotes synchronized gamma oscillations in hippocampal interneuron networks. Proc Natl Acad Sci U S A *99*, 13222-13227.

Bauman, M.L., and Kemper, T.L. (2005). Neuroanatomic observations of the brain in autism: a review and future directions. Int J Dev Neurosci *23*, 183-187.

Beierlein, M., Gibson, J.R., and Connors, B.W. (2003). Two dynamically distinct inhibitory networks in layer 4 of the neocortex. J Neurophysiol *90*, 2987-3000.

Bell, C.C., and Kawasaki, T. (1972). Relations among climbing fiber responses of nearby Purkinje Cells. J Neurophysiol *35*, 155-169.

Benardo, L.S., and Foster, R.E. (1986). Oscillatory behavior in inferior olive neurons: mechanism, modulation, cell aggregates. Brain Res Bull *17*, 773-784.

Bengtsson, F., and Hesslow, G. (2006). Cerebellar control of the inferior olive. Cerebellum *5*, 7-14.

Bennett, M.V. (1966). Physiology of electrotonic junctions. Ann N Y Acad Sci *137*, 509-539.

Bennett, M.V., Aljure, E., Nakajima, Y., and Pappas, G.D. (1963). Electrotonic junctions between teleost spinal neurons: electrophysiology and ultrastructure. Science *141*, 262-264.

Berciano, J., Boesch, S., Perez-Ramos, J.M., and Wenning, G.K. (2006). Olivopontocerebellar atrophy: toward a better nosological definition. Mov Disord *21*, 1607-1613.

Berens, P. (2009). CircStat: A MATLAB Toolbox for Circular Statistics. Journal of Statistical Software *31*, 1-21.

Best, A.R., and Regehr, W.G. (2008). Serotonin evokes endocannabinoid release and retrogradely suppresses excitatory synapses. J Neurosci *28*, 6508-6515.

Best, A.R., and Regehr, W.G. (2009). Inhibitory regulation of electrically coupled neurons in the inferior olive is mediated by asynchronous release of GABA. Neuron *62*, 555-565.

Biscoe, T.J., Duggan, A.W., Headley, P.M., and Lodge, D. (1973). Proceedings: Rhythmical field potentials induced in the inferior olive complex by iontophoretically applied harmaline and other unrelated alkaloids. Br J Pharmacol *49*, 174P-175P.

Bishop, G.A., and Ho, R.H. (1984). Substance P and serotonin immunoreactivity in the rat inferior olive. Brain Res Bull *12*, 105-113.

Blenkinsop, T.A., and Lang, E.J. (2006). Block of inferior olive gap junctional coupling decreases Purkinje cell complex spike synchrony and rhythmicity. J Neurosci *26*, 1739-1748.

Bloedel, J.R., and Ebner, T.J. (1984). Rhythmic discharge of climbing fibre afferents in response to natural peripheral stimuli in the cat. J Physiol *352*, 129-146.

Bloedel, J.R., and Roberts, W.J. (1971). Action of climbing fibers in cerebellar cortex of the cat. J Neurophysiol *34*, 17-31.

Bloodgood, B.L., and Sabatini, B.L. (2005). Neuronal activity regulates diffusion across the neck of dendritic spines. Science *310*, 866-869.

Bosman, L.W., and Konnerth, A. (2009). Activity-dependent plasticity of developing climbing fiber-Purkinje cell synapses. Neuroscience *162*, 612-623.

Bowman, M.H., and King, J.S. (1973). The conformation, cytology and synaptology of the opossum inferior olivary nucleus. J Comp Neurol *148*, 491-523.

Boyden, E.S., Katoh, A., Pyle, J.L., Chatila, T.A., Tsien, R.W., and Raymond, J.L. (2006). Selective engagement of plasticity mechanisms for motor memory storage. Neuron *51*, 823-834.

Boyden, E.S., Katoh, A., and Raymond, J.L. (2004). Cerebellum-dependent learning: the role of multiple plasticity mechanisms. Annu Rev Neurosci *27*, 581-609.

Bukauskas, F.F., and Verselis, V.K. (2004). Gap junction channel gating. Biochim Biophys Acta *1662*, 42-60.

Cachope, R., Mackie, K., Triller, A., O'Brien, J., and Pereda, A.E. (2007). Potentiation of electrical and chemical synaptic transmission mediated by endocannabinoids. Neuron *56*, 1034-1047.

Cavanagh, J.B. (1994). Is Purkinje cell loss in Leigh's disease an excitotoxic event secondary to damage to inferior olivary nuclei? Neuropathol Appl Neurobiol *20*, 599-603.

Chang, Y.Y., Tsai, T.C., Shih, P.Y., and Liu, J.S. (1993). Unilateral symptomatic palatal myoclonus: MRI evidence of contralateral inferior olivary lesion. Gaoxiong Yi Xue Ke Xue Za Zhi *9*, 371-376.

Charpantier, E., Cancela, J., and Meda, P. (2007). Beta cells preferentially exchange cationic molecules via connexin 36 gap junction channels. Diabetologia *50*, 2332-2341.

Chklovskii, D.B., Vitaladevuni, S., and Scheffer, L.K. (2010). Semi-automated reconstruction of neural circuits using electron microscopy. Curr Opin Neurobiol *20*, 667-675.

Choi, S., Yu, E., Kim, D., Urbano, F.J., Makarenko, V., Shin, H.S., and Llinas, R.R. (2010). Subthreshold membrane potential oscillations in inferior olive neurons are dynamically regulated by P/Q- and T-type calcium channels: a study in mutant mice. J Physiol *588*, 3031-3043.

Chorev, E., Yarom, Y., and Lampl, I. (2007). Rhythmic episodes of subthreshold membrane potential oscillations in the rat inferior olive nuclei in vivo. J Neurosci *27*, 5043-5052.

Clark, B.A., Monsivais, P., Branco, T., London, M., and Hausser, M. (2005). The site of action potential initiation in cerebellar Purkinje neurons. Nat Neurosci *8*, 137-139.

Connors, B.W., and Long, M.A. (2004). Electrical synapses in the mammalian brain. Annu Rev Neurosci *27*, 393-418.

Crépel, F., Hemart, D., D., J., and Daniel, H. (1996). Cellular mechanisms of long-term depression in the cerebellum. Behavioral and Brain Sciences *19*, 347-353.

Crill, W.E. (1970). Unitary multiple-spiked responses in cat inferior olive nucleus. J Neurophysiol *33*, 199-209.

Crill, W.E., and Kennedy, T.T. (1967). Inferior olive of the cat: intracellular recording. Science *157*, 716-718.

Cuntz, H., Forstner, F., Borst, A., and Hausser, M. (2011). The TREES toolbox--probing the basis of axonal and dendritic branching. Neuroinformatics *9*, 91-96.

Davie, J.T., Clark, B.A., and Hausser, M. (2008). The origin of the complex spike in cerebellar Purkinje cells. J Neurosci *28*, 7599-7609.

de Montigny, C., and Lamarre, Y. (1973). Rhythmic activity induced by harmaline in the olivo-cerebello-bulbar system of the cat. Brain Res *53*, 81-95.

De Montigny, C., and Lamarre, Y. (1974). Activity in the olivo-cerebello-bulbar system of the cat during ibogaline- and oxotremorine-induced tremor. Brain Res *82*, 369-373.

De Zeeuw, C.I., Chorev, E., Devor, A., Manor, Y., Van Der Giessen, R.S., De Jeu, M.T., Hoogenraad, C.C., Bijman, J., Ruigrok, T.J., French, P.*, et al.* (2003). Deformation of network connectivity in the inferior olive of connexin 36-deficient mice is compensated by morphological and electrophysiological changes at the single neuron level. J Neurosci *23*, 4700-4711.

De Zeeuw, C.I., Hertzberg, E.L., and Mugnaini, E. (1995a). The dendritic lamellar body: a new neuronal organelle putatively associated with dendrodendritic gap junctions. J Neurosci *15*, 1587-1604.

De Zeeuw, C.I., Hoebeek, F.E., Bosman, L.W., Schonewille, M., Witter, L., and Koekkoek, S.K. (2011). Spatiotemporal firing patterns in the cerebellum. Nat Rev Neurosci *12*, 327-344.

de Zeeuw, C.I., Holstege, J.C., Ruigrok, T.J., and Voogd, J. (1989). Ultrastructural study of the GABAergic, cerebellar, and mesodiencephalic innervation of the cat medial accessory olive: anterograde tracing combined with immunocytochemistry. J Comp Neurol *284*, 12-35.

de Zeeuw, C.I., Holstege, J.C., Ruigrok, T.J., and Voogd, J. (1990a). Mesodiencephalic and cerebellar terminals terminate upon the same dendritic spines in the glomeruli of the cat and rat inferior olive: an ultrastructural study using a combination of [3H]leucine and wheat germ agglutinin coupled horseradish peroxidase anterograde tracing. Neuroscience *34*, 645-655.

De Zeeuw, C.I., Koekkoek, S.K., Wylie, D.R., and Simpson, J.I. (1997). Association between dendritic lamellar bodies and complex spike synchrony in the olivocerebellar system. J Neurophysiol *77*, 1747-1758.

De Zeeuw, C.I., Lang, E.J., Sugihara, I., Ruigrok, T.J., Eisenman, L.M., Mugnaini, E., and Llinas, R. (1996). Morphological correlates of bilateral synchrony in the rat cerebellar cortex. J Neurosci *16*, 3412-3426.

De Zeeuw, C.I., and Ruigrok, T.J. (1994). Olivary projecting neurons in the nucleus of Darkschewitsch in the cat receive excitatory monosynaptic input from the cerebellar nuclei. Brain Res *653*, 345-350.

de Zeeuw, C.I., Ruigrok, T.J., Holstege, J.C., Jansen, H.G., and Voogd, J. (1990b). Intracellular labeling of neurons in the medial accessory olive of the cat: II. Ultrastructure of dendritic spines and their GABAergic innervation. J Comp Neurol *300*, 478-494.

de Zeeuw, C.I., Ruigrok, T.J., Holstege, J.C., Schalekamp, M.P., and Voogd, J. (1990c). Intracellular labeling of neurons in the medial accessory olive of the cat: III. Ultrastructure of axon hillock and initial segment and their GABAergic innervation. J Comp Neurol *300*, 495-510.

De Zeeuw, C.I., Simpson, J.I., Hoogenraad, C.C., Galjart, N., Koekkoek, S.K., and Ruigrok, T.J. (1998). Microcircuitry and function of the inferior olive. Trends Neurosci *21*, 391-400.

De Zeeuw, C.I., Wylie, D.R., Stahl, J.S., and Simpson, J.I. (1995b). Phase relations of Purkinje cells in the rabbit flocculus during compensatory eye movements. J Neurophysiol *74*, 2051-2064.

Dean, P., and Porrill, J. (2008). Adaptive-filter models of the cerebellum: computational analysis. Cerebellum *7*, 567-571.

Dean, P., and Porrill, J. (2010). The cerebellum as an adaptive filter: a general model? Funct Neurol *25*, 173-180.

Dean, P., and Porrill, J. (2011). Evaluating the adaptive-filter model of the cerebellum. J Physiol *589*, 3459-3470.

Dean, P., Porrill, J., and Stone, J.V. (2002). Decorrelation control by the cerebellum achieves oculomotor plant compensation in simulated vestibulo-ocular reflex. Proceedings *269*, 1895-1904.

Denk, W., and Horstmann, H. (2004). Serial block-face scanning electron microscopy to reconstruct three-dimensional tissue nanostructure. PLoS Biol *2*, e329.

Destexhe, A., Rudolph, M., Fellous, J.M., and Sejnowski, T.J. (2001). Fluctuating synaptic conductances recreate in vivo-like activity in neocortical neurons. Neuroscience *107*, 13-24.

Deutch, A.Y., Rosin, D.L., Goldstein, M., and Roth, R.H. (1989). 3-Acetylpyridine-induced degeneration of the nigrostriatal dopamine system: an animal model of olivopontocerebellar atrophy-associated parkinsonism. Exp Neurol *105*, 1-9.

Devor, A. (2002). The great gate: control of sensory information flow to the cerebellum. Cerebellum *1*, 27-34.

Devor, A., Fritschy, J.M., and Yarom, Y. (2001). Spatial distribution and subunit composition of GABA(A) receptors in the inferior olivary nucleus. J Neurophysiol *85*, 1686-1696.

Devor, A., and Yarom, Y. (2000). GABAergic modulation of olivary oscillations. Prog Brain Res *124*, 213-220.

Devor, A., and Yarom, Y. (2002a). Coherence of subthreshold activity in coupled inferior olivary neurons. Ann N Y Acad Sci *978*, 508.

Devor, A., and Yarom, Y. (2002b). Electrotonic coupling in the inferior olivary nucleus revealed by simultaneous double patch recordings. J Neurophysiol *87*, 3048-3058.

Devor, A., and Yarom, Y. (2002c). Generation and propagation of subthreshold waves in a network of inferior olivary neurons. J Neurophysiol *87*, 3059-3069.

Dias-Ferreira, E., Sousa, N., and Costa, R.M. (2010). Frontocerebellar Connectivity: Climbing through the Inferior Olive. Front Neurosci *4*.

Dittman, J.S., and Regehr, W.G. (1998). Calcium dependence and recovery kinetics of presynaptic depression at the climbing fiber to Purkinje cell synapse. J Neurosci *18*, 6147-6162.

Dugue, G.P., Brunel, N., Hakim, V., Schwartz, E., Chat, M., Levesque, M., Courtemanche, R., Lena, C., and Dieudonne, S. (2009). Electrical coupling mediates tunable low-frequency oscillations and resonance in the cerebellar Golgi cell network. Neuron *61*, 126-139.

Ebner, T.J., and Bloedel, J.R. (1981). Role of climbing fiber afferent input in determining responsiveness of Purkinje cells to mossy fiber inputs. J Neurophysiol *45*, 962-971.

Eccles, J.C., Ito, M., and Szentagothai, J. (1967). The Cerebellum as a Neuronal Machine (Berlin, Heidelberg, New York, Springer-Verlag).

Eccles, J.C., Llinas, R., and Sasaki, K. (1966). The excitatory synaptic action of climbing fibres on the purinje cells of the cerebellum. J Physiol *182*, 268-296.

Ekerot, C.F., Garwicz, M., and Schouenborg, J. (1991). Topography and nociceptive receptive fields of climbing fibres projecting to the cerebellar anterior lobe in the cat. J Physiol *441*, 257-274.

Ekerot, C.F., and Kano, M. (1985). Long-term depression of parallel fibre synapses following stimulation of climbing fibres. Brain Res *342*, 357-360.

Elble, R.J. (1996). Central mechanisms of tremor. J Clin Neurophysiol *13*, 133-144.

Fish, K.N., Sweet, R.A., Deo, A.J., and Lewis, D.A. (2008). An automated segmentation methodology for quantifying immunoreactive puncta number and fluorescence intensity in tissue sections. Brain Res *1240*, 62-72.

Gellman, R., Gibson, A.R., and Houk, J.C. (1985). Inferior olivary neurons in the awake cat: detection of contact and passive body displacement. J Neurophysiol *54*, 40-60.

Gellman, R., Houk, J.C., and Gibson, A.R. (1983). Somatosensory properties of the inferior olive of the cat. J Comp Neurol *215*, 228-243.

Gibson, J.R., Beierlein, M., and Connors, B.W. (1999). Two networks of electrically coupled inhibitory neurons in neocortex. Nature *402*, 75-79.

Gonzalez-Nieto, D., Gomez-Hernandez, J.M., Larrosa, B., Gutierrez, C., Munoz, M.D., Fasciani, I., O'Brien, J., Zappala, A., Cicirata, F., and Barrio, L.C. (2008). Regulation of neuronal connexin-36 channels by pH. Proc Natl Acad Sci U S A *105*, 17169-17174.

Groenewegen, H.J., Voogd, J., and Freedman, S.L. (1979). The parasagittal zonation within the olivocerebellar projection. II. Climbing fiber distribution in the intermediate and hemispheric parts of cat cerebellum. J Comp Neurol *183*, 551-601.

Grunditz, A., Holbro, N., Tian, L., Zuo, Y., and Oertner, T.G. (2008). Spine neck plasticity controls postsynaptic calcium signals through electrical compartmentalization. J Neurosci *28*, 13457-13466.

Gwyn, D.G., Nicholson, G.P., and Flumerfelt, B.A. (1977). The inferior olivary nucleus of the rat: a light and electron microscopic study. J Comp Neurol *174*, 489-520.

Gwyn, D.G., Rutherford, J.G., and Nicholson, G.P. (1983). An electron microscopic study of the direct spino-olivary projection to the inferior olivary nucleus in the rat. Neurosci Lett *42*, 243-248.

Hanani, M. (2011). Lucifer yellow - an angel rather than the Devil. J Cell Mol Med.

Hansel, C., and Linden, D.J. (2000). Long-term depression of the cerebellar climbing fiber--Purkinje neuron synapse. Neuron *26*, 473-482.

Harris, A., and Locke, D. (2009). Connexins: A guide (New York, Humana Press).

Hashimoto, K., Watanabe, M., Kurihara, H., Offermanns, S., Jiang, H., Wu, Y., Jun, K., Shin, H.S., Inoue, Y., Wu, D*., et al.* (2000). Climbing fiber synapse elimination during postnatal cerebellar development requires signal transduction involving G alpha q and phospholipase C beta 4. Prog Brain Res *124*, 31-48.

Hatton, G.I. (1998). Synaptic modulation of neuronal coupling. Cell Biol Int *22*, 765-780.

Headley, P.M., and Lodge, D. (1976). Studies on field potentials and on single cells in the inferior olivary complex of the rat. Brain Res *101*, 445-459.

Headley, P.M., Lodge, D., and Duggan, A.W. (1976). Drug-induced rhythmical activity in the inferior olivary complex of the rat. Brain Res *101*, 461-478.

Hesslow, G., and Ivarsson, M. (1996). Inhibition of the inferior olive during conditioned responses in the decerebrate ferret. Exp Brain Res *110*, 36-46.

Hines, M.L., and Carnevale, N.T. (1997). The NEURON simulation environment. Neural Comput *9*, 1179-1209.

Hines, M.L., and Carnevale, N.T. (2001). NEURON: a tool for neuroscientists. Neuroscientist *7*, 123-135.

Hobson, J.A., and McCarley, R.W. (1972). Spontaneous discharge rates of cat cerebellar Purkinje cells in sleep and waking. Electroencephalogr Clin Neurophysiol *33*, 457-469.

Hoebeek, F.E., Witter, L., Ruigrok, T.J., and De Zeeuw, C.I. (2010). Differential olivo-cerebellar cortical control of rebound activity in the cerebellar nuclei. Proc Natl Acad Sci U S A *107*, 8410-8415.

Hoge, G., Davidson, K.G., Yasumura, T., Castillo, P.E., Rash, J.E., and Pereda, A.E. (2010). The extent and strength of electrical coupling between inferior olivary neurons is heterogeneous. J Neurophysiol.

Hoge, G.J., Davidson, K.G., Yasumura, T., Castillo, P.E., Rash, J.E., and Pereda, A.E. (2011). The extent and strength of electrical coupling between inferior olivary neurons is heterogeneous. J Neurophysiol *105*, 1089-1101.

Holmes, G. (1917). The symptoms of acute cerebellar injuries due to gunshot injuries. Brain *40*, 461-535.

Houk, J.C., Buckingham, J.T., and Barto, A.G. (1996). Models of the cerebellum and motor learning. Behavioral and Brain Sciences *19*, 368-383.

Ito, M. (2001). Cerebellar long-term depression: characterization, signal transduction, and functional roles. Physiological reviews *81*, 1143-1195.

Ito, M., Sakurai, M., and Tongroach, P. (1982). Climbing fibre induced depression of both mossy fibre responsiveness and glutamate sensitivity of cerebellar Purkinje cells. J Physiol *324*, 113-134.

Jacobson, G.A., Lev, I., Yarom, Y., and Cohen, D. (2009). Invariant phase structure of olivo-cerebellar oscillations and its putative role in temporal pattern generation. Proc Natl Acad Sci U S A *106*, 3579-3584.

Jacobson, G.A., Rokni, D., and Yarom, Y. (2008). A model of the olivo-cerebellar system as a temporal pattern generator. Trends Neurosci *31*, 617-625.

Kaila, K., and Voipio, J. (1987). Postsynaptic fall in intracellular pH induced by GABA-activated bicarbonate conductance. Nature *330*, 163-165.

Kanaporis, G., Brink, P.R., and Valiunas, V. (2011). Gap junction permeability: selectivity for anionic and cationic probes. Am J Physiol Cell Physiol *300*, C600-609.

Kano, M., Rexhausen, U., Dreessen, J., and Konnerth, A. (1992). Synaptic excitation produces a long-lasting rebound potentiation of inhibitory synaptic signals in cerebellar Purkinje cells. Nature *356*, 601-604.

Katori, Y., Lang, E.J., Onizuka, M., Kawato, M., and Aihara, K. (2010). Quantitative Modeling of Spatio-Temporal Dynamics of Inferior Olive Neurons with a Simple Conductance-Based Model. Int J Bifurcat Chaos *20*, 583-603.

Kawato, M., and Gomi, H. (1992). A computational model of four regions of the cerebellum based on feedback-error learning. Biol Cybern *68*, 95-103.

Kazantsev, V.B., Nekorkin, V.I., Makarenko, V.I., and Llinas, R. (2003). Olivo-cerebellar cluster-based universal control system. Proc Natl Acad Sci U S A *100*, 13064-13068.

Kazantsev, V.B., Nekorkin, V.I., Makarenko, V.I., and Llinas, R. (2004). Self-referential phase reset based on inferior olive oscillator dynamics. Proc Natl Acad Sci U S A *101*, 18183-18188.

Keating, J.G., and Thach, W.T. (1995). Nonclock behavior of inferior olive neurons: interspike interval of Purkinje cell complex spike discharge in the awake behaving monkey is random. J Neurophysiol *73*, 1329-1340.

Keating, J.G., and Thach, W.T. (1997). No clock signal in the discharge of neurons in the deep cerebellar nuclei. J Neurophysiol *77*, 2232-2234.

Kennelly, A.E. (1899). The equivalence of triangles and three-pointed stars in conducting networks. Elec World *36*, 413-414.

Khaliq, Z.M., and Raman, I.M. (2005). Axonal propagation of simple and complex spikes in cerebellar Purkinje neurons. J Neurosci *25*, 454-463.

Khosrovani, S., Van Der Giessen, R.S., De Zeeuw, C.I., and De Jeu, M.T. (2007). In vivo mouse inferior olive neurons exhibit heterogeneous subthreshold oscillations and spiking patterns. Proc Natl Acad Sci U S A *104*, 15911-15916.

Kim, J.S., Moon, S.Y., Choi, K.D., Kim, J.H., and Sharpe, J.A. (2007). Patterns of ocular oscillation in oculopalatal tremor: imaging correlations. Neurology *68*, 1128-1135.

Kistler, W.M., De Jeu, M.T., Elgersma, Y., Van Der Giessen, R.S., Hensbroek, R., Luo, C., Koekkoek, S.K., Hoogenraad, C.C., Hamers, F.P., Gueldenagel, M., *et al.* (2002). Analysis of Cx36 knockout does not support tenet that olivary gap junctions are required for complex spike synchronization and normal motor performance. Ann N Y Acad Sci *978*, 391-404.

Kistler, W.M., and De Zeeuw, C.I. (2005). Gap junctions synchronize synaptic input rather than spike output of olivary neurons. Prog Brain Res *148*, 189-197.

Kitajima, M., Korogi, Y., Shimomura, O., Sakamoto, Y., Hirai, T., Miyayama, H., and Takahashi, M. (1994). Hypertrophic olivary degeneration: MR imaging and pathologic findings. Radiology *192*, 539-543.

Kitazawa, S., Kimura, T., and Yin, P.B. (1998). Cerebellar complex spikes encode both destinations and errors in arm movements. Nature *392*, 494-497.

Kitazawa, S., and Wolpert, D.M. (2005). Rhythmicity, randomness and synchrony in climbing fiber signals. Trends Neurosci *28*, 611-619.

Koch, C., Poggio, T., and Torre, V. (1982). Retinal ganglion cells: a functional interpretation of dendritic morphology. Philos Trans R Soc Lond B Biol Sci *298*, 227-263.

Koch, C., Poggio, T., and Torre, V. (1983). Nonlinear interactions in a dendritic tree: localization, timing, and role in information processing. Proc Natl Acad Sci U S A *80*, 2799-2802.

Koeppen, A.H. (2005). The pathogenesis of spinocerebellar ataxia. Cerebellum *4*, 62-73.

Kole, M.H. (2011). First node of ranvier facilitates high-frequency burst encoding. Neuron *71*, 671-682.

Lampl, I., and Yarom, Y. (1993). Subthreshold oscillations of the membrane potential: a functional synchronizing and timing device. J Neurophysiol *70*, 2181-2186.

Lampl, I., and Yarom, Y. (1997). Subthreshold oscillations and resonant behavior: two manifestations of the same mechanism. Neuroscience *78*, 325-341.

Landisman, C.E., Long, M.A., Beierlein, M., Deans, M.R., Paul, D.L., and Connors, B.W. (2002). Electrical synapses in the thalamic reticular nucleus. J Neurosci *22*, 1002-1009.

Lang, E.J. (2001). Organization of olivocerebellar activity in the absence of excitatory glutamatergic input. J Neurosci *21*, 1663-1675.

Lang, E.J. (2002). GABAergic and glutamatergic modulation of spontaneous and motor-cortex-evoked complex spike activity. J Neurophysiol *87*, 1993-2008.

Lang, E.J., and Blenkinsop, T.A. (2011). Control of Cerebellar Nuclear Cells: A Direct Role for Complex Spikes? Cerebellum.

Lang, E.J., Llinas, R., and Sugihara, I. (2006a). Isochrony in the olivocerebellar system underlies complex spike synchrony. J Physiol *573*, 277-279; author reply 281-272.

Lang, E.J., Sugihara, I., and Llinas, R. (1996). GABAergic modulation of complex spike activity by the cerebellar nucleoolivary pathway in rat. J Neurophysiol *76*, 255-275.

Lang, E.J., Sugihara, I., and Llinas, R. (1997). Differential roles of apamin- and charybdotoxin-sensitive K+ conductances in the generation of inferior olive rhythmicity in vivo. J Neurosci *17*, 2825-2838.

Lang, E.J., Sugihara, I., and Llinas, R. (2006b). Olivocerebellar modulation of motor cortex ability to generate vibrissal movements in rat. J Physiol *571*, 101-120.

Lang, E.J., Sugihara, I., Welsh, J.P., and Llinas, R. (1999). Patterns of spontaneous purkinje cell complex spike activity in the awake rat. J Neurosci *19*, 2728-2739.

Lansky, P., and Lanska, V. (1987). Diffusion approximation of the neuronal model with synaptic reversal potentials. Biol Cybern *56*, 19-26.

Latham, A., and Paul, D.H. (1970). Climbing iibre responses of cerebellar Purkinje cells. J Physiol *207*, 56P-57P.

Lee, K.W., and Singh, S.N. (2011). Bifurcation of orbits and synchrony in inferior olive neurons. J Math Biol.

Leznik, E., and Llinas, R. (2005). Role of gap junctions in synchronized neuronal oscillations in the inferior olive. J Neurophysiol *94*, 2447-2456.

Leznik, E., Makarenko, V., and Llinas, R. (2002). Electrotonically mediated oscillatory patterns in neuronal ensembles: an in vitro voltage-dependent dye-imaging study in the inferior olive. J Neurosci *22*, 2804-2815.

Lidierth, M., and Apps, R. (1990). Gating in the spino-olivocerebellar pathways to the c1 zone of the cerebellar cortex during locomotion in the cat. J Physiol *430*, 453-469.

Llinas, R. (1974). Eighteenth Bowditch lecture. Motor aspects of cerebellar control. Physiologist *17*, 19-46.

Llinas, R., Baker, R., and Sotelo, C. (1974). Electrotonic coupling between neurons in cat inferior olive. J Neurophysiol *37*, 560-571.

Llinas, R., Lang, E.J., and Welsh, J.P. (1997). The cerebellum, LTD, and memory: alternative views. Learn Mem *3*, 445-455.

Llinas, R., and Sasaki, K. (1989). The Functional Organization of the Olivo-Cerebellar System as Examined by Multiple Purkinje Cell Recordings. Eur J Neurosci *1*, 587-602.

Llinas, R., and Volkind, R.A. (1973). The olivo-cerebellar system: functional properties as revealed by harmaline-induced tremor. Exp Brain Res *18*, 69-87.

Llinas, R., and Welsh, J.P. (1993). On the cerebellum and motor learning. Curr Opin Neurobiol *3*, 958-965.

Llinas, R., and Yarom, Y. (1981a). Electrophysiology of mammalian inferior olivary neurones in vitro. Different types of voltage-dependent ionic conductances. J Physiol *315*, 549-567.

Llinas, R., and Yarom, Y. (1981b). Properties and distribution of ionic conductances generating electroresponsiveness of mammalian inferior olivary neurones in vitro. J Physiol *315*, 569-584.

Llinas, R., and Yarom, Y. (1986). Oscillatory properties of guinea-pig inferior olivary neurones and their pharmacological modulation: an in vitro study. J Physiol *376*, 163-182.

Llinas, R.R. (2009). Inferior olive oscillation as the temporal basis for motricity and oscillatory reset as the basis for motor error correction. Neuroscience *162*, 797-804.

Loewenstein, Y. (2002). A possible role of olivary gap-junctions in the generation of physiological and pathological tremors. Mol Psychiatry *7*, 129-131.

Loewenstein, Y., Mahon, S., Chadderton, P., Kitamura, K., Sompolinsky, H., Yarom, Y., and Hausser, M. (2005). Bistability of cerebellar Purkinje cells modulated by sensory stimulation. Nat Neurosci *8*, 202-211.

Long, M.A., Deans, M.R., Paul, D.L., and Connors, B.W. (2002). Rhythmicity without synchrony in the electrically uncoupled inferior olive. J Neurosci *22*, 10898-10905.

Long, M.A., Jutras, M.J., Connors, B.W., and Burwell, R.D. (2005). Electrical synapses coordinate activity in the suprachiasmatic nucleus. Nat Neurosci *8*, 61-66.

Lou, J.S., and Bloedel, J.R. (1992a). Responses of sagittally aligned Purkinje cells during perturbed locomotion: relation of climbing fiber activation to simple spike modulation. J Neurophysiol *68*, 1820-1833.

Lou, J.S., and Bloedel, J.R. (1992b). Responses of sagittally aligned Purkinje cells during perturbed locomotion: synchronous activation of climbing fiber inputs. J Neurophysiol *68*, 570-580.

Mann-Metzer, P., and Yarom, Y. (1999). Electrotonic coupling interacts with intrinsic properties to generate synchronized activity in cerebellar networks of inhibitory interneurons. J Neurosci *19*, 3298-3306.

Mano, N. (1970). Changes of simple and complex spike activity of cerebellar purkinje cells with sleep and waking. Science *170*, 1325-1327.

Manor, Y., Rinzel, J., Segev, I., and Yarom, Y. (1997). Low-amplitude oscillations in the inferior olive: a model based on electrical coupling of neurons with heterogeneous channel densities. JNeurophysiol *77*, 2736-2752.

Manor, Y., Yarom, Y., Chorev, E., and Devor, A. (2000). To beat or not to beat: a decision taken at the network level. J Physiol Paris *94*, 375-390.

Marina, N., Becker, D.L., and Gilbey, M.P. (2008). Immunohistochemical detection of connexin36 in sympathetic preganglionic and somatic motoneurons in the adult rat. Auton Neurosci *139*, 15-23.

Marr, D. (1969). A theory of cerebellar cortex. JPhysiol *202*, 437-470.

Marshall, S.P., and Lang, E.J. (2004). Inferior olive oscillations gate transmission of motor cortical activity to the cerebellum. J Neurosci *24*, 11356-11367.

Marshall, S.P., and Lang, E.J. (2009). Local changes in the excitability of the cerebellar cortex produce spatially restricted changes in complex spike synchrony. J Neurosci *29*, 14352-14362.

Maruta, J., Hensbroek, R.A., and Simpson, J.I. (2007). Intraburst and interburst signaling by climbing fibers. J Neurosci *27*, 11263-11270.

Mathy, A., Ho, S.S., Davie, J.T., Duguid, I.C., Clark, B.A., and Hausser, M. (2009). Encoding of oscillations by axonal bursts in inferior olive neurons. Neuron *62*, 388-399.

Mauk, M.D., Medina, J.F., Nores, W.L., and Ohyama, T. (2000). Cerebellar function: coordination, learning or timing? Curr Biol *10*, R522-525.

Mauk, M.D., Steinmetz, J.E., and Thompson, R.F. (1986). Classical conditioning using stimulation of the inferior olive as the unconditioned stimulus. Proc Natl Acad Sci U S A *83*, 5349-5353.

Medina, J.F., Nores, W.L., and Mauk, M.D. (2002). Inhibition of climbing fibres is a signal for the extinction of conditioned eyelid responses. Nature *416*, 330-333.

Miall, R.C., Weir, D.J., Wolpert, D.M., and Stein, J.F. (1993). Is the cerebellum a smith predictor? J Mot Behav *25*, 203-216.

Mills, S.L., and Massey, S.C. (1995). Differential properties of two gap junctional pathways made by AII amacrine cells. Nature *377*, 734-737.

Monsivais, P., Clark, B.A., Roth, A., and Hausser, M. (2005). Determinants of action potential propagation in cerebellar Purkinje cell axons. J Neurosci *25*, 464-472.

Nagy, J.I., Dudek, F.E., and Rash, J.E. (2004). Update on connexins and gap junctions in neurons and glia in the mammalian nervous system. Brain Res Brain Res Rev *47*, 191-215.

Nagy, J.I., Ionescu, A.V., Lynn, B.D., and Rash, J.E. (2003). Coupling of astrocyte connexins Cx26, Cx30, Cx43 to oligodendrocyte Cx29, Cx32, Cx47: Implications from normal and connexin32 knockout mice. Glia *44*, 205-218.

Onodera, S. (1984). Olivary projections from the mesodiencephalic structures in the cat studied by means of axonal transport of horseradish peroxidase and tritiated amino acids. J Comp Neurol *227*, 37-49.

Oscarsson, O. (1980). Functional organization of olivary projection to the cerebellar anterior lobe. In The Inferior Olivary Nucleus, Anatomy and Physiology, J. COURVILLE, C.D. MONTIGNY, and Y. LAMARRE, eds. (New York, Raven Press).

Palmer, L.M., and Stuart, G.J. (2009). Membrane potential changes in dendritic spines during action potentials and synaptic input. J Neurosci *29*, 6897-6903.

Park, Y.G., Park, H.Y., Lee, C.J., Choi, S., Jo, S., Choi, H., Kim, Y.H., Shin, H.S., Llinas, R.R., and Kim, D. (2010). Ca(V)3.1 is a tremor rhythm pacemaker in the inferior olive. Proc Natl Acad Sci U S A *107*, 10731-10736.

Pereda, A., O'Brien, J., Nagy, J.I., Smith, M., Bukauskas, F., Davidson, K.G., Kamasawa, N., Yasumura, T., and Rash, J.E. (2003). Short-range functional interaction between connexin35 and neighboring chemical synapses. Cell Commun Adhes *10*, 419-423.

Pfeuty, B., Mato, G., Golomb, D., and Hansel, D. (2005). The combined effects of inhibitory and electrical synapses in synchrony. Neural Comput *17*, 633-670.

Placantonakis, D., and Welsh, J. (2001). Two distinct oscillatory states determined by the NMDA receptor in rat inferior olive. J Physiol *534*, 123-140.

Placantonakis, D.G., Bukovsky, A.A., Aicher, S.A., Kiem, H.P., and Welsh, J.P. (2006). Continuous electrical oscillations emerge from a coupled network: a study of the inferior olive using lentiviral knockdown of connexin36. J Neurosci *26*, 5008-5016.

Placantonakis, D.G., Bukovsky, A.A., Zeng, X.H., Kiem, H.P., and Welsh, J.P. (2004). Fundamental role of inferior olive connexin 36 in muscle coherence during tremor. Proc Natl Acad Sci U S A *101*, 7164-7169.

Placantonakis, D.G., Schwarz, C., and Welsh, J.P. (2000). Serotonin suppresses subthreshold and suprathreshold oscillatory activity of rat inferior olivary neurones in vitro. J Physiol *524 Pt 3*, 833-851.

Ramon y Cajal, S. (1911). Histologie du système nerveux de l'homme et des vertébrés. (Maloine, Paris.).

Rash, J.E., Davidson, K.G., Kamasawa, N., Yasumura, T., Kamasawa, M., Zhang, C., Michaels, R., Restrepo, D., Ottersen, O.P., Olson, C.O.*, et al.* (2005). Ultrastructural localization of connexins (Cx36, Cx43, Cx45), glutamate receptors and aquaporin-4 in rodent olfactory mucosa, olfactory nerve and olfactory bulb. J Neurocytol *34*, 307-341.

Rash, J.E., Yasumura, T., Davidson, K.G., Furman, C.S., Dudek, F.E., and Nagy, J.I. (2001). Identification of cells expressing Cx43, Cx30, Cx26, Cx32 and Cx36 in gap junctions of rat brain and spinal cord. Cell Commun Adhes *8*, 315-320.

Richardson, M.J., and Gerstner, W. (2005). Synaptic shot noise and conductance fluctuations affect the membrane voltage with equal significance. Neural Comput *17*, 923-947.

Richardson, M.J., and Gerstner, W. (2006). Statistics of subthreshold neuronal voltage fluctuations due to conductance-based synaptic shot noise. Chaos *16*, 026106.

Roth, A., and Hausser, M. (2001). Compartmental models of rat cerebellar Purkinje cells based on simultaneous somatic and dendritic patch-clamp recordings. J Physiol *535*, 445-472.

Ruigrok, T.J. (1997). Cerebellar nuclei: the olivary connection. Prog Brain Res *114*, 167-192.

Ruigrok, T.J., de Zeeuw, C.I., van der Burg, J., and Voogd, J. (1990a). Intracellular labeling of neurons in the medial accessory olive of the cat: I. Physiology and light microscopy. J Comp Neurol *300*, 462-477.

Ruigrok, T.J., de Zeeuw, C.I., and Voogd, J. (1990b). Hypertrophy of inferior olivary neurons: a degenerative, regenerative or plasticity phenomenon. Eur J Morphol *28*, 224-239.

Ruigrok, T.J., and Voogd, J. (1990). Cerebellar nucleo-olivary projections in the rat: an anterograde tracing study with Phaseolus vulgaris-leucoagglutinin (PHA-L). J Comp Neurol *298*, 315-333.

Ruigrok, T.J., and Voogd, J. (2000). Organization of projections from the inferior olive to the cerebellar nuclei in the rat. J Comp Neurol *426*, 209-228.

Rushmer, D.S., Roberts, W.J., and Augter, G.K. (1976). Climbing fiber responses of cerebellar Purkinje cells to passive movement of the cat forepaw. Brain Res *106*, 1-20.

Safo, P., and Regehr, W.G. (2008). Timing dependence of the induction of cerebellar LTD. Neuropharmacology *54*, 213-218.

Sasaki, K., Bower, J.M., and Llinas, R. (1989). Multiple Purkinje Cell Recording in Rodent Cerebellar Cortex. Eur J Neurosci *1*, 572-586.

Scheibel, M.E., and Scheibel, A.B. (1955). The inferior olive; a Golgi study. J Comp Neurol *102*, 77-131.

Schmitz, D., Schuchmann, S., Fisahn, A., Draguhn, A., Buhl, E.H., Petrasch-Parwez, E., Dermietzel, R., Heinemann, U., and Traub, R.D. (2001). Axo-axonal coupling. a novel mechanism for ultrafast neuronal communication. Neuron *31*, 831-840.

Schonewille, M., Gao, Z., Boele, H.J., Veloz, M.F., Amerika, W.E., Simek, A.A., De Jeu, M.T., Steinberg, J.P., Takamiya, K., Hoebeek, F.E.*, et al.* (2011). Reevaluating the role of LTD in cerebellar motor learning. Neuron *70*, 43-50.

Schonewille, M., Khosrovani, S., Winkelman, B.H., Hoebeek, F.E., De Jeu, M.T., Larsen, I.M., Van der Burg, J., Schmolesky, M.T., Frens, M.A., and De Zeeuw, C.I. (2006). Purkinje cells in awake behaving animals operate at the upstate membrane potential. Nat Neurosci *9*, 459-461; author reply 461.

Schultz, S.R., Kitamura, K., Post-Uiterweer, A., Krupic, J., and Hausser, M. (2009). Spatial pattern coding of sensory information by climbing fiber-evoked calcium signals in networks of neighboring cerebellar Purkinje cells. J Neurosci *29*, 8005-8015.

Schweighofer, N., Doya, K., Fukai, H., Chiron, J.V., Furukawa, T., and Kawato, M. (2004). Chaos may enhance information transmission in the inferior olive. Proc Natl Acad Sci U S A *101*, 4655-4660.

Schweighofer, N., Doya, K., and Kawato, M. (1999). Electrophysiological properties of inferior olive neurons: A compartmental model. J Neurophysiol *82*, 804-817.

Sears, L.L., and Steinmetz, J.E. (1991). Dorsal accessory inferior olive activity diminishes during acquisition of the rabbit classically conditioned eyelid response. Brain Res *545*, 114-122.

Sedgwick, E.M., and Williams, T.D. (1967). Responses of single units in the inferior olive to stimulation of the limb nerves, peripheral skin receptors, cerebellum, caudate nucleus and motor cortex. J Physiol *189*, 261-279.

Shinoda, Y., Sugihara, I., Wu, H.S., and Sugiuchi, Y. (2000). The entire trajectory of single climbing and mossy fibers in the cerebellar nuclei and cortex. Prog Brain Res *124*, 173-186.

Shu, X., Lev-Ram, V., Deerinck, T.J., Qi, Y., Ramko, E.B., Davidson, M.W., Jin, Y., Ellisman, M.H., and Tsien, R.Y. (2011). A genetically encoded tag for correlated light and electron microscopy of intact cells, tissues, and organisms. PLoS Biol *9*, e1001041.

Silver, R.A., Momiyama, A., and Cull-Candy, S.G. (1998). Locus of frequency-dependent depression identified with multiple-probability fluctuation analysis at rat climbing fibre-Purkinje cell synapses. J Physiol *510 (Pt 3)*, 881-902.

Simoes de Souza, F.M., and De Schutter, E. (2011). Robustness effect of gap junctions between Golgi cells on cerebellar cortex oscillations. Neural Syst Circuits *1*, 7.

Simpson, J.I., Wylie, D.R., and De Zeeuw, C.I. (1996). On climbing fiber signals and their consequences. Behavioral and Brain Sciences *19*, 384 - 398.

Sjolund, B., Bjorklund, A., and Wiklund, L. (1977). The indolaminergic innervation of the inferior olive. 2. Relation to harmaline induced tremor. Brain Res *131*, 23-37.

Smith, M., and Pereda, A.E. (2003). Chemical synaptic activity modulates nearby electrical synapses. Proc Natl Acad Sci U S A *100*, 4849-4854.

Smith, S.S. (1998). Step cycle-related oscillatory properties of inferior olivary neurons recorded in ensembles. Neuroscience *82*, 69-81.

Sotelo, C. (2003). Viewing the brain through the master hand of Ramon y Cajal. Nat Rev Neurosci *4*, 71-77.

Sotelo, C., and Llinas, R. (1972). Specialized membrane junctions between neurons in the vertebrate cerebellar cortex. J Cell Biol *53*, 271-289.

Sotelo, C., Llinas, R., and Baker, R. (1974). Structural study of inferior olivary nucleus of the cat: morphological correlates of electrotonic coupling. J Neurophysiol *37*, 541-559.

Spira, M.E., and Bennett, M.V. (1972). Synaptic control of electrotonic coupling between neurons. Brain Res *37*, 294-300.

Spira, M.E., Spray, D.C., and Bennett, M.V. (1980). Synaptic organization of expansion motoneurons of Navanax inermis. Brain Res *195*, 241-269.

Srinivas, M., Rozental, R., Kojima, T., Dermietzel, R., Mehler, M., Condorelli, D.F., Kessler, J.A., and Spray, D.C. (1999). Functional properties of channels formed by the neuronal gap junction protein connexin36. J Neurosci *19*, 9848-9855.

Sugihara, I., Lang, E.J., and Llinas, R. (1995). Serotonin modulation of inferior olivary oscillations and synchronicity: a multiple-electrode study in the rat cerebellum. Eur J Neurosci *7*, 521-534.

Sugihara, I., Wu, H., and Shinoda, Y. (1999). Morphology of single olivocerebellar axons labeled with biotinylated dextran amine in the rat. J Comp Neurol *414*, 131-148.

Sugihara, I., Wu, H.S., and Shinoda, Y. (2001). The entire trajectories of single olivocerebellar axons in the cerebellar cortex and their contribution to Cerebellar compartmentalization. J Neurosci *21*, 7715-7723.

Svoboda, K., Tank, D.W., and Denk, W. (1996). Direct measurement of coupling between dendritic spines and shafts. Science *272*, 716-719.

Szapiro, G., and Barbour, B. (2007). Multiple climbing fibers signal to molecular layer interneurons exclusively via glutamate spillover. Nat Neurosci *10*, 735-742.

Szentagothai, J., and Rajkovits, K. (1959). Uber den Ursprung der Kletterfasern des Kleinhirns. Z Anat EntwGesch *121*, 130-141.

Urbano, F.J., Simpson, J.I., and Llinas, R.R. (2006). Somatomotor and oculomotor inferior olivary neurons have distinct electrophysiological phenotypes. Proc Natl Acad Sci U S A *103*, 16550-16555.

Uusisaari, M., Obata, K., and Knopfel, T. (2007). Morphological and electrophysiological properties of GABAergic and non-GABAergic cells in the deep cerebellar nuclei. J Neurophysiol *97*, 901-911.

Van Der Giessen, R.S., Koekkoek, S.K., van Dorp, S., De Gruijl, J.R., Cupido, A., Khosrovani, S., Dortland, B., Wellershaus, K., Degen, J., Deuchars, J., *et al.* (2008). Role of olivary electrical coupling in cerebellar motor learning. Neuron *58*, 599-612.

van Essen, T.A., van der Giessen, R.S., Koekkoek, S.K., Vanderwerf, F., Zeeuw, C.I., van Genderen, P.J., Overbosch, D., and de Jeu, M.T. (2010). Anti-Malaria Drug Mefloquine Induces Motor Learning Deficits in Humans. Front Neurosci *4*, 191.

Velarde, M.G., Nekorkin, V.I., Kazantsev, V.B., Makarenko, V.I., and Llinas, R. (2002). Modeling inferior olive neuron dynamics. Neural Netw *15*, 5-10.

Vervaeke, K., Lorincz, A., Gleeson, P., Farinella, M., Nusser, Z., and Silver, R.A. (2010). Rapid desynchronization of an electrically coupled interneuron network with sparse excitatory synaptic input. Neuron *67*, 435-451.

Volman, V., Levine, H., and Sejnowski, T.J. (2010). Shunting inhibition controls the gain modulation mediated by asynchronous neurotransmitter release in early development. PLoS Comput Biol *6*, e1000973.

Voogd, J., and Glickstein, M. (1998). The anatomy of the cerebellum. Trends Neurosci *21*, 370-375.

Walberg, F., and Ottersen, O.P. (1989). Demonstration of GABA immunoreactive cells in the inferior olive of baboons (Papio papio and Papio anubis). Neurosci Lett *101*, 149-155.

Wang, S.S., Denk, W., and Hausser, M. (2000). Coincidence detection in single dendritic spines mediated by calcium release. Nat Neurosci *3*, 1266-1273.

Weiss, C., Houk, J.C., and Gibson, A.R. (1990). Inhibition of sensory responses of cat inferior olive neurons produced by stimulation of red nucleus. J Neurophysiol *64*, 1170-1185.

Welsh, J.P., Ahn, E.S., and Placantonakis, D.G. (2005a). Is autism due to brain desynchronization? Int J Dev Neurosci *23*, 253-263.

Welsh, J.P., Han, V.Z., Rossi, D.J., Mohr, C., Odagiri, M., Daunais, J.B., and Grant, K.A. (2011). Bidirectional plasticity in the primate inferior olive induced by chronic ethanol intoxication and sustained abstinence. Proc Natl Acad Sci U S A *108*, 10314-10319.

Welsh, J.P., Lang, E.J., Suglhara, I., and Llinas, R. (1995). Dynamic organization of motor control within the olivocerebellar system. Nature *374*, 453-457.

Welsh, J.P., Yamaguchi, H., Zeng, X.H., Kojo, M., Nakada, Y., Takagi, A., Sugimori, M., and Llinas, R.R. (2005b). Normal motor learning during pharmacological prevention of Purkinje cell long-term depression. Proc Natl Acad Sci U S A *102*, 17166-17171.

Wiklund, L., Sjolund, B., and Bjorklund, A. (1981). Morphological and functional studies on the serotoninergic innervation of the inferior olive. J Physiol (Paris) *77*, 183-186.

Williams, S.R., and Stuart, G.J. (1999). Mechanisms and consequences of action potential burst firing in rat neocortical pyramidal neurons. J Physiol *521 Pt 2*, 467-482.

Willoughby, D., and Schwiening, C.J. (2002). Electrically evoked dendritic pH transients in rat cerebellar Purkinje cells. J Physiol *544*, 487-499.

Wise, A.K., Cerminara, N.L., Marple-Horvat, D.E., and Apps, R. (2010). Mechanisms of synchronous activity in cerebellar Purkinje cells. J Physiol *588*, 2373-2390.

Yarom, Y., and Llinas, R. (1987). Long-term modifiability of anomalous and delayed rectification in guinea pig inferior olivary neurons. J Neurosci *7*, 1166-1177.

Yizhar, O., Fenno, L.E., Davidson, T.J., Mogri, M., and Deisseroth, K. (2011). Optogenetics in neural systems. Neuron *71*, 9-34.

Yokota, T., Hirashima, F., Furukawa, T., Tsukagoshi, H., and Yoshikawa, H. (1989). MRI findings of inferior olives in palatal myoclonus. J Neurol *236*, 115-116.